UNIVERSITY OF TARTU
Faculty of Science and Technology
Institute of Technology

Viacheslav Kiselev

Cdk1-mediated phosphoregulation of NLS-NES modules

Bachelor's Thesis (12 ECTS)

Curriculum Science and Technology

Supervisor(s):
Associate Professor, PhD Ilona Faustova
Researcher, PhD Mihkel Örd

Tartu 2022

Cdk1-mediated phosphoregulation of NLS-NES modules

Abstract:

Cyclin-dependent kinases (CDKs) are central regulators of the cell cycle that form complexes with various cyclins to phosphorylate hundreds of targets required for cell cycle progression. CDK-mediated phosphorylation affects various aspects of the target proteins, for example their localization. In this study we aimed to understand how the CDK specificity mechanisms affect the regulation of protein nuclear localization by Cdk1. We focused on the impact of phosphorylation site mutations to alanine or switching phospho-acceptor from threonine to serine in a Cdk1-inactivated nuclear localization module of Psy4. The experiments revealed that inactivation of different phosphorylation sites created localization modules with very different nuclear exit dynamics in the cell cycle. The results showed that threonines are phosphorylated significantly later in the cell cycle presumably due to high counteracting phosphatase activity.

Keywords: Cell cycle, Phosphorylation, Cyclin-dependent kinase

CERCS: P310 Proteins, enzymology

Valkude tuuma lokalisatsiooni regulatsioon kinaasi Cdk1 poolt

***Lühikokkuvõte*:**

Tsükliinist sõltuvad kinaasid (CDK-d) on kesksed rakutsükli regulaatorid, mis seondudes erinevate tsükliinidega fosforüleerivad sadu rakutsükli valke. CDK-vahendatud fosforüleerimine mõjutab erinevaid valkude omadusi, näiteks nende paiknemist rakus. Käesoleva töö eesmärk on uurida, kuidas CDK substraatide valiku mehhanimsid mõjutavad valkude tuuma lokalisatsiooni reguleerimist. Töös keskenduti fosforüleerimissaitide inaktiveerimisele ja treoniin-seriin mutatsioonidele Psy4 valgu tuuma lokalisatsiooni moodulis. Eri saitide inaktiveerimisel saadi väga erineva ekspordi dünaamikaga moodulid. Katsed näitasid, et treoniinid fosforüleeritakse rakutsüklis oluliselt hiljem ja et treoniin-seriin mutatsioonid võivad omada eripidist mõju. Moodulite erinev ekspordi dünaamika rakutsüklis näitas, et osade saitide fosforüleerimine jõuab kiiresti kinaasi ja fosfataasi vahelise tasakaaluni, samas kui teiste saitide fosforüleerimine koguneb aeglaselt.

Võtmesõnad: Rakutsükkel, Fosforüleerimine, Tsükliinist sõltuvad kinaasid

CERCS: P310 Proteiinid, ensümoloogia

TABLE OF CONTENTS

TERMS, ABBREVIATIONS AND NOTATIONS

APC – anaphase-promoting complex

CDK – cyclin-dependent kinase

clonNAT – nourseothricin

CSM – complete supplement mixture

DMSO - dimethyl sulfoxide

EDTA – ethylenediaminetetraacetic acid

GFP – green fluorescent protein

LB – Luria-Bertani media

MAP – mitogen-activated protein

MCM - minichromosome maintenance protein complex

NES – nuclear export signal

NLS – nuclear localization signal

OD – optical density

SC-HIS – Synthetic complete media without histidine

SDS - PAGE - sodium dodecyl sulfate polyacrylamide gel electrophoresis

SLiM – short linear interaction motif

TE buffer – Tris-EDTA buffer

WT - wild type

YPD -Yeast extract, peptone, dextrose media

INTRODUCTION

The cell cycle is a precisely timed series of events that take place in four different phases. The crucial components of the cell cycle control system which governs the sequence of events are cyclin-dependent kinases (CDKs). CDKs are a group of kinases whose activity oscillates in the cell cycle, and which phosphorylate a large variety of cell cycle proteins, thus controlling the activity, localization, stability, protein-protein interactions and other aspects of these downstream proteins. By phosphorylating hundreds of cell cycle proteins, CDKs regulate most cell cycle events. To carry out their role, CDKs must form a complex with activating proteins known as cyclins. Distinct cyclins are expressed at different cell cycle phases, allowing CDKs to from phase-specific cyclin-CDK complexes and also phosphorylation of phase-specific substrates, as different cyclins guide the kinase subunit to their substrates via recognition of specific substrate docking motifs. In addition to cyclin-specific phosphorylation, cell cycle progression depends on an increasing CDK activity, as low CDK activity is needed for phosphorylation of G1 and S phase substrates, but phosphorylation of mitotic substrates requires high kinase activity. These different mechanisms allow CDKs to phosphorylate distinct substrates in different time periods during the cell cycle.

CDK-mediated phosphorylation affects various aspects of the target proteins, for example their localization. Many cell cycle proteins, for example transcriptional regulators, are controlled by nuclear shuttling. Proteins have to carry nuclear localization signals (NLS) for nuclear import or nuclear export signals (NES) for regulated export. These signals are often controlled by CDK. Depending on the position of the phosphorylation site, phosphorylation can either activate or inactivate NLS or NES motifs, enabling CDK to trigger nuclear import or export of proteins.

Previous studies have demonstrated several examples of CDK-mediated control of protein nuclear localization and have showed that localization switches take place at different cell cycle stages. This raises a question about the mechanisms determining the timing of these switches. Previous research investigating the timing of CDK phosphorylation events was carried out on degrons which led to an irreversible output. Nuclear shuttling, however, is reversible and is constantly counteracted by phosphatases. For this reason, the dynamic regulation of nuclear localization is expected to be different.

In this study, we investigated the regulation of CDK-dependent nuclear shuttling using an NLS-NES module from Psy4 as a model system. We focused on how threonine-to-serine mutations determine the phosphorylation thresholds and affect the localization dynamics.

1 LITERATURE REVIEW

1.1. Eukaryotic cell cycle

Cell cycle is a highly ordered chain of events that leads to cell division. This cycle usually consists of four phases: G1, S, G2 and M phase (**Figure 1**). During G1 phase cell conducts its regular functions and grows. After the cell reaches a sufficient size and proliferation is promoted by extracellular signals, the cell proceeds to S phase, where DNA is replicated, leading to duplication of chromosomes. Upon completion of DNA replication, the cell enters G2 phase in which it continues to grow and makes necessary preparations for the division. G2 phase leads to the final phase – M phase, where the cell divides, creating two genetically identical daughter cells (Morgan, 2007).

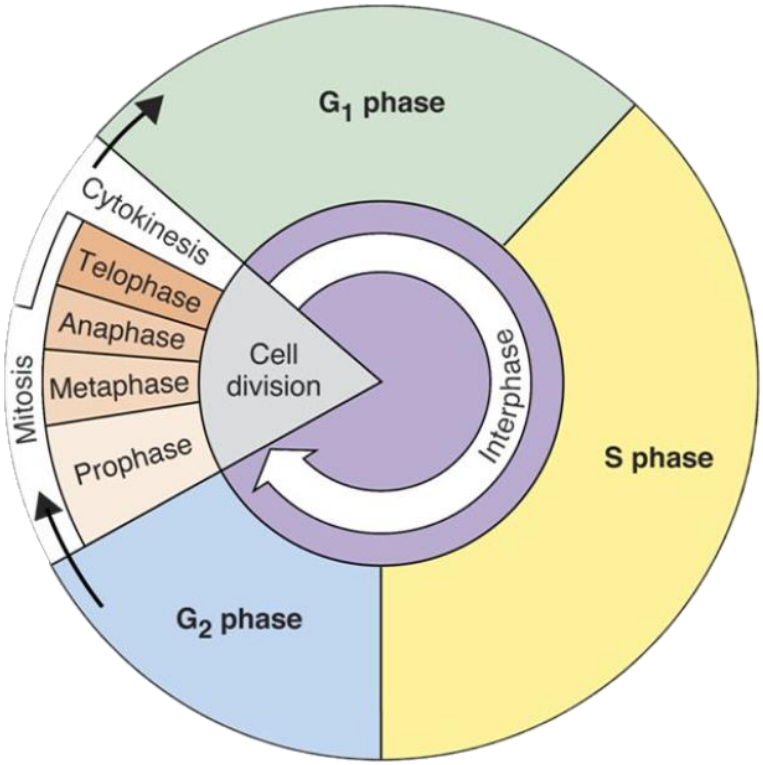

Figure 1. Graphical representation of the cell cycle. The cell cycle is divided into four phases with distinct events occurring in each phase. G1, S and G2 phases are part of interphase, followed by mitosis and cytokinesis that constitute cell division. In more detail, mitosis is divided into distinct subphases. Figure adapted from https://onlinesciencenotes.com/cell-cycle-its-different-phases-and-duration.

The gap phases, G1 and G2, also provide time to integrate external and internal signals to determine if conditions are favourable and all preparations are done, allowing cells to commit to the cell cycle or segregation of chromosomes, respectively (Alberts *et al*., 2017). During these phases cell can pass a border to make an irreversible commitment to continuation of the cell cycle. The first decision point is during the G1 phase. When conditions are not suitable, or anti-proliferative signals are present, cells either stay in G1 phase or enter a non-dividing G0 phase, also known as quiescence. When conditions become favourable again and signals that promote proliferation are present, cells go through the commitment point and progress with DNA replication and cell division. Importantly, after the commitment point negative signals cannot affect the progress of the cell cycle until the next commitment point. The second commitment point is in G2 phase. At that point cells either commit to M phase, leading to chromatin condensation and alignment, or they arrest in G2 phase, for example in case of DNA damage (Matthews *et al*., 2022)

1.1.1 Cyclin-dependent kinase is the master cell cycle regulator

The key regulator of the cell cycle is cyclin-dependent kinase (CDK). Changes in the CDK activity promote cell cycle entry, progression, and completion (Morgan, 2007). For example, CDK initiates the commitment to cell cycle entry at G1 phase and triggers DNA replication in S phase. During M phase CDK activity initiates chromosome condensation, makes nuclear envelope permeable, initiates alignment of the replicated chromosomes and is required for chromosome segregation. *S. cerevisiae* contains six CDKs, four of which regulate transcription and two, Cdk1 and Pho85, are involved in cell cycle control (Malumbres, 2014). Pho85 is non-essential and coordinates metabolism and cell cycle, but Cdk1 alone is sufficient and essential to control cell cycle events from G1 to M phase (Jiménez *et al*., 2013).

CDKs are active only when they are in complex with cyclins. The conformation of Cdk1 changes by binding to cyclins. The most important changes happen in the T-loop of Cdk1 – after cyclin binding it no longer obstructs the binding site for the substrates (Andzelm *et al*., 1995). Also, changes occur at the ATP-binding site, thus correctly positioning ATP phosphates for phosphotransfer reaction. These changes in confirmation allow the formed CDK/cyclin complex to bind and phosphorylate substrate proteins.

Due to the cell-cycle-regulated transcription and controlled activation of protein degradation, specific cyclins accumulate during distinct stages of the cell cycle (Bloom &

Cross, 2007). Importantly, transcription and protein degradation that is regulated by cell cycle also depends on CDK activity, creating a system that makes the cell cycle sequential and unidirectional. Progression of the cell cycle is driven by accumulation of CDK activity from interphase to M phase. To return to interphase CDK activity must decrease and for this, cyclins must be degraded (Wäsch & Cross, 2002). The loss of CDK activity in late mitosis is achieved through anaphase-promoting complex/cyclosome (APC/C) activity that causes degradation of cyclins. In late G1 and S phase, the accumulating cyclin-CDK complexes in turn phosphorylate and inactivate APC/C (Zachariae *et al*., 1998). These feedback loops between CDK and APC/C make the cell cycle behave in oscillatory manner (Matthews *et al*., 2022; Morgan, 2007; Peters, 2006).

Through the cell cycle, transition from one phase to another is connected to the activating partners of CDKs – cyclins, which are expressed at different cell cycle phases. Different cyclins possess similar structure, and they contain the cyclin box – a conserved region that binds CDK (Tatum & Endicott, 2020). In budding yeast, Cdk1 is regulated by cyclins Cln1-3 and Clb1-6 (Bloom & Cross, 2007). In late G1, Cln3-Cdk1 activates the transcription of G1/S cyclins Cln2 and Cln1. These three cyclins promote commitment to cell cycle in G1 phase. Cln1- and Cln2-Cdk1 promote bud formation and expression of subsequent S phase cyclins Clb5 and Clb6. In addition to triggering DNA replication, Clb6- and Clb5-Cdk1 in turn activate the expression of G2 and M cyclins Clb1-4. Cyclins also differ in subcellular localization, as the major G1/S cyclin Cln2 is predominantly cytoplasmic, while S cyclin Clb5 is nuclear and G2 and M cyclins Clb3 and Clb2 are mainly nuclear, but also present in the cytoplasm at lower levels (Miller & Cross, 2000; Örd, Möll, *et al*., 2019a). Quantitative analysis of expression of Clb cyclins revealed that Clb5 and Clb2 are expressed at higher level than the others (**Figure 2**). Also, this analysis showed that in a normal 90-minute yeast cell cycle, the S, G2 and M cyclins are expressed with around 15-minute intervals (**Figure 2**). (Enserink & Kolodner, 2010; Merrick & Fisher, 2010; Morgan, 2007; Örd & Loog, 2019).

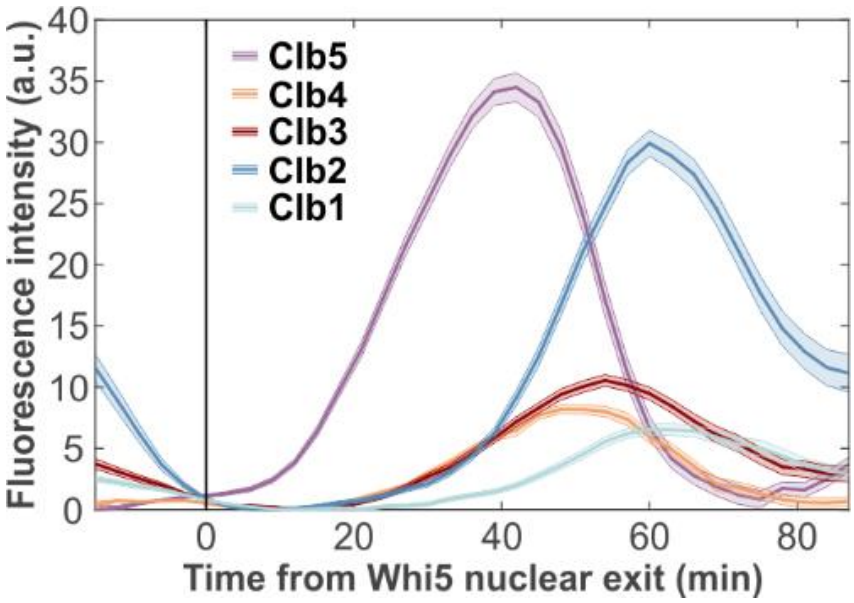

Figure 2. Expression profiles of Clb cyclins. Plot showing the nuclear levels of Clb-Citrine measured in time-lapse microscopy experiments. Whi5 nuclear exit marks the Start point of cell cycle, in late G1 phase (Örd, Möll, *et al*., 2019a).1.2 Mechanisms allowing temporally resolved phosphorylation of CDK targets

1.1.2.1 Quantitative and qualitative models of CDK function

CDK activity plays a central part in ordering the cell cycle. There are two models that describe the control of cell cycle by CDK. The qualitative model by which cell cycle events are ordered by distinct substrate specificities of successive cyclin-CDK waves and the quantitative model where the increasing CDK activity leads to phosphorylation of different target proteins, with low activity required for phosphorylation of G1 substrates to maximal activity required for mitotic targets (Uhlmann *et al*., 2011). According to the quantitative model that was initially based on fission yeast, one mitotic cyclin-CDK complex is enough to drive the cell cycle, however, other cyclins are needed to phosphorylate specific targets in their respectful phases in other organisms. For example, budding yeast is dependent on G1 cyclins for polarization and growing buds (Ercan *et al*., 2021). The quantitative model suggests that as CDK activity rises with cell cycle progression, it orders the cell cycle by phosphorylating different proteins at different kinase activity levels. This is possible due to later substrates being less optimal for the kinase and thus they require more active CDK complexes to be sufficiently phosphorylated, while earlier substrates are more optimal, making their sufficient phosphorylation by earlier CDK complexes possible (Swaffer *et al*., 2016).

1.1.2.2 The active site specificity of cyclin-Cdk1 complexes

Cyclin-Cdk1 complexes phosphorylate sites with the minimal consensus S/TP and the full consensus S/TPxK/R (where S/T is the phosphorylation site, P is proline, x is any amino acid and K/R is lysine or arginine (Leiss *et al*., 1992). Biochemical assays have revealed that the phosphorylation efficiency between different minimal and full consensus sites varies over 10-fold, with positively charged residues in positions +2 to +5 from the phosphorylation site having a positive effect on phosphorylation rate. Also, a two-fold preference for phosphorylation of serines over threonines was found for Cdk1 (Örd, Möll, *et al*., 2019a; Suzuki *et al*., 2015). The proline in position +1 is a key determinant for CDK phosphorylation sites, yet there are many examples of weaker Cdk1 phosphorylation sites that lack the +1 proline. To promote phosphorylation of a weaker site there can be additional factors which increase active site specificity (for example, positively charged residues in +2 to +5 positions) and distant docking interactions (**Figure 3**) (Faustova *et al*., 2021; Örd, Möll, *et al*., 2019a; Suzuki *et al*., 2015).

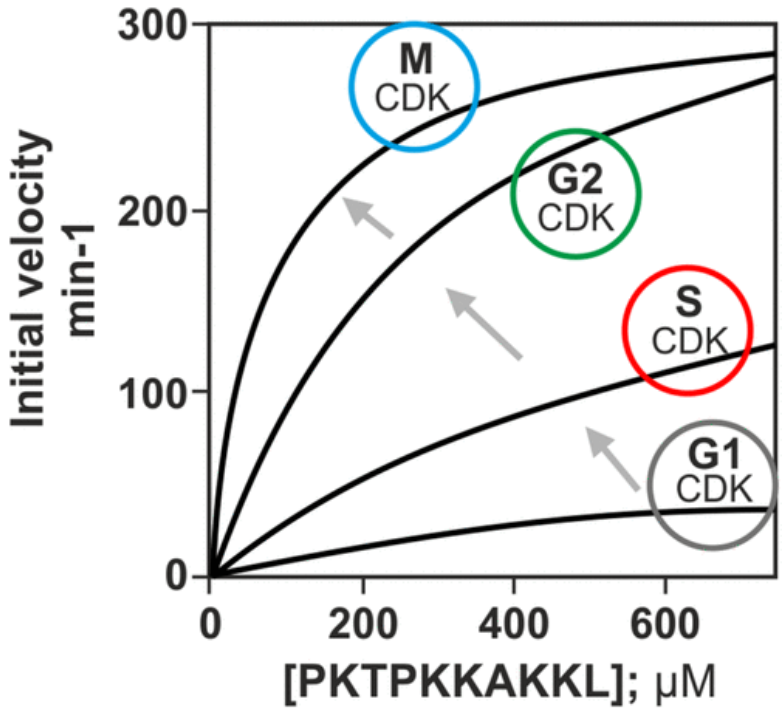

Figure 3. The activity of cyclin-CDK complexes rises in the order of expression of the cyclins in the cell cycle. The figure shows the different activity of cyclin-Cdk1 complexes towards a substrate peptide with a consensus CDK phosphorylation site (PKTPKKAKKL). Figure adapted from Örd & Loog, 2019.

Various cyclins promote different events during the cell cycle, which is partially possible because cyclins confer different specificity to the CDK complex. For example, S phase Clb5-Cdk1 complex is more efficient in phosphorylating targets involved in S phase events compared to mitotic Clb2-Cdk1 (Loog & Morgan, 2005. This was shown by replacing *CLB5* with *CLB2* gene, which led to a decrease in phosphorylation of Clb5-specific targets during S phase. However, Clb2-Cdk1 has higher intrinsic activity than Clb5-Cdk1, allowing it to phosphorylate a broader range of substrates irrespective of cyclin-substrate docking motifs (Loog & Morgan, 2005). This led to a key discovery that with cell cycle progression the activity of subsequent cyclin-CDK complexes increases so that complexes of later phases are more active compared to earlier complexes (**Figure 3**), allowing complexes with higher intrinsic activity to phosphorylate less optimal substrates (Kõivomägi *et al*., 2011; Topacio *et al*., 2019). The increasing intrinsic activity could also be a mechanism that prevents early cyclin-Cdk1 complexes from phosphorylating targets from later phases and offers an explanation to the observation that later cyclins are in many cases able to carry out the functions of earlier cyclin-Cdk1 complexes. (Loog & Morgan, 2005; Morgan, 2007; Örd & Loog, 2019).

1.1.2.3 Cks1 promotes multisite phosphorylation

Cks1 is phopshoadapter which binds to the catalytic subunit of Cdk1 and increases the efficiency of multisite phosphorylation of CDK substrates (**Figure 4**) (Köivomägi *et al*., 2011).

Cks1 binds to phosphorylated threonine based CDK consensus sites, but it does not bind to phosphorylated SP sites (Kõivomägi *et al*., 2013; McGrath *et al*., 2013). Another factor that affects the Cks1-mediated multisite phosphorylation is the relative positioning and distance between the Cks1 priming site and the secondary phosphorylation sites (**Figure 4**). It was found that the efficiency of secondary site phosphorylation is maximal when the secondary site is 12-16 amino acid residues C-terminal of the Cks1 binding site. No effect of the Cks1 docking was observed when the two sites were less than 12 amino acid residues apart and the multiphosphorylation efficiency declined rapidly at distances greater than 20 or 30 amino acids (Kõivomägi *et al*., 2013; Örd *et al*., 2019).

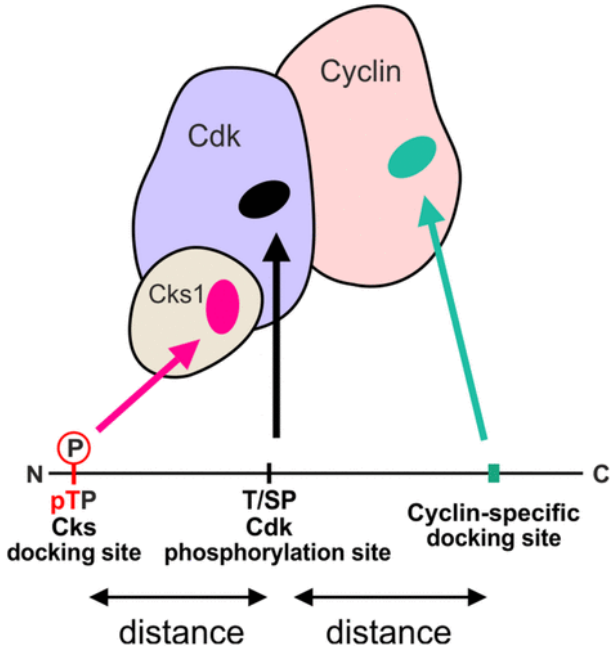

Figure 4. Diagram displaying the main interactions between substrate proteins and the CDK complex that determine the phosphorylation rate and specificity. The CDK active site phosphorylates phosphorylation sites with consensus S/TP. The phosphorylation rate of a site can be increased by: Cks1 binding to phosphorylated TP sites and cyclins interacting with substrates via specific short linear motifs. The effect of docking is dependent on the relative positioning of docking sites and phosphorylation sites along the disordered substrate. (Örd & Loog, 2019).

The distance-dependency of Cks1 docking connections could create an order in phosphorylation of multisite networks, as Cks1 docking enhances phosphorylation of C-terminal sites at a specific distance. Substitution of threonine with serine in CDK phosphorylation site can disrupt the Cks1 docking connection, , leading to changes in phosphorylation mode from ordered and semi-processive to random distributive, where phosphorylation of one site does not depend on other sites . Thus, distribution of serines and threonines in phosphorylation sites is one of the mechanisms of controlling how efficiency CDK activity is transferred through the multisite phosphorylation networks (Kõivomägi *et al*., 2013; Örd, Möll, *et al*., 2019a).

1.1.2.4 Cyclin-substrate docking

CDKs are activated by various cyclins during the cell cycle. Apart from being activators of CDKs, cyclins also guide the kinase subunit to specific substrates by recognizing certain linear motifs. Linear motifs are short protein sequences (usually 3-10 amino acid residues long) that mediate dynamic protein interactions and that usually act as modification or ligand binding sites (Van Roey *et al*., 2014).

In budding yeast, specific cyclin-substrate docking motifs have been characterised for cyclins in all cell cycle phases (**Figure 4**). For example, LP motif is recognised by late G1 cyclins, Cln2 and Cln1 (Bhaduri & Pryciak, 2011; Kõivomägi *et al*., 2011). LP docking interactions help Cln1/2-Cdk1 to phosphorylate specific substrates efficiently. The substrates with LP motifs include Whi5, the repressor of cell cycle transcription, Sic1, the inhibitor of Clb-Cdk1 complexes, mating pathway proteins Ste5 and Ste20, and others (Bhaduri & Pryciak, 2011; Kõivomägi *et al*., 2011).

The NLxxxL motif was found to help the phosphorylation and degradation of Far1 at G1/S stage in yeast (Faustova *et al*., 2021). Far1 is a Cdk1 inhibitor that is activated by mating pheromone signalling and it must be degraded following commitment to cell cycle (Blondel *et al*., 2000).NLxxxL motif is recognized only by Clb5/Clb6-Cdk1 complexes that are present in S phase and the motif was also found in several other S phase Cdk1 targets (Faustova *et al*., 2021). Another cyclin-substrate docking motif, the RxL motif, is used by all Clb1-6 cyclins, in contrast to the S-phase-specific NLxxxL motif (**Figure 5**) (Faustova *et al*., 2021). Therefore, the RxL motif would promote substrate phosphorylation from S phase through mitosis, whereas NLxxxL motif is targeted only in S phase. Indeed, the NLxxxL motif was found on several proteins that must be dephosphorylated in mitosis (Faustova *et al*., 2021). This illustrates how the specificity of cyclin-substrate docking motifs affects both the timing of phosphorylation and dephosphorylation.

Another docking motif that is specific for a certain cyclin-CDK complex is PxxPxF motif. This motif is recognized by G2 cyclin Clb3 and is needed for the G2 cyclin functions in *S. cerevisiae*. PxxPxF is required for transcriptional activation of mitotic cyclins and for regulation of the spindle pole bodies (Örd *et al*., 2020).

LxF is an M phase cyclin docking motif that mediates binding of Cdc6, a replication factor, to M phase cyclin (Örd, Möll, *et al*., 2019a). Binding to this motif drives inhibition of M-CDK by Cdc6, which allows for Cdc6 accumulation and isolation during mitosis. Mutual inhibition between M-CDK and tyrosine kinase Swe1 is also facilitated by LxF motif

and Cks1, showing that the same interaction modules regulate the binding of the Cdk1 complex to its substrates and inhibitors. In addition to mediating interactions with inhibitory proteins, the LxF motif is also crucial for guiding M-CDK to phosphorylate certain mitotic regulators like Spo12.

Therefore, cyclin docking motifs are important in regulation of substrate phosphorylation in all cell cycle phases and while some motifs (LP, NLxxxL, PxxPxF, LxF) are specific to one pair of cyclins, the RxL motif is used by a wider range of cyclins (**Figure 4**). The motifs with different specificity can enable CDK to regulate its targets with high precision and with various dynamics, while the common RxL motifs could enable stable phosphorylation of proteins throughout S, G2 and M phases. The latter is important for example to keep replication proteins phosphorylated after G1/S transition to avoid re-replication (Wilmes *et al*., 2004). Similarly to Cks1 docking, the effect of cyclin-substrate docking on substrate phosphorylation is dependent on the positioning of the docking motif to phosphorylation sites. While the LP motifs are more flexible in respect to the position of the phosphorylation site, the RxL motifs promote phosphorylation of sites that are N-terminal of the docking motif (**Figure 5**) (Kõivomägi *et al*., 2013).

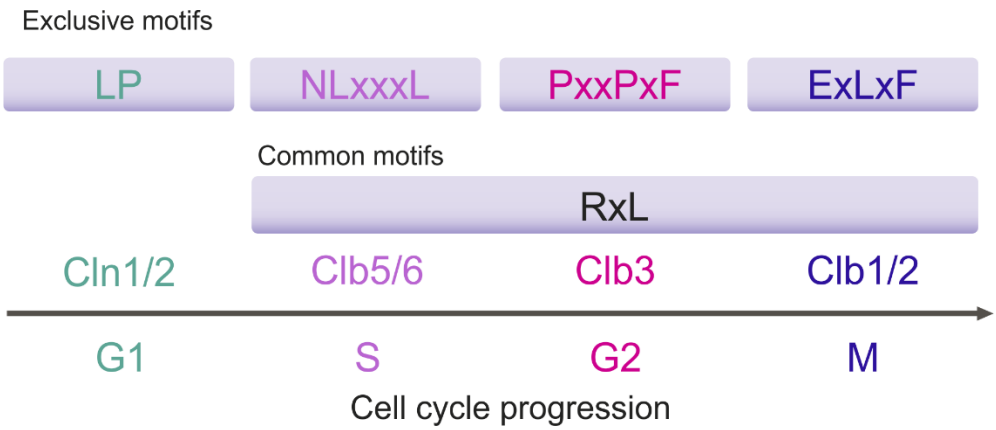

Figure 5. Examples of exclusive and common cyclin docking motifs. The exclusive motifs bind to cyclins expressed in one cell cycle phase, whereas the common RxL motifs bind to cyclins expressed from S phase to M phase (Clb1-6). Figure modified from Örd, 2021.

1.1.2.5 Pattern of linear motifs determines the timing of Cdk1 substrate phosphorylation

Cdk1 substrates differ from each other in their pattern of linear motifs that mediate the phosphorylation, for example the number of phosphorylation sites and the distances between them, the positioning of cyclin docking motifs, and the distribution of serine and threonines as phopshoacceptors (Örd, Möll, *et al*., 2019a). Variation of these parameters not only differentiates the substrates between cell cycle phases, but also provides a variety of CDK thresholds in the cycle. This allows CDK to discriminate between hundreds of substrate proteins to mediate their timely phosphorylation. (Kõivomägi *et al*., 2013; Örd, Venta, *et al*., 2019)

The impact of different multisite phosphorylation network parameters on the timing of phosphorylation in the cell cycle has been studied using phospho-degrons as a detectable output of phosphorylation (Faustova *et al*., 2021; Örd, Möll, *et al*., 2019a). The N terminus of Sic1 contains eight Cdk1 phosphorylation sites, but the limiting step was found to be phosphorylation of a non-proline site in a phospho-degron. While 50% the wild-type Sic1 degron module was degraded in S phase around 25 minutes after the Start point of the cell cycle, an increase of the distance of the degron from a Cks1 binding site by just four amino acid residues caused an enormous 30-minute delay in degradation, resulting in incomplete degradation of Sic1 during the whole cell cycle (Örd, Möll, *et al*., 2019a). The delay caused by decreased Cks1 docking could be rescued by addition of specific cyclin docking motifs such as RxL or LxF motifs, which further demonstrated that linear motifs contribute to determining the timing of phosphorylation in the cell cycle. A variety of such manipulations to the CDK specificity of the Sic1 degron were made and it was found that the Cks1 binding sites and the cyclin docking motifs act as a helper network can that tune the timing of degron phosphorylation throughout the cell cycle (**Figure 6**). Importantly, these interactions were found to be especially important for phosphorylation of sites with poor active site specificity, such as the non-proline site in Sic1 degron, as the helper network can compensate for the weak phosphorylation specificity of such sites.

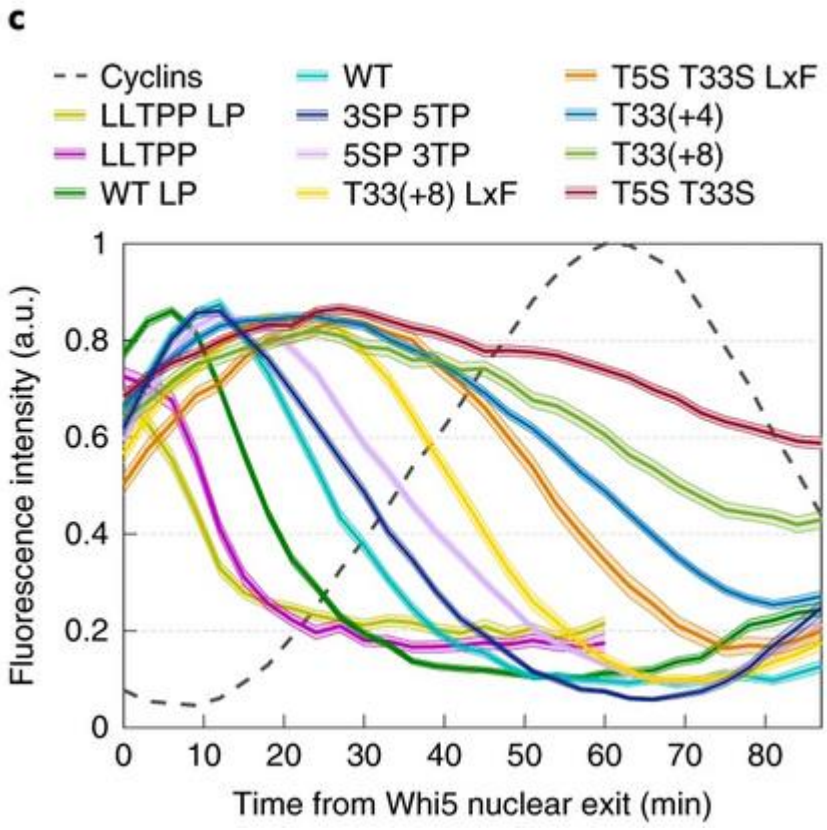

Figure 6. The pattern of motifs in multisite phosphorylation network affects the timing of Sic1 degron phosphorylation. Plot shows the timing of degradation of various Sic1-based proteins, where the parameters of multisite phosphorylation networks, including the distances between the sites, the presence of cyclin docking motifs and threonine/serine distribution in phosphorylation sites, were manipulated. Whi5 nuclear exit marks the Start point of cell cycle in late G1 phase. (Örd *et al*., 2019)

1.1.2.6 Phosphatases counteracting Cdk1 activity

In addition to differences in CDK specificity, various Cdk1 substrates can also differ in their specificity to phosphatases. Recent work has revealed that by counteracting CDK activity, phosphatases play an important role in determining the timing of different phosphorylation events. $PP2A^{Cdc55}$ is the major phosphatase that counteracts CDK phosphorylation during interphase and contributes to ordering the cell cycle by delaying phosphorylation of some sites (Godfrey *et al*., 2017). $PP2A^{Cdc55}$ especially focuses on threonine dephosphorylation, leading to threonine-directed phosphorylation to accumulate later in the cycle (Godfrey *et al*., 2017). Thus, the CDK-counteracting phosphatases also contribute to ordering the cell cycle by affecting CDK thresholds, based on distribution of threonine and serine residues on the substrate phosphorylation sites. Phosphatase activity can also be targeted to distinct proteins. For example, the PxL motif guides phosphatase

Cdc14 to dephosphorylate distinct targets during mitotic exit, and its removal delays the dephosphorylation events (Godfrey *et al*., 2017; Kataria *et al*., 2018). Furthermore, specific docking motifs have been found for the major phosphatases PP2A and PP1 in humans (Heroes *et al*., 2013; Hertz *et al*., 2016), but knowledge of specific substrate docking interactions for these phosphatases in yeast is limited.

1.3. Regulation of nuclear localization by CDK

Nuclear localization signals (NLS) are short peptide sequences which signal the import of the protein from cytoplasm into nucleus. This process is facilitated by importins in the process of NLS-dependent protein recognition. Examples of the motifs that mediate nuclear import: PKKKRKV, RRARRPR xKxKRx, RxRK, RRARRPR. (Lu *et al*., 2021)

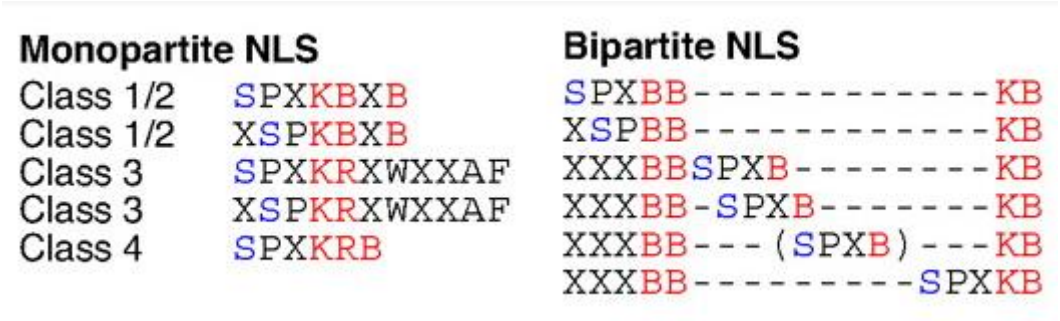

Figure 7. Regulation of monopartite and bipartite NLS by phosphorylation. Amino acids that constitute monopartite and bipartite NLS are marked in red, CDK phosphorylation sites are marked in blue. Phosphorylation of sites immediately N-terminal of the NLS inactivate the motif, whereas phosphorylation of the linker region in bipartite NLS can enhance nuclear import (Kosugi *et al*., 2009)

Typically, NLS contains one or two clusters of basic amino acids, resulting in monopartite and bipartite NLS motifs (**Figure 7**). Monopartite NLSs have 4-5 of such amino acids, while bipartite NLSs have two clusters that are separated by around 10 amino acid residues (Zhu *et al*., 2015).

Transport in and out of the nucleus is an essential cellular function and the nuclear transport of proteins is controlled by several mechanisms, including phosphorylation. Phosphorylation can either switch on or off biological pathways and enzymes. Phosphorylation has either enhancing or inhibitory effect on nuclear import, depending on the position of the phosphorylation site relative to the NLS (**Figure 7**) (Nardozzi *et al*., 2010). An example of inhibitory effect of phosphorylation is the bipartite NLS of Psy4. It

has two Cdk1 phosphorylation sites located at both parts of NLS, and phosphorylation of these sites abolishes the binding of importins to this NLS and thus inactivates the NLS (Kosugi *et al*., 2009). An example of nuclear import enhancing effect of phosphorylation is Dna2, which is imported into the nucleus upon phosphorylation of a CDK consensus site that is in the linker region of a bipartite NLS.

Nuclear Export Signals (NES) drive the export of proteins from the nucleus. NES motifs are recognized by exportins, such as Crm1 and Msn5 in yeast (Kosugi *et al*., 2009). While the Crm1-dependent NES is well-characterized and consists of 3-4 hydrophobic residues, the Msn5-dependent NES motifs are often longer protein segments with no clear determinants(Belanger *et al*., 2022). For proteins whose nuclear localization is regulated during the cell cycle, the presence of both NLS and NES is necessary (Liku *et al*., 2005), as the balance of the two activities determines the localization. For example, the minichromosome maintenance protein complex (MCM) helicase complex is exported from the nucleus upon phosphorylation by Cdk1 and this is dependent on both inactivation of NLS and the presence of NES. The presence of both motifs also enables rapid localization switches, as the shuttling is actively regulated in both direction and is not dependent on diffusion through the nuclear pores.

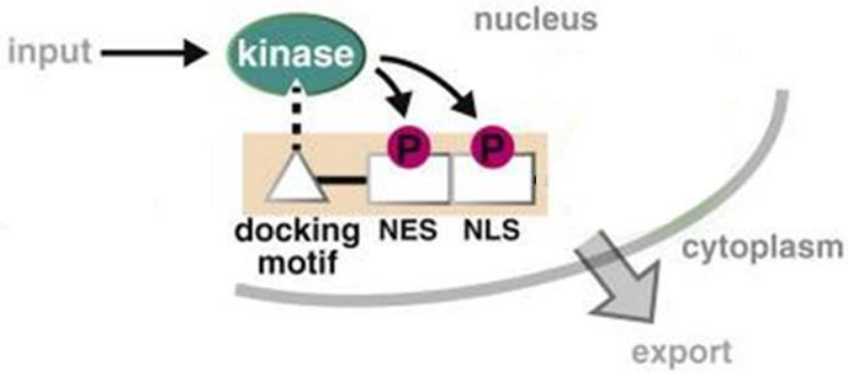

Figure 8. Diagram shows principle of nuclear shuttling controlled by a kinase. Kinase docks to its docking motif and phosphorylates NES or NLS promoting export or import (Russell MGordley *et al*., 2016)

Nuclear shuttling (**Figure 8**) of more than thirty proteins in *S. cerevisiae* is regulated by Cdk1 (Kosugi *et al*., 2009). Four of them (Swi5, Cdh1, Acm1, and Pds1) are responsible for M phase to G1 transition, five of them (Swi6, Whi5, Msa1, Mcm3, and Dna2) G1-S transition, some of them are G1-specific transcription factors. Dna2 is being targeted by CDK especially during S and G2 phases to control its localization to ensure proper processing of DNA. Whi5 is a negative regulator of cell cycle progression in G1 phase. In early G1 phase Whi5 binds and inhibits transcriptional complexes that are required for entry into the cell cycle. G1-Cdk1 complex phosphorylates and inactivates Whi5, dissociating it from the complexes and marking it for nuclear export, thus allowing cell cycle to progress (Kosugi *et al*., 2009; Wagner *et al*., 2009).

These examples show that Cdk1-controlled nuclear localization of various proteins takes place at different times in the cell cycle. This raises a question that which mechanisms govern the timing of these phosphorylation switches in the cell cycle. While previous studies have investigated the timing of degron phosphorylation by Cdk1 (Faustova *et al*., 2021; Örd, Möll, *et al*., 2019), the localization modules are expected to behave differently, as the phosphorylation and output is reversible in case of localization and irreversible in case of degradation. Also, while prior studies have focused on phosphorylation in the nucleus, nuclear shuttling depends on phosphorylation in both nucleus and cytoplasm.

2 THE AIMS OF THE THESIS

Cdk1 controls the phosphorylation of hundreds of proteins in a timely-resolved manner, leading to a question what parameters determine the dynamics of Cdk1-regulated switches. The timing of CDK phosphorylation events has been studied using phosphorylation-activated protein degradation as the output. While degradation is an irreversible output, most CDK phosphorylation events, including those that regulate protein localization, are likely reversible. We set out to investigate how changes into CDK specificity determinants affect the phosphorylation of a nuclear localization module to gain an insight into the dynamic regulation of protein localization. We used a localization module from Psy4 that contains a bipartite NLS and six CDK phosphorylation sites as a model system.

The aims of the thesis are:

- To study the impact of inactivating different phosphorylation sites in the Psy4 localization module.
- To analyse how threonine-to-serine mutations at phosphorylation sites affect the localization and phosphorylation dynamics of the Psy4 module in the cell cycle.
- To investigate the phosphorylation of CDK sites in Psy4 in G1-arrested cells.

3 EXPERIMENTAL PART

3.1 MATERIALS AND METHODS

3.1.1 DNA cloning

The materials used in DNA cloning are described in **Table 1** and the plasmids used in the study are characterized in **Table 2**. The restriction enzyme cutting sites and the desired mutations to phosphorylation sites were introduced with the primers during PCR, followed by restriction digestion of the PCR product with SalI and EcoRI. Inserts were cloned to pRG203MX-based vector, which contained *ACT1* promoter upstream from the insert and green fluorescent protein coding sequence for C-terminal tagging of the NLS-NES module. Resulting plasmids were isolated and amplified by transformation to competent *E. coli* Turbo cells, purified and then integrated into the yeast genome by homologous recombination.

Table 1. Materials used in DNA cloning

Nr.	Materials	Components
1	Competent Turbo *Escherichia coli* cells	Competent *E. coli* Turbo (New England Biolabs)
2	Luria-Bertani media (LB) media	10 g/L Sodium Chloride (Chempur), 10 g/L Tryptone (Formedium), 5 g/L Yeast Extract (Formedium)
3	LB agar plates with ampicillin	LB media, 100 µg/mL ampicillin (Fisher bioreagents)
4	1% or 2% agarose TAE gel	1% or 2% agarose, 40 mM Tris-Acetate pH 8.3, 4 µL/mL Atlas ClearSight DNA stain (BioAtlas), 1 mM ethylenediaminetetraacetic acid (EDTA)
5	TAE buffer	40 mM Tris-Acetate pH 8.3, 1 mM EDTA

Table 2. Plasmids used in the study

Nr.	Plasmid	Backbone	Promoter	Description	Tag	Source
1	pNLS 86	pRG203MX	ACT1	Psy4(315-441 wild type (wt))	sfGFP	Ilona Faustova/ Mihkel Örd
2	pNLS 97			Psy4(315-441 T347A)		
3	pNLS 123			Psy4 315-441 T320A T347A		
4	pNLS 146			Psy4(315-441 S364A S409A S434A)		
5	pNLS 199			Psy4(314-441 AP)		
6	pNLS 206			Psy4(315-441 T320S T347S S364A S409A S434A)		
7	pNLS 211			Psy4(315-441 AP T320)		
8	pNLS 212			Psy4(315-441 AP S320)		
9	pNLS 248			Psy4(315-441 T320S T347A)		This study

3.1.1.1 PCR

PCRs were done using oligonucleotides from Integrated DNA Technologies and Phusion High-Fidelity DNA Polymerase from Thermo Scientific. Reactions were performed with the mixture and program showed in **Tables 3** and **4**. The PCR products were loaded on 1% TAE agarose gel and separated by gel electrophoresis to verify and isolate the DNA fragments. PCR products were extracted from gel and purified with Favorgens's FavorPrep GEL/PCR purification kit as stated in manufacturers instruction.

Table 3. PCR mixture

Reagent	Volume
5x Phusion HF buffer	10 µL
Forward + Reverse primers 10 µM	1.5 + 1.5 µL
Template plasmid DNA ~5 ng/µL	1 µL
dNTPs 25 mM	0.5 µL
Phusion DNA polymerase	0.5 µL

Table 4. PCR program

Step	Temperature	Time	Repeats
Initial denaturation	98 °C	5 m	
Denaturation	98 °C	15 s	32
Annealing	Tm (calculated from length and composition of the primer) °C	20 s	
Extension	72 °C	30 s per 1 kb	
Final extension	72 °C	5 min	

3.1.1.2 Restriction digestion

Both the PCR product and the vector were restricted with SalI and EcoRI to later ligate the insert into the vector. The DNA was restricted with Thermo Fisher's FastDigest enzymes in compliance with the manufacturer's instructions. The mixtures for restrictions are presented in **Tables 5** and **6**.

Table 5. Vector restriction

Compound	Volume
10x FastDigest Green buffer	2 µL
Vector	1500 ng
Enzymes (SalI and EcoRI)	1 µL + 1 µL
FastAP (Thermo Fisher Alkaline phosphatase)	0.5 µL
MQ H_2O	Up to 20 µL

Table 6. PCR product restriction

Compound	Volume
10x FastDigest buffer	2 µL
PCR product	8 µL
Enzymes (SalI and EcoRI)	1 µL + 1 µL
MQ H_20	6.5 µL

The restriction mixtures were incubated at 37 °C for 30 minutes. After incubation, vector was loaded into 1% TAE agarose gel, the fragments were separated by electrophoresis, cut out and purified with Favorgen's FavorPrep GEL/PCR Purification Kit. The PCR product restriction mixture was placed into a thermostat to heat inactivate the enzymes, according to manufacturer's instructions.

3.1.1.3 Ligation

Digested fragments were mixed in 3:1 insert:vector molar ratio in the ligation mixture presented in **Table 7**. Ligation mixtures were kept at 18 °C for at least one hour and then transformed to competent *E. coli* cells.

Table 7. Ligation mixture.

Compound	Volume
10x T4 DNA ligase buffer	1 µL
Insert	3 µL
Vector ~50 ng	1 µL
T4 DNA ligase (Thermo Fisher)	0.5 µL
MQ H_20	4.5 µL

3.1.1.4 Bacterial transformation

For isolation and purification of the correct plasmids, the ligations were transformed into competent *E. coli* turbo cells, provided by New England Biolabs. Transformation procedure was conducted as follows:

1. Cells were taken from -80 °C storage and thawed on ice
2. 2 µl of ligation was mixed with 50 µL of the cells
3. After adding DNA to cells they were incubated for 30 minutes on ice
4. Then, the cells were heatshocked for 30 seconds at 42 °C, followed by placing the mixture on ice for 5 minutes
5. Next, 500 µL of LB media was added to the transformation mixture
6. Then the mixture was incubated at 37 °C under constant shaking at 200 rpm for 45 minutes
7. The cells were spinned down by centrifugation at 6000 rpm for 1 minute
8. After centrifugation 400 µL of the media was removed and cells were resuspended in the remaining 100 µL of media
9. The cells were plated out on LB agar plates with ampicillin and left at 37 °C to incubate overnight.

3.1.1.5 Plasmid purification

After overnight incubation, colonies from the transformation plates were placed to grow in 5 mL LB media with ampicillin at 37 °C with constant shaking at 200 rpm for 6 to 16 hours. After the cultures had grown enough, the plasmids were puruifed with Favorgen's FavorPrep Plasmid DNA Extraction Mini Kit accoridng to manual provided with the kit.

After purification the plasmids were analysed for correct assembly and sequence by Sanger sequencing in the Institute of Genomics Core Facility.

3.1.2 Yeast transformation

Table 8. Yeast strains used in this study.

Nr.	Strains	Genotype	Source
1	MO571	*bar1Δ::HISG Padh1::Padh1-Mcm2/3 NLS-NES-mCherry::TRP1 his3::Pact1-Psy4(315-441 WT)-sfGFP::HIS3*	Ilona Faustova/Mihkel Örd
2	MO586	*bar1Δ::HISG Padh1::Padh1-Mcm2/3 NLS-NES-mCherry::TRP1 his3::Pact1-Psy4(315-441 WT)-sfGFP-6HA-naNT2::HIS3*	Ilona Faustova/Mihkel Örd
3	MO599	*bar1Δ::HISG Padh1::Padh1-Mcm2/3 NLS-NES-mCherry::TRP1 his3::Pact1-Psy4(315-441 T347A)-sfGFP::HIS3*	Ilona Faustova/Mihkel Örd
4	MO625	*bar1Δ::HISG Padh1::Padh1-Mcm2/3 NLS-NES-mCherry::TRP1 his3::Pact1-Psy4(315-441 T320A T347A)-sfGFP::HIS3*	Ilona Faustova/Mihkel Örd
5	MO646	*bar1Δ::HISG Padh1::Padh1-Mcm2/3 NLS-NES-mCherry::TRP1 his3::Pact1-Psy4(315-441 AP T320 T347)-sfGFP::HIS3*	Ilona Faustova/Mihkel Örd
6	MO744	*bar1Δ::HISG Padh1::Padh1-Mcm2/3 NLS-NES-mCherry::TRP1 his3::Pact1-Psy4(315-441 AP)-sfGFP::HIS3*	This study
7	MO762	*bar1Δ::HISG Padh1::Padh1-Mcm2/3 NLS-NES-mCherry::TRP1 his3::Pact1-Psy4(315-441 AP T320S T347S)-sfGFP::HIS3*	Ilona Faustova/Mihkel Örd

8	MO854	*bar1Δ::HISG Padh1::Padh1-Mcm2/3 NLS-NES-mCherry::TRP1 his3::Pact1-Psy4(315-441 AP T320 T347)-sfGFP::HIS3 swe1::URA3 clb5::CLB2*	This study
9	MO855	*bar1Δ::HISG Padh1::Padh1-Mcm2/3 NLS-NES-mCherry::TRP1 his3::Pact1-Psy4(315-441 AP T320S T347S)-sfGFP::HIS3 swe1::URA3 clb5::CLB2*	
10	MO856	*bar1Δ::HISG Padh1::Padh1-Mcm2/3 NLS-NES-mCherry::TRP1 his3::Pact1-Psy4(315-441 AP T320 T347)-sfGFP-6HA-naNT2::HIS3*	
11	MO857	*bar1Δ::HISG Padh1::Padh1-Mcm2/3 NLS-NES-mCherry::TRP1 his3::Pact1-Psy4(315-441 AP T320S T347S)-sfGFP-6HA-naNT2::HIS3*	
12	MO859	*bar1Δ::HISG Padh1::Padh1-Mcm2/3 NLS-NES-mCherry::TRP1 his3::Pact1-Psy4(315-441 AP T320)-sfGFP-6HA-naNT2::HIS3*	
13	MO860	*bar1Δ::HISG Padh1::Padh1-Mcm2/3 NLS-NES-mCherry::TRP1 his3::Pact1-Psy4(315-441 AP T320S)-sfGFP-6HA-naNT2::HIS3*	This study
14	MO861	*bar1Δ::HISG Padh1::Padh1-Mcm2/3 NLS-NES-mCherry::TRP1 his3::Pact1-Psy4(315-441 AP T320 T347)-sfGFP-6HA-naNT2::HIS3 swe1::URA3 clb5::CLB2*	
15	MO862	*bar1Δ::HISG Padh1::Padh1-Mcm2/3 NLS-NES-mCherry::TRP1 his3::Pact1-Psy4(315-441 AP T320S T347S)-sfGFP-6HA-naNT2::HIS3 swe1::URA3 clb5::CLB2*	
16	MO863	*bar1Δ::HISG Padh1::Padh1-Mcm2/3 NLS-NES-mCherry::TRP1 his3::Pact1-Psy4(315-441 T320S T347A)-sfGFP::HIS3*	

Table 9. Materials for yeast transformation

Nr.	Materials	Components
1	Yeast extract, peptone, dextrose media (YPD) media	20 g/L Glucose, 20 g/L Peptone (Formedium), 10 g/L Yeast Extract (Formedium)
2	1x Tris-EDTA buffer (TE buffer)	10 mM Tris-hydrochloride (Tris-HCI) pH 8, 1 mM EDTA
3	PL1 buffer	0.5xTE buffer, 100 mM Lithium Acetate (LiAc)
4	PL2 buffer	0.5xTE buffer, 40% Polyethylene glycol (PEG) 3350, 100 mM LiAc
5	YPD plates	20 g/L Bacto agar (Formedium), YPD media
6	Synthetic complete media without histidine (SC-HIS plates)	Yeast Nitrogen Base w/o amino acids 7 g/L (BD Biosciences), Glucose 20 g/L, Agar 14 g/L, -HIS dropout according to manufacturer's instructions (MP Biomedicals), 1% ADE/TRP
7	YPD + nourseothricin (clonNAT) plates	20 g/L Glucose, 20 g/L Peptone (Formedium), 10 g/L Yeast Extract (Formedium), Agar 14 g/L 1% ADE/TRP, 100 ug/mL

To analyze the effect of different mutations in the NLS-NES modules, the plasmids were next trasformed into yeast, where the expression construct integrated into the genome via homologous recombination. Before transformation, 500-1000 ng of the pRG203MX-based plasmids were linerised with FastDigest SgsI (Thermo Fisher) to create the homologous DNA ends with yeast genome. The yeast strains used in the study are presented in **Table 8**. The materials used for yeast transformation are shown in **Table 9**. The protocol used for yeast transformation is presented below:

1. Yeast strains were grown in 25 mL of YPD (for one transformation) at 30 °C, shaking set to 160 rpm, until optical density at 600 nm (OD) of 0.4 to 0.8.
2. Cells were collected by centrifugation at 3200 rpm for 1 minute.
3. The pellet formed by centrifugation was resuspended in 1 mL of PL1 buffer.
4. Then, the cells were centrifuged again at 3200 rpm for 1 minute.

5. After centrifugation the buffer was removed, cells were resuspended in two times the cell volume of PL1, and left to incubate for 10 minutes at room temperature.
6. At the same time, Salmon sperm DNA solution (SS DNA), 5 mg/mL, was boiled at 100 °C for 10 minutes to ensure it is single stranded, and after heating the SS DNA was cooled down on ice.
7. 10 µL of the SgsI-restricted plasmid was mixed with 10 µL of SS DNA followed by addition of 100 µL of cells/PL1 mixture.
8. Then 700 µL of PL2 buffer and 48 µL of dimethyl sulfoxide (DMSO) were added to the solution and the solution was mixed well.
9. The transformation mixture was then incubated at 42 °C for 40 minutes, after which the cells were chilled on ice.
10. The cells were spinned down by centrifugation at 3200 rpm for 1 minute.
11. Supernatant was removed, cells were resuspended in 1 mL 1xTE and centrifuged again with the same parameters.
12. Buffer was removed again, cells were resuspended in 1xTE, plated on SC - HIS/glucose selection plates and left in 30 °C incubator for 48 hours.

3.1.3 Time-lapse fluorescence microscopy

Table 10. Materials used in time-lapse microscopy experiments.

Nr.	Materials	Componets
1	Complete supplement mixture (CSM) media with 2% glucose	20 g/L glucose (Oriola, 0.79 g/L CSM powder (Formedium), 7 g/L yeast nitrogen base without amino acids (BD Biosciences),
2	2% agarose/glucose or agarose/glucose/α-factor gel	10 g/L CSM (Formedium), 7 g/L yeast nitrogen base without amino acids (BD Biosciences), 20 g/L glucose (Oriola), 2% NuSieve GTG agarose (Thermo Fisher), 1 µg/mL α-factor (if needed)

The yeast strains obtained from the transformation were analyzed in microscopy experiments. Single colonies from the SC-HIS/glucose plates were streaked on a new SC-HIS/glucose plate and later used to inoculate 3 mL of 2% CSM media with 2% glucose and were set to grow at 30 °C with 160 rpm for 4-8 hours untill they reached OD 0.6.

Then, 0.5 µL of the culture was pipetted onto a 0.08 mm thick cover glass (24x50 mm), covered with 1 mm thick 2% agarose gel pieces (made with CSM with 2% glucose (**Table 10**)), which were in turn covered with a smaller 20x20 mm cover glass to prevent the gels from drying. Finally, the assembly was covered with a plastic container that further prevents the agar pieces from drying out.

The assembled sample was placed onto Zeiss Axio Observed Z1 microscope with 63x/1.4 Oil M27 Plan-Apochromat objective and Axiocam 506 mono camera. Time-lapse imaging was performed using ZEN automated software with8 hours for experiment duration and 3-minute intervals between the time points. Definite focus was used to keep the images in focus throughout the experiment. The fluorescent proteins sfGFP and mCherry were excited by 470 LED and 540-580 LED Colibri modules, respectively, at 25% power. The exposure times were set at 15 ms for sfGFP and 450 ms for mCherry and the filter set 61 HE (Zeiss) was used. In addition to the fluorescence images, also a phase contrast image was taken at each time point. Temperature of the sample was kept constant at 30 °C using TempControl 37-2 (Pecon).

Segmentation, tracking and quantification of the cells was done using The MathWorks Inc. software MATLAB and custom-made scripts described in (Doncic *et al*., 2013; Örd, Möll, *et al*., 2019a). In the analysis, the phase contrast image was used to locate and segment the cells, followed by quantification of the nuclear and cytoplasmic signals of sfGFP- and mCherry-tagged proteins from the fluorescence images. Next, individual cells were synchronized at G1/S transition, detected by the time when 50% of Mcm2/3-NLS-NES-mCherry is exported from the nucleus. The mean nuclear fluorescence with SEM error bars of a population of cells over the duration of the cell cycle is plotted.

To analyze the nuclear accumulation of Psy4 NLS-NES module in G1 phase, the microscopy sample was prepared as described above, with the addition that 1 µg/mL α-factor was added to the CSM glucose agar used for the experiment. These time-lapse experiments were ran for 4 hours. During the analysis, the cells were synchronized at the point of 50% nuclear entry of the Mcm2/3-NLS-NES-mCherry sensor, marking the time of entry into G1 phase.

3.1.4 6 HA tagging for western blotting

To directly monitor Psy4 NLS-NES module phosphorylation, the module was tagged with 6HA epitope tag in the microscopy strains. The 6HA tag together with natNT2 selection marker was PCR-amplified from a template (pYM17 (Janke *et al.*, 2004)) with the PCR mixture and program shown in **Tables 3** and **4**. The PCR primers contained homologous ends with the Psy4 expression vector, so that the 6HA tag would integrate C-terminally of sfGFP in the same reading frame. The obtained DNA fragments were separated on 1% agarose TAE gel and purified. After purification the PCR products were transformed into yeast accourding to the same yeast transformation protocol as shown in chapter 3.1.2 but 40 µL of DNA was taken. After transformation, the cells were plated on YPD plates, left overnight at room temperature, next day replica plated onto YPD+clonNAT plates and placed into 30 °C incubator for 2 days. The integration of 6HA tag was confirmed by PCR.

3.1.5 Western blot

Table 11. Materials used for Western blotting.

Nr.	Materials	Components/Recipe
1	Urea lysis buffer	8M Urea (Sigma), 2M Thiourea (Sigma), 4% CHAPS (Sigma), 1% DTT (Sigma), 50 mM NaF, 89 mM beta-glycerol phosphate (BGP), 20 mM Tris pH 7.4, 1 mM Na_3VO_4
2	Phos-tag sodium dodecyl sulfate polyacrylamide gel electrophoresis (SDS-PAGE)	Separating gel : 8% polyacrylamide, 375 mM Tris-HCI pH 8.8, Phos-tag 50 µM, 100 µM $MnCl_2$, 0.1% SDS , 0.1% APS , 0.006% TEMED Stacking gel: 15% polyacrylamide, 125 mM Tris-HCI pH 6.8, 0.1% SDS, 0.1% APS , 0.01% TEMED
3	6xSDS loading buffer	12% SDS (Sodium Dodecyl Sulphate), 50% Glycerol, 0.06% Bromophenol blue
4	Semi-dry transfer buffer	192 mM glycine, 25 mM Tris-HCI, 0.1% SDS
5	1xTBS-T buffer	150 mM NaCl, 20 mM Tris-HCI, 0.1% Tween20 (Biomed)
6	Blocking solution	1xTBS-T buffer, 5% fat-free milk powder (BurËnka Inc.)
7	Primary antibody solution	1xTBS-T buffer, 3% milk powder (BurËnka Inc.), 1:500 anti-HA.11-antibody (clone 16B12, BioLegend Cat. No. 901501)
8	Secondary antibody solution	1xTBS-T buffer, 3% milk powder (BurËnka Inc.), 1:7500 HRP-conjugated anti-mouse IgG antibody (LabAS)

3.1.5.1 Western Blot sample preparation

Yeast cultures were diluted to OD 0.07 into 3x5 ml of YPD and grown for 3-5 hours to reach OD 0.3 - 0.4.

After the samples had reached the required OD they were exposed to three different conditions:

- G1 phase arrest by addition of 1 μg/mL of α-factor to the culture, followed by growing the cultures for 2.5 hours.
- S phase arrest by addition of 200 mM hydroxyurea (HU), followed by 2 hours of growth.
- M phase arrest with nocodazole (NOC). First, 1% DMSO added to the cultures, followed by incubation for 30 minutes and addition of 20 μg/mL of nocodazole. The samples were then grown for another 2 hours.

To collect the cells, the cultures were centrifuged at 3200 rpm for 1 minute. The media was poured away, the tubes were dried with tissue paper, the samples were frozen in liquid nitrogen and stored in -80 °C freezer.

3.1.5.2 Western blot procedure

The cell pellet was resuspended with 200 μL of urea lysis buffer (**Table 11**). Silica beads were placed in 1.5 mL centrifuge tubes and the cell suspension was moved to that tube. Samples were then placed into a FastPrep-24 homogenizer (MP Biomedicals) for 40 seconds at 4 m/s to break the cells. The lysates were then centrifuged for 10 minutes at 13200 rpm. The supernatant was transferred to new tubes. The total protein concentrations in the lysates were measured with Bio-Rad Protein assay dye (Biorad). For this, 200 μL of the diluted dye was pipetted into the wells of 96-well plate. 2 μL of each sample was added and then the absorbance of the dye at 595 nm wavelength was measured with Sunrise microplate reader and Magellan software (Tecan Life Sciences). Based on the measurements, an equal amount of total protein was loaded to SDS-PAGE gels. The samples were mixed with 2x SDS sample buffer supplemented with 1 mM $MnCl_2$, followed by heating for 5 minutes at 72 °C. 8% polyacrylamide SDS-PAGE gels supplemented with 50 μM Phos-tag and 100 μM $MnCl_2$ were used. SDS-PAGE electrophoresis ran for 1.5 hours with constant current of 15 mA per gel. Next, the gel was soaked in Semi-dry transfer buffer supplemented with 10 mM EDTA for 2x15 minutes and then for 5 minutes in Semi-dry transfer buffer. Four pieces of

filter paper and the nitrocellulose membrane were soaked in Semi-dry transfer buffer for at least 15 minutes. The transfer sandwiches were assembled in the following way: first two pieces of filter paper on the anode, then the membrane, gel, and finally two pieces of filter paper. Transfer was carried out using standard semi-dry program in Pierce G2 Fast Blotter (Thermo Scientific). After the transfer, the membrane was placed into blocking solution for one hour with gentle agitation. After blocking the membrane was rinsed with TBS-T solution and placed into primary antibody solution for one hour with gentle agitation. Then, the membrane was washed with TBS-T for 15 minutes with intense shaking followed by 3x5 minutes of washing with TBS-T. The membrane was then placed into secondary antibody solution for 30 minutes also with gentle agitation. The membrane was washed again with TBS-T for 15 minutes with intense shaking followed by 3x5 minutes of washing with TBS-T. The SuperSignal West Pico PLUS Chemiluminescent Substrate (Thermo Fisher Scientific) was used for detection. The membrane was covered with the chemiluminescent solution and wrapped in plastic. Then AGFA Medical Xray film blue was exposed to the membrane, after which the film was developed in G150 AGFA developer, washed in water, and fixed with AGFA G354 fixer. Finally, film was washed with water, dried and scanned.

3.2 RESULTS AND DISSCUSION

Control of NLS and NES by phosphorylation is important for regulation of protein signaling and is tightly connected to regulation of cell cycle proteins. The shuttling of over 30 cell cycle proteins between the nucleus and cytoplasm is controlled by CDK (Kosugi *et al*., 2009). While detailed studies on the parameters that determine the phosphorylation timing of degrons have been published (Faustova *et al*., 2021; Örd, Möll, *et al*., 2019a), it can be expected that localization modules will behave differently, because localization is a reversible output that depends on phosphorylation in multiple cellular compartments. In this thesis, the CDK specificity determinants in Psy4 NLS-NES nuclear localization module are manipulated, followed by analysis of the effect of these mutations on localization and directly on phosphorylation.

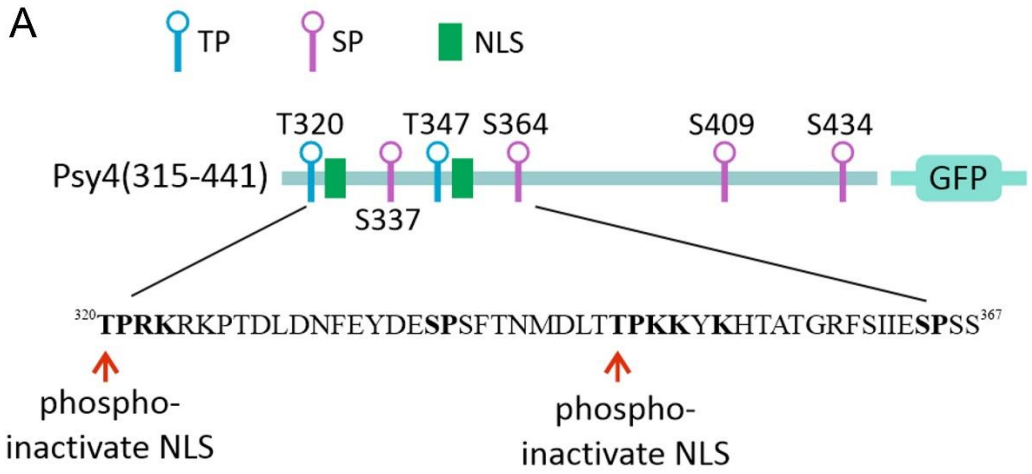

Figure 9. Scheme showing the C terminus (positions 315-441) of Psy4. The region contains six CDK consensus phosphorylation sites and a bipartite NLS that is flanked by T320 and T347, whose phosphorylation inactivates the NLS (Kosugi *et al*., 2009).

The Psy4 NLS-NES module (the intrinsically disordered C terminus of Psy4, positions 315-441, **Figure 9**) was used as a model for CDK-regulated bipartite NLS. Psy4 contains a bipartite NLS, where both NLS parts have a CDK phosphorylation site (T320 and T347) N-terminal of the NLS. Phosphorylation of these sites is known to inactivate the NLS, causing nuclear exit of Psy4 (Kosugi *et al*., 2009). The dynamics of this regulation and the function of four additional minimal consensus CDK phosphorylation sites in Psy4 are not known.

3.2.1 Ser/Thr mutations could impact multiple mechanisms

Previous studies have shown that mutation of T320 and T347 to alanine abolishes the nuclear exit of Psy4 in the cell cycle (Kosugi *et al.*, 2009), but the effects of single site mutations or the impact of mutations that affect CDK specificity have not been described. We used time-lapse fluorescence microscopy to study the localization dynamics (**Figure 10A**). For this, we transformed Psy4 NLS-NES-GFP expression constructs to a yeast strain that is expressing the Mcm2/3 NLS-NES-mCherry cell cycle reporter protein.

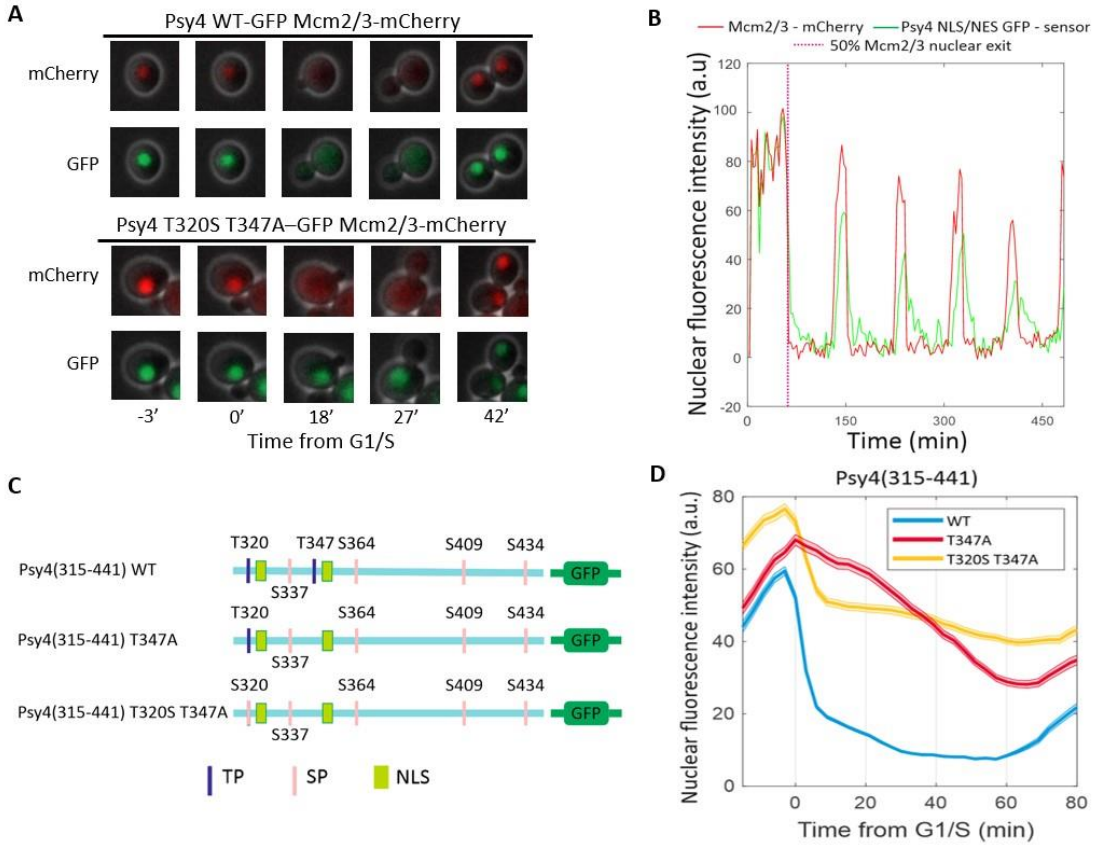

Figure 10. The complex effect of Thr/Ser mutation at position 320. (A) Image**s** showing example of time series acquired from microscopy experiments. (B) Example of the oscillations of nuclear levels of Psy4 NLS/NES-GFP and Mcm2/3-mCherry in a single cell over five cell cycles. For further analysis, individual cells were synchronized at the 50% nuclear exit of Mcm2/3-mCherry. (C) Schemes showing the Psy4 mutants used in the experiment presented in panel 'D'. (D) Time-lapse microscopy analysis of nuclear fluorescence intensities of the indicated Psy4(315–441)- GFP constructs. Values are average of a population of cells. Error bars are +/- S.E.M.

The Mcm2/3-based reporter that is exported from the nucleus at G1/S and is imported back in anaphase was used here as a reference point for G1/S to synchronize the cells during the analysis (**Figure 10B**) (Örd, Venta, *et al*., 2019). First, we compared the wild type Psy4 module and a mutant with T347 site disabled by mutation to alanine (**Figure 10C**). Time-lapse microscopy revealed that the majority of wild type Psy4 module was exported rapidly around the time of G1/S, followed by a period of slower nuclear exit and nuclear accumulation at around 60 minutes after G1/S, at which point the cells have reached anaphase (**Figure 10D**). Disabling the T347 site led to Psy4 being exported gradually over the cell cycle, with some nuclear fraction even in mitotic cells (**Figure 10D**). This suggested that T347 site is a major site that controls nuclear export, but its mutation does not cause complete loss of nuclear exit. The gradual exit profile of the T347A mutant indicates that this mutant is highly sensitive to CDK activity and therefore it could be a suitable background to study the effect of mutations that affect the CDK specificity of the module. Next, we mutated T320 to serine in the T347A background (**Figure 10C**). Interestingly, the T320S T347A mutant had very different localization dynamics, as it was rapidly partially exported in G1/S, followed by a very slow decline in nuclear levels during the rest of the cell cycle (**Figure 10D**). The T320S mutation is expected to affect three mechanisms: 1) Cdk1 preferentially phosphorylates serines; 2) PP2A-Cdc55, the major phosphatase that counteracts Cdk1, preferentially dephosphorylates threonines; 3) Cks1 only binds phosphotreonines (Godfrey *et al*., 2017; Kõivomägi *et al*., 2013; Örd, Möll, *et al*., 2019a; Suzuki *et al*., 2015). The T320S mutation is expected to enhance nuclear exit due to the first two mechanisms but decrease exit due to the loss of Cks1 binding, which could reduce phosphorylation of additional sites. This suggests that the initial gain in exit rate at G1/S compared to T347A mutant, is from increased phosphorylation at 320. Interestingly, the nuclear levels of T320S T347A mutant in later phases of the cell cycle are higher than those of T347A mutant, indicating Cks1-mediated phosphorylation of the minimal consensus sites (S364, S409, S434, **Figure 10C**) could be necessary for efficient exit of the module. The different localization dynamics of these three constructs show how different multisite phosphorylation clusters can have very different response dynamics to the changes in CDK activity during the cell cycle. This highlights the importance of detailed examination of the CDK specificity mechanisms.

3.2.2 Thr-to-Ser mutations have a profound impact phosphorylation efficiency

While time-lapse microscopy enables precise analysis of the phosphorylation-controlled localization changes, it does not directly show phosphorylation of different sites, because the impact of different phosphorylation events on localization can be different. To get a more direct view on the effect of Thr-to-Ser mutations on phosphorylation dynamics of these sites, we conducted western blotting with several Psy4 NLS-NES variants. To simplify the phosphorylation analysis, we decreased the number of phosphorylation sites in the module. We created constructs with S320 or T320 as the only CDK site (AP T320 and AP S320, where all other CDK consensus sites are mutated to alanine) (**Figure 11A**). We investigated phosphorylation of these constructs in cells arrested in different cell cycle phases. We used α-factor to arrest cells in G1 phase, hydroxyurea to arrest in S phase and nocodazole for M phase arrest. We used Phos-tag SDS-PAGE to separate 6HA-tagged Psy4 proteins based on phosphorylation.

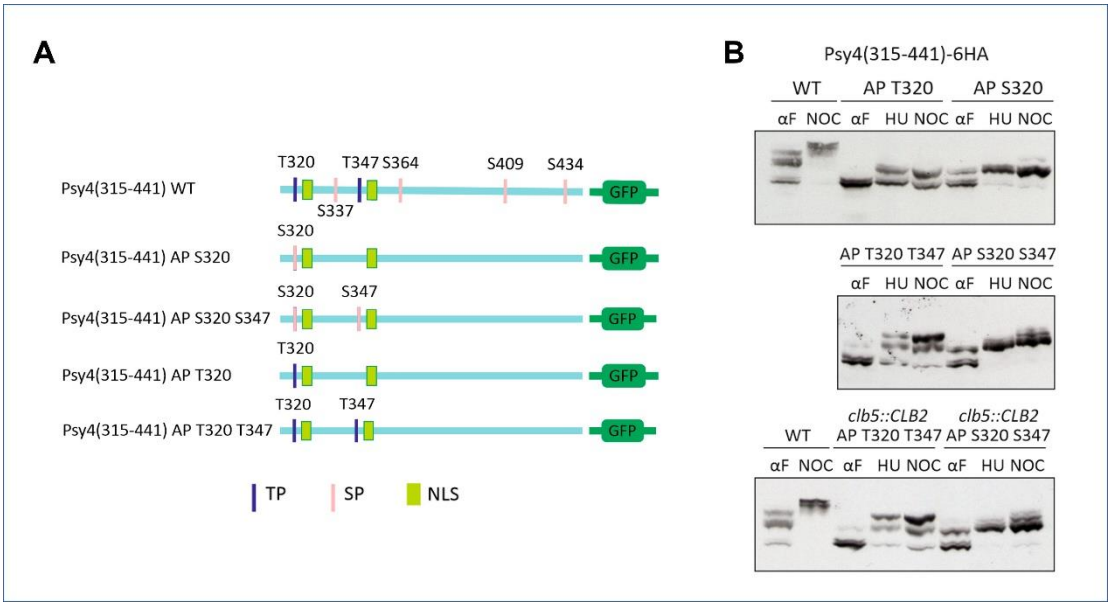

Figure 11. Low and delayed phosphorylation of TP sites compared to SP sites. (A) Schemes of the Psy4 variants used in western blots. (B) Phosphorylation of Psy4 modules was studied using Phos-tag SDS-PAGE western blotting of cell cultures synchronized with α-factor (αF), hydroxyurea (HU) or nocodazole (NOC). AP means that all CDK consensus sites apart from the ones shown are disabled. In *clb5::CLB2* strains *SWE1* was deleted and an additional copy of *CLB2* was expressed from *CLB5* locus.

The experiments revealed that wild type Psy4 module was partially phosphorylated in G1 phase, but much higher phosphorylation was observed in M phase (**Figure 11B**). Psy4 AP T320 was not phosphorylated in G1 phase, but it was partially phosphorylated in S and M phases. Interestingly, a similar module but with serine in the same position showed a very different behavior, as S320 was partially phosphorylated already in G1 and fully phosphorylated in S and M phases. This difference indicates that phosphorylation of T320 occurs later in the cell cycle and requires more Cdk1 activity compared to S320.

We also investigated the phosphorylation of Psy4 modules with T320 and T347 or S320 and S347 as the only two CDK consensus sites (AP T320 T347 and AP S320 S347, **Figure 11A**). Psy4 AP T320 T347 followed the same pattern of phosphorylation as AP T320, although it was more phosphorylated in M phase (**Figure 11B**). The profound impact of Thr-to-Ser mutations was also apparent in these constructs, as AP S320 S347 was efficiently multiphosphorylated already in S phase. These two constructs further suggest that serines require less Cdk1 activity than threonines for phosphorylation.

To test the sensitivity of T320 and T347 to Cdk1 activity, we studied the phosphorylation of Psy4 AP T320 T347 and AP S320 S347 in a strain with increased Cdk1 activity. In this strain, an extra copy of mitotic cyclin *CLB2* gene is introduced into S phase cyclin *CLB5* locus (*clb5::CLB2*). This leads to an increase in Cdk1 activity in S phase, as Clb2-Cdk1 has much higher intrinsic activity compared to Clb5-Cdk1 (Kõivomägi *et al*., 2011). Surprisingly, there was only a minor increase in phosphorylation of the AP T320 T347 module in S phase and the protein was not fully phosphorylated even in M phase (**Figure 11B**). The pattern of AP S320 S347 phosphorylation did not change, confirming that these sites are fully phosphorylated already in the wild type strain. The results of the phosphorylation analysis indicate that serines are phosphorylated to much greater extent at both 320 and 347 positions and shows that optimal threonine-based sites are not fully phosphorylated during the cell cycle even in *clb5::CLB2* cells that have higher than wild type Cdk1 activity.

The Cdk1 preference of serine over threonines is twofold (Örd, Möll, *et al*., 2019a), but the effect of the swap on phosphorylation is very strong (**Figure 11B**). This can be due to a significant preference of phospho-threonines by phosphatases, which has been found for PP2A-Cdc55, a key phosphatase that counteracts CDK activity (Godfrey *et al*., 2017).

3.2.3 Biphasic export profile of Psy4 modules with two phosphorylation sites

Next, we analyzed the Psy4 AP T320 T347 and Psy4 AP S320 S347 constructs in time-lapse microscopy. Interestingly, the AP T320 T347 mutant exited the nucleus in a step-wise manner, forming a ca 20-minute plateau after an initial drop in nuclear levels in G1/S, followed by another wave of increased exit around 30 minutes after G1/S (**Figure 12**). This exit profile is in contrast with the wild type Psy4 that contains additional minimal consensus sites S364, S409 and S434 and that was rapidly almost fully exported (**Figure 10D**). This indicates that the minimal consensus sites are important for the regulation of Psy4 localization module. Phosphorylation of these sites could affect the activity of a NES or it could inhibit the NLS via some additional mechanisms. The AP S320 S347 construct that was fully phosphorylated in S and M phases (**Figure 11B**), exited the nucleus rapidly at G1/S and to a much greater extent than AP T320 T347 **(Figure 12**). However, it remained more nuclear than the wild type Psy4, indicating that the additional minimal consensus sites are critical for efficient shuttling of Psy4 even when positions 320 and 347 are fully phosphorylated. Next, we analyzed these constructs in the *clb5::CLB2* strain with increased Cdk1 activity. AP T320 T347 exited the nucleus more rapidly in *clb5::CLB2* cells, further showing that threonine sites have higher phosphorylation thresholds (**Figure 12**). AP S320 S347, however, behaved in the same manner in both strains, confirming that serines are fully phosphorylated at G1/S, as this substrate is not sensitive to an increase in Cdk1 activity.

When compared to the rapid exit of the wild type Psy4 module and the gradual exit of T347A mutant, the two-step exit with an S phase plateau of the Psy4 AP T320 T347 module shows that different CDK targets can have very different response dynamics to the increasing CDK activity that drives the cell cycle progression. This provides several interesting insights into cell cycle regulation. First, the presence of a plateau indicates a rapid switch from low to high S phase CDK activity at G1/S, rather than a gradual increase in activity during the S phase. Secondly, the formation of a plateau suggests that an equilibrium in phosphorylation and dephosphorylation is reached in the AP T320 T347 mutant, in contrast to T347A mutant, where the equilibrium is not achieved in this time period and the sensor exits gradually. Interestingly, in AP T320 T347, the exit is dependent on phosphorylation of full consensus TP sites that are rapidly targeted both by Cdk1 and by phosphatase PP2A-Cdc55. In T347A, however, the gradual exit could be due to slow accumulation of phosphorylation at S364, S409 and S434, which are minimal consensus Cdk1 sites and

suboptimal PP2A-Cdc55 sites as they are serines. These differences indicate that the equilibrium is not reached rapidly for all CDK substrates. Finally, such plateaus were not observed in studies investigating the phosphorylation dynamics of phospho-degrons (Faustova *et al*., 2021; Örd, Möll, *et al*., 2019a). In case of degrons, different mutations had an effect on the timing of degradation in the cell cycle, but the degradation was always a gradual and one-step process. This could be because degradation is an irreversible output, so an equilibrium is not established. Taken together, these results illustrate the multitude of parameters that affect the dynamics of CDK substrate phosphorylation and highlight the importance of phosphatases and the output function in determining the phosphorylation threshold.

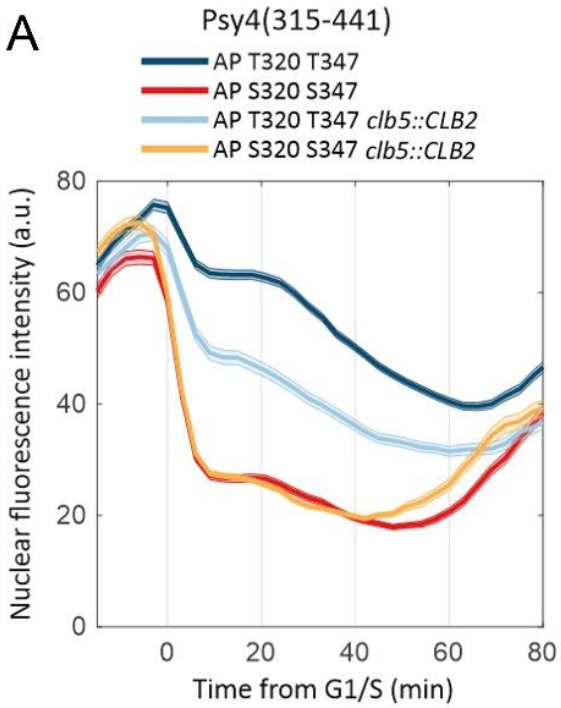

Figure 12. Mutation of S364, S409 and S434 causes biphasic export of the Psy4 module. Psy4 AP T320 T347 and AP S320 S347 have all sites except for 320 and 347mutated to alanine. In *clb5::CLB2* strains, *SWE1* is deleted and an additional copy of *CLB2* is expressed from the *CLB5* locus. Values are average of a population of cells. Error bars are +/- S.E.M.

3.2.4 Serines are phosphorylated in pheromone-induced G1 arrest.

Previous studies have shown that SP motifs can be phosphorylated in G1 phase to a greater extent than TP sites (Örd *et al*., 2019b; Venta *et al*., 2020). Here, partial phosphorylation of the Psy4-based sensors that contain SP sites was observed in G1 arrested cells, while T320 and T347 were not phosphorylated in these cells (**Figure 11B**). To study the effect of the S364, S409 and S434 phosphorylation on the localization dynamics in G1 phase, we investigated the nuclear accumulation of the module during entry into G1 phase in the presence of α-factor (**Figure 13A**). In the AP mutant the module accumulation into the nucleus was higher compared to Psy4 T320A T347A mutant, which had only S364, S409 and S434 sites (**Figure 13B, C**). This suggests that the C-terminal minimal consensus SP sites promote nuclear exit of the module also in G1 phase and even when T320 and T347 are mutated to alanine. Further, this indicates that these sites are partially phosphorylated by other kinases during G1 phase, as Cdk1 is inactive in pheromone-arrested cells (Gartner *et al*., 1998). Pheromone leads to activation of the mitogen-activated protein (MAP) kinase signaling pathway that contains proline-directed kinases, which could target the same phosphorylation sites as CDKs (Bardwell, 2004). In contrast to CDKs, however, MAP kinase activity results in cell cycle arrest. The data presented here indicates that the TP sites T320 and T347 could act as a specificity filter for kinase signaling, in contrast to the SP sites. The increased kinase activity threshold for threonine phosphorylation likely emerges from higher phosphatase specificity towards phospho-threonines over phospho-serines (Godfrey *et al*., 2017). Thus, in addition to affecting the timing of phosphorylation during the cell cycle, the Thr-to-Ser mutations can affect the phosphorylation specificity and input from other kinases.

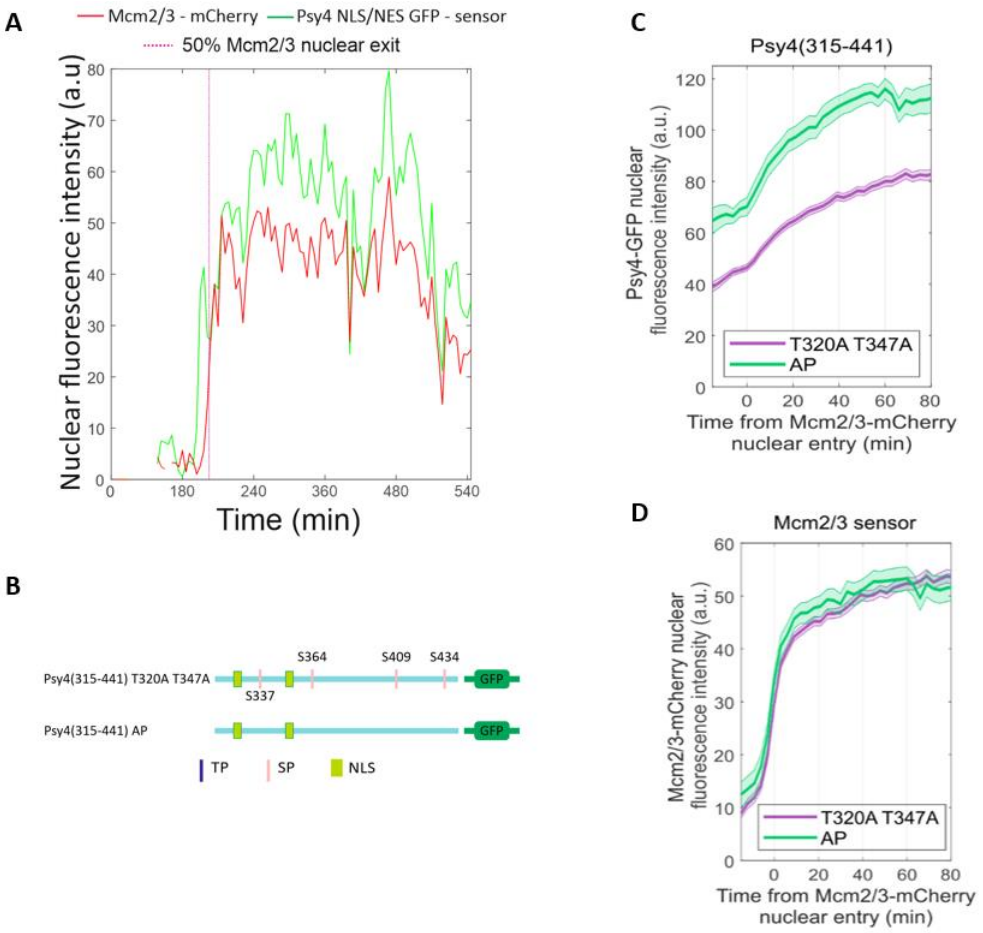

Figure 13. S364, S409 and S434 affect Psy4 nuclear levels also in G1 phase. (A) Example of the fluorescence microscopy data of a single cell. For analysis presented in panels 'C' and 'D', single cells were synchronized at the 50% nuclear entry of Mcm2/3-mCherry, which marks the entry into G1 phase. (B). Psy4 mutants used in panels 'C' and 'D'. (C) The nuclear levels of the indicated Psy4 NLS-NES modules in cells arrested in G1 phase with α-factor. (D) Plot showing the nuclear levels of Mcm2/3-NLS-NES-mCherry reporter in the cells expressing the indicated Psy4 construct. The values in panels 'C' and 'D' are average of a population of cells. Error bars are +/- S.E.M.

SUMMARY

In this work we studied the impact of different phosphorylation site mutations on the localization dynamics of a Cdk1-regulated nuclear localization NLS-NES module from Psy4 using time-lapse fluorescence microscopy. Phosphorylation of Psy4 module at T320 and T347 causes inactivation of the NLS and nuclear exit of the module. However, the dynamics and the functions of four additional sites in the module had not been characterized previously.

We found that mutations of different phosphorylation sites to alanine or mutations of Thr-to-Ser had a profound impact on the nuclear exit dynamics of the localization module during the cell cycle. While the wild type module exited the nucleus rapidly at G1/S transition, the T347A mutant exited gradually over the whole cell cycle. When additionally, to T347A mutation T320 was mutated to serine, the localization module was rapidly partially exported at G1/S, followed by a stable plateau and higher nuclear levels in mitosis compared to T347A mutant. This suggested that the Thr-to-Ser mutations can affect multiple mechanisms in different ways. From one side, the preferences in kinase and phosphatase site specificity lead to increased phosphorylation of serines, On the other hand, only phospho-threonines can bind to Cks1, and thus Thr-to-Ser mutations can cause decreased phosphorylation of other sites.

The microscopy results indicated that phosphorylation of threonines is considerably delayed in the cell cycle. We performed Phos-tag western blotting to directly analyse phosphorylation. We confirmed that S320 and S347 are fully phosphorylated in S phase, whereas T320 and T347 remain partially phosphorylated even in M phase and in cells with increased Cdk1 activity. The extensive delay suggests that phosphatases play a major role in delaying threonine phosphorylation, as the kinase preference for serines is only twofold.

Next, we found that the module containing T320 and T347 as the only CDK sites exited the nucleus in a stepwise manner with a 20-minute plateau after G1/S. This indicates a rapid switch from low to high CDK activity at G1/S and that an equilibrium between CDK and phosphatase activity is reached. Interestingly, the gradual exit of T347A mutant indicates that no equilibrium is reached with that module. These results show that phosphoregulation by CDK is affected by many factors, illustrating the importance of phosphatases and the output function in determining the phosphorylation threshold and dynamics.

Finally, we analyzed the nuclear levels of different Psy4 modules in pheromone-arrested G1 phase cells, revealing that the serine-based sites in Psy4 can be phosphorylated by other kinases. This suggests a role for threonines as specificity filters, as the kinase activity threshold for threonine phosphorylation is higher. Thus, apart from affecting the timing of phosphorylation, Thr-to-Ser mutations can affect the phosphorylation specificity and input from other kinases.

Characterization of phospho-regulatable localization modules with different response dynamics to kinase activity creates a basis to use phosphorylation in synthetic signalling networks. These localization modules together with previously characterized phospho-controlled degradation modules make up a comprehensive phospho-processor toolbox. The modules are intrinsically disordered and consist of independent linear motifs, thus by fusing them with other proteins, the phospho-regulation can be transferred. These modules would enable dynamic control over protein stability or localization to fine-tune the protein activities in cell factories and other synthetic biology applications.

The results presented in this study are included in the manuscript in Appendix.

REFERENCES

Alberts, B., Johnson, A., Lewis, J., Morgan, D., Raff, M., Roberts, K., & Walter, P. (2017). Molecular Biology of the Cell. In *Molecular Biology of the Cell*. https://doi.org/10.1201/9781315735368

Andzelm, E. R., Lew, J., & Taylor, S. (1995). Bound to activate: conformational consequences of cyclin binding to CDK2. *Structure*, *3*(11). https://doi.org/10.1016/S0969-2126(01)00249-0

Bardwell, L. (2004). A walk-through of the yeast mating pheromone response pathway. In *Peptides* (Vol. 25, Issue 9). https://doi.org/10.1016/j.peptides.2003.10.022

Belanger, K. D., Yewdell, W. T., Barber, M. F., Russo, A. N., Pettit, M. A., Damuth, E. K., Hussain, N., Geier, S. J., & Belanger, K. G. (2022). Exportin Crm1 is important for Swi6 nuclear shuttling and MBF transcription activation in Saccharomyces cerevisiae. *BMC Molecular and Cell Biology*, *23*(1). https://doi.org/10.1186/s12860-022-00409-6

Bhaduri, S., & Pryciak, P. M. (2011). Cyclin-specific docking motifs promote phosphorylation of yeast signaling proteins by G1/S Cdk complexes. *Current Biology*, *21*(19). https://doi.org/10.1016/j.cub.2011.08.033

Blondel, M., Galan, J. M., Chi, Y., Lafourcade, C., Longaretti, C., Deshaies, R. J., & Peter, M. (2000). Nuclear-specific degradation of Far1 is controlled by the localization of the F-box protein Cdc4. *EMBO Journal*, *19*(22). https://doi.org/10.1093/emboj/19.22.6085

Bloom, J., & Cross, F. R. (2007). Multiple levels of cyclin specificity in cell-cycle control. In *Nature Reviews Molecular Cell Biology* (Vol. 8, Issue 2). https://doi.org/10.1038/nrm2105

Doncic, A., Eser, U., Atay, O., & Skotheim, J. M. (2013). An Algorithm to Automate Yeast Segmentation and Tracking. *PLoS ONE*, *8*(3). https://doi.org/10.1371/journal.pone.0057970

Enserink, J. M., & Kolodner, R. D. (2010). An overview of Cdk1-controlled targets and processes. In *Cell Division* (Vol. 5). https://doi.org/10.1186/1747-1028-5-11

Ercan, D. P., Chrétien, F., Chakravarty, P., Flynn, H. R., Snijders, A. P., & Uhlmann, F. (2021). Budding yeast relies on G1 cyclin specificity to couple cell cycle progression with morphogenetic development. *Science Advances*, *7*(23). https://doi.org/10.1126/sciadv.abg0007

Faustova, I., Bulatovic, L., Matiyevskaya, F., Valk, E., Örd, M., & Loog, M. (2021). A new linear cyclin docking motif that mediates exclusively S-phase CDK-specific signaling. *The EMBO Journal*, *40*(2). https://doi.org/10.15252/embj.2020105839

Gartner, A., Jovanovic´, A., Jovanovic´, J., Jeoung, D.-I., Bourlat, S., Cross, F. R., & Ammerer, G. (1998). Pheromone-Dependent G 1 Cell Cycle Arrest Requires Far1 Phosphorylation, but May Not Involve Inhibition of Cdc28-Cln2 Kinase, *In Vivo*. In *MOLECULAR AND CELLULAR BIOLOGY* (Vol. 18, Issue 7).

Godfrey, M., Touati, S. A., Kataria, M., Jones, A., Snijders, A. P., & Uhlmann, F. (2017). PP2ACdc55 Phosphatase Imposes Ordered Cell-Cycle Phosphorylation by Opposing Threonine Phosphorylation. *Molecular Cell*, *65*(3). https://doi.org/10.1016/j.molcel.2016.12.018

Heroes, E., Lesage, B., Görnemann, J., Beullens, M., van Meervelt, L., & Bollen, M. (2013). The PP1 binding code: A molecular-lego strategy that governs specificity. In *FEBS Journal* (Vol. 280, Issue 2). https://doi.org/10.1111/j.1742-4658.2012.08547.x

Hertz, E. P. T., Kruse, T., Davey, N. E., López-Méndez, B., Sigurðsson, J. O., Montoya, G., Olsen, J. v., & Nilsson, J. (2016). A Conserved Motif Provides Binding Specificity to the PP2A-B56 Phosphatase. *Molecular Cell*, *63*(4). https://doi.org/10.1016/j.molcel.2016.06.024

Janke, C., Magiera, M. M., Rathfelder, N., Taxis, C., Reber, S., Maekawa, H., Moreno-Borchart, A., Doenges, G., Schwob, E., Schiebel, E., & Knop, M. (2004). A versatile toolbox for PCR-based tagging of yeast genes: New fluorescent proteins, more markers and promoter substitution cassettes. *Yeast*, *21*(11). https://doi.org/10.1002/yea.1142

Jiménez, J., Ricco, N., Grijota-Martínez, C., Fadó, R., & Clotet, J. (2013). Redundancy or specificity? the role of the CDK Pho85 in cell cycle control. In *International Journal of Biochemistry and Molecular Biology* (Vol. 4, Issue 3).

Kataria, M., Mouilleron, S., Seo, M. H., Corbi-Verge, C., Kim, P. M., & Uhlmann, F. (2018). A PxL motif promotes timely cell cycle substrate dephosphorylation by the Cdc14 phosphatase. *Nature Structural and Molecular Biology*, *25*(12). https://doi.org/10.1038/s41594-018-0152-3

Kõivomägi, M., Örd, M., Iofik, A., Valk, E., Venta, R., Faustova, I., Kivi, R., Balog, E. R. M., Rubin, S. M., & Loog, M. (2013). Multisite phosphorylation networks as signal processors for Cdk1. *Nature Structural and Molecular Biology*, *20*(12). https://doi.org/10.1038/nsmb.2706

Köivomägi, M., Valk, E., Venta, R., Iofik, A., Lepiku, M., Balog, E. R. M., Rubin, S. M., Morgan, D. O., & Loog, M. (2011). Cascades of multisite phosphorylation control Sic1 destruction at the onset of S phase. *Nature*, *480*(7375). https://doi.org/10.1038/nature10560

Kõivomägi, M., Valk, E., Venta, R., Iofik, A., Lepiku, M., Morgan, D. O., & Loog, M. (2011). Dynamics of Cdk1 Substrate Specificity during the Cell Cycle. *Molecular Cell*, *42*(5). https://doi.org/10.1016/j.molcel.2011.05.016

Kosugi, S., Hasebe, M., Tomita, M., & Yanagawa, H. (2009). Systematic identification of cell cycle-dependent yeast nucleocytoplasmic shuttling proteins by prediction of composite motifs. *Proceedings of the National Academy of Sciences of the United States of America*, *106*(25). https://doi.org/10.1073/pnas.0900604106

Leiss, D., Felix, M. A., & Karsenti, E. (1992). Association of cyclin-bound p34(cdc2) with subcellular structures in Xenopus eggs. *Journal of Cell Science*, *102*(2). https://doi.org/10.1242/jcs.102.2.285

Liku, M. E., Nguyen, V. Q., Rosales, A. W., Irie, K., & Li, J. J. (2005). CDK phosphorylation of a novel NLS-NES module distributed between two subunits of the Mcm2-7 complex prevents chromosomal rereplication. *Molecular Biology of the Cell*, *16*(10). https://doi.org/10.1091/mbc.E05-05-0412

Loog, M., & Morgan, D. O. (2005). Cyclin specificity in the phosphorylation of cyclin-dependent kinase substrates. *Nature*, *434*(7029). https://doi.org/10.1038/nature03329

Lu, J., Wu, T., Zhang, B., Liu, S., Song, W., Qiao, J., & Ruan, H. (2021). Types of nuclear localization signals and mechanisms of protein import into the nucleus. In *Cell Communication and Signaling* (Vol. 19, Issue 1). https://doi.org/10.1186/s12964-021-00741-y

Malumbres, M. (2014). Cyclin-dependent kinases. *Genome Biology*, *15*(6). https://doi.org/10.1186/gb4184

Matthews, H. K., Bertoli, C., & de Bruin, R. A. M. (2022). Cell cycle control in cancer. In *Nature Reviews Molecular Cell Biology* (Vol. 23, Issue 1). https://doi.org/10.1038/s41580-021-00404-3

McGrath, D. A., Balog, E. R. M., Kõivomägi, M., Lucena, R., Mai, M. v., Hirschi, A., Kellogg, D. R., Loog, M., & Rubin, S. M. (2013). Cks confers specificity to phosphorylation-dependent CDK signaling pathways. *Nature Structural and Molecular Biology*, *20*(12). https://doi.org/10.1038/nsmb.2707

Merrick, K. A., & Fisher, R. P. (2010). Putting one step before the other: Distinct activation pathways for Cdk1 and Cdk2 bring order to the mammalian cell cycle. In *Cell Cycle* (Vol. 9, Issue 4). https://doi.org/10.4161/cc.9.4.10732

Miller, M. E., & Cross, F. R. (2000). Distinct Subcellular Localization Patterns Contribute to Functional Specificity of the Cln2 and Cln3 Cyclins of Saccharomyces cerevisiae . *Molecular and Cellular Biology*, *20*(2). https://doi.org/10.1128/mcb.20.2.542-555.2000

Morgan, D. O. (2007). Cell Cycle: Principles of Control. *The Yale Journal of Biology and Medicine*, *80*(3).

Nardozzi, J. D., Lott, K., & Cingolani, G. (2010). Phosphorylation meets nuclear import: A review. In *Cell Communication and Signaling* (Vol. 8). https://doi.org/10.1186/1478-811X-8-32

Örd, M., & Loog, M. (2019). How the cell cycle clock ticks. In *Molecular Biology of the Cell* (Vol. 30, Issue 2). https://doi.org/10.1091/mbc.E18-05-0272

Örd, M., Möll, K., Agerova, A., Kivi, R., Faustova, I., Venta, R., Valk, E., & Loog, M. (2019a). Multisite phosphorylation code of CDK. *Nature Structural and Molecular Biology*, *26*(7). https://doi.org/10.1038/s41594-019-0256-4

Örd, M., Möll, K., Agerova, A., Kivi, R., Faustova, I., Venta, R., Valk, E., & Loog, M. (2019b). Multisite phosphorylation code of CDK. *Nature Structural & Molecular Biology*, *26*(7), 649–658. https://doi.org/10.1038/s41594-019-0256-4

Örd, M., Puss, K. K., Kivi, R., Möll, K., Ojala, T., Borovko, I., Faustova, I., Venta, R., Valk, E., Kõivomägi, M., & Loog, M. (2020). Proline-Rich Motifs Control G2-CDK Target Phosphorylation and Priming an Anchoring Protein for Polo Kinase Localization. *Cell Reports*, *31*(11). https://doi.org/10.1016/j.celrep.2020.107757

Örd, M., Venta, R., Möll, K., Valk, E., & Loog, M. (2019). Cyclin-Specific Docking Mechanisms Reveal the Complexity of M-CDK Function in the Cell Cycle. *Molecular Cell*, *75*(1). https://doi.org/10.1016/j.molcel.2019.04.026

Peters, J. M. (2006). The anaphase promoting complex/cyclosome: A machine designed to destroy. In *Nature Reviews Molecular Cell Biology* (Vol. 7, Issue 9). https://doi.org/10.1038/nrm1988

Suzuki, K., Sako, K., Akiyama, K., Isoda, M., Senoo, C., Nakajo, N., & Sagata, N. (2015). Identification of non-Ser/Thr-Pro consensus motifs for Cdk1 and their roles in mitotic regulation of C2H2 zinc finger proteins and Ect2. *Scientific Reports*, *5*. https://doi.org/10.1038/srep07929

Swaffer, M. P., Jones, A. W., Flynn, H. R., Snijders, A. P., & Nurse, P. (2016). CDK Substrate Phosphorylation and Ordering the Cell Cycle. *Cell*, *167*(7). https://doi.org/10.1016/j.cell.2016.11.034

Tatum, N. J., & Endicott, J. A. (2020). Chatterboxes: the structural and functional diversity of cyclins. In *Seminars in Cell and Developmental Biology* (Vol. 107). https://doi.org/10.1016/j.semcdb.2020.04.021

Topacio, B. R., Zatulovskiy, E., Cristea, S., Xie, S., Tambo, C. S., Rubin, S. M., Sage, J., Kõivomägi, M., & Skotheim, J. M. (2019). Cyclin D-Cdk4,6 Drives Cell-Cycle Progression via the Retinoblastoma Protein's C-Terminal Helix. *Molecular Cell*, *74*(4). https://doi.org/10.1016/j.molcel.2019.03.020

Uhlmann, F., Bouchoux, C., & López-Avilés, S. (2011). A quantitative model for cyclin-dependent kinase control of the cell cycle: Revisited. In *Philosophical Transactions of the Royal Society B: Biological Sciences* (Vol. 366, Issue 1584). https://doi.org/10.1098/rstb.2011.0082

van Roey, K., Uyar, B., Weatheritt, R. J., Dinkel, H., Seiler, M., Budd, A., Gibson, T. J., & Davey, N. E. (2014). Short linear motifs: Ubiquitous and functionally diverse protein interaction modules directing cell regulation. In *Chemical Reviews* (Vol. 114, Issue 13). https://doi.org/10.1021/cr400585q

Venta, R., Valk, E., Örd, M., Košik, O., Pääbo, K., Maljavin, A., Kivi, R., Faustova, I., Shtaida, N., Lepiku, M., Möll, K., Doncic, A., Kõivomägi, M., & Loog, M. (2020). A processive phosphorylation circuit with multiple kinase inputs and mutually diversional routes controls G1/S decision. *Nature Communications*, *11*(1), 1836. https://doi.org/10.1038/s41467-020-15685-z

Wagner, M. v., Smolka, M. B., de Bruin, R. A. M., Zhou, H., Wittenberg, C., & Dowdy, S. F. (2009). Whi5 regulation by site specific CDK-phosphorylation in Saccharomyces cerevisiae. *PLoS ONE*, *4*(1). https://doi.org/10.1371/journal.pone.0004300

Wäsch, R., & Cross, F. R. (2002). APC-dependent proteolysis of the mitotic cyclin Clb2 is essential for mitotic exit. *Nature*, *418*(6897). https://doi.org/10.1038/nature00856

Wilmes, G. M., Archambault, V., Austin, R. J., Jacobson, M. D., Bell, S. P., & Cross, F. R. (2004). Interaction of the S-phase cyclin Clb5 with an "RXL" docking sequence in the initiator protein Orc6 provides an origin-localized replication control switch. *Genes and Development*, *18*(9). https://doi.org/10.1101/gad.1202304

Zachariae, W., Schwab, M., Nasmyth, K., & Seufert, W. (1998). Control of cyclin ubiquitination by CDK-regulated binding of Hct1 to the anaphase promoting complex. *Science*, *282*(5394). https://doi.org/10.1126/science.282.5394.1721

Zhu, M., Fang, T., Li, S., Meng, K., & Guo, D. (2015). Bipartite Nuclear Localization Signal Controls Nuclear Import and DNA-Binding Activity of IFN Regulatory Factor 3. *The Journal of Immunology*, *195*(1). https://doi.org/10.4049/jimmunol.1500232

Appendix

Science Advances
AAAS

FRONT MATTER

Title

- **Full title: A synthetic biology approach reveals diverse and dynamic CDK response profiles via multisite phosphorylation of NLS-NES modules**

- **Short title: Diverse CDK response profiles of NLS-NES modules**

Authors
Ilona Faustova[1], Mihkel Örd[1], Viacheslav Kiselev[1], Dmytro Fedorenko[1], Irina Borovko[1], Dags Macs[1], Kaur Pääbo[1], Marko Lõoke[1], and Mart Loog[1]*

Affiliations
[1] Institute of Technology, University of Tartu, Tartu, 50411, Estonia

Corresponding author: Mart Loog, mart.loog@ut.ee

Abstract
The complexity of multisite phosphorylation mechanisms in regulating nuclear localization (NLS) and export (NES) signals is not understood and its potential has not been used in synthetic biology. The nucleo-cytoplasmic shuttling of many proteins is regulated by cyclin-dependent kinases (CDKs) that rely on multisite phosphorylation patterns and short linear motifs (SLiMs) to dynamically control proteins in the cell cycle. We studied the role of motif patterns in nucleo-cytoplasmic shuttling using sensors based on CDK targets Dna2, Psy4, and Mcm2/3 of S. cerevisiae. We designed multisite phosphorylation modules by rearranging phosphorylation sites, cyclin-specific SLiMs, phospho-priming, phosphatase specificity, and NLS/NES phospho-regulation, and obtained very different substrate localization dynamics. These included ultrasensitive responses with and without a delay, graded responses, and different homeostatic plateaus. Thus, CDK can do much more than trigger sequential switches during the cell cycle, but can drive complex patterns of protein localization and activity by using multisite phosphorylation networks.

Teaser
A synthetic biology approach to engineer multisite phosphorylation networks for dynamic regulation of NLS-NES modules.

MAIN TEXT

Introduction

Major cellular reorganizations and state changes, such as cell division or cell differentiation, require complex regulatory mechanisms and large spatially coordinated signaling networks. In the eukaryotic cell division cycle, the cyclin-dependent kinases (CDKs) are central regulators. In freely proliferating cells, CDK activity displays oscillatory dynamics due to the wavelike synthesis and degradation of cyclins (*1*). At each cell cycle stage, different versions of cyclins are expressed. In G1, the total CDK activity is at its minimum due to the very low expression of cyclins and the low intrinsic activity of early CDK complexes (*2–4*). CDK activity starts to rise at the G1/S transition, peaks in mitosis and drops again at the M/G1 transition (*5*).

The cell cycle is regulated by hundreds of CDK targets, leading to chains of downstream events triggered by the phosphates added to target proteins (in *S. cerevisiae* there are ~700 CDK targets (*6*), which is >10% of the proteome). However, it is not clear how simple oscillatory dynamics of a single protein kinase activity can be processed into properly timed, dosed, and precisely localized molecular events leading to synthesis, segregation, and division. One way CDK regulates protein activity is through the phospho-regulation of protein shuttling between the nucleus and cytoplasm (*7, 8*). However, little is known about how CDK is able to precisely temporally control the ratio of nuclear and cytoplasmic concentrations to produce distinct protein activity dynamics.

Nucleo-cytoplasmic shuttling is mediated by the nuclear pore complex (NPC) and karyopherins – importins and exportins that catalyze transport into the nucleus and cytoplasm, respectively. To be recognized, a target protein has to carry an NLS (nuclear localization signal) and/or NES (nuclear export signal): amino acid sequences that are often regulated by multiple adjacent phosphorylation sites (*9*). In fact, most CDK targets are phosphorylated at multiple sites (*10*). Multisite phosphorylation systems have been shown to introduce ultrasensitivity to kinase output switches (*11, 12*), create multi-stability (*13–15*), facilitate multi-input signal processing (*16–19*), allosteric regulation (*20*), regulate kinase scaffolds (*21, 22*), produce negative-feedback (*23*), and form phospho-degrons (*24, 25*).

Our recent studies exemplified the power of the synthetic biology concept “build to understand” by demonstrating how multisite phosphorylation networks can act as “timing

tags" that trigger specific events at distinct CDK thresholds. Using a model system based derived from the Cdk1 target Sic1, we were able to change the order of the sequence elements within phosphorylation site clusters to program the execution times over the whole time-span of the budding yeast cell cycle (Örd *et al*., 2019a, Faustova *et al*., 2020). The mechanisms that drive multisite phosphorylation by CDK included SLiM-based cyclin docking interactions, priming phosphorylation, and docking of primed sites to the CDK complex's phospho-adaptor subunit Cks1. The more optimal the phosphorylation parameter set, or the "multisite phosphorylation code", of a phosphorylation cluster, the more efficiently CDK phosphorylates it up to the execution threshold of a switch. Thus, CDK function was translated into a simple principle: lower CDK activity at early cell cycle stages would require a stronger set of parameters in early targets, while the mitotic switches at higher CDK levels can contain sites or clusters with a relatively weak set of CDK multisite phosphorylation parameters. In this sense, a target can be compared to a resistor in electronics. The higher the resistance, the later the switch.

In these previous studies we focused solely on how the multisite phosphorylation parameters that lead to faster or slower phosphorylation can control a fixed output condition; generation of a phospho-degron (*26*, *27*). Yet, there are many types of outputs of CDK signaling (*7*), which can be regulated in multiple ways: complex formation/disruption, localization change, enzyme activation/inactivation, protein degradation, etc. Moreover, outputs of the same type may have different affinities or execution rates for the subsequent downstream processes. Thus, it remains an open question whether phosphorylation efficiency is a generalizable predictor of output timing – i.e., such that poor CDK sites (or sites with low CDK/phosphatase specificity ratio) are later switches, while optimal CDK sites or docking-potentiated sites are early switches. One mechanism that can subvert this direct relationship is cyclin-specific docking (*18*, *27–33*). Cyclin specificity can enforce a well-resolved temporal order of substrate phosphorylation independent of the identity of the phosphorylated sites (*26*). This was also elegantly demonstrated in a recent study comparing the phosphorylation dynamics of Cdk1 substrates in wild-type strains to a strain with just one B-type cyclin, Clb2, instead of six (Clb1-6) (*10*). Similarly, the relationship between phosphorylation efficiency and output timing can also become confounded, when the rates of downstream steps are taken into account. For example, substrates with the same timing of CDK phosphorylation can have different timing of the resulting output effects, like nuclear exit, due to differences in the kinetics of downstream steps (**Fig S1A**).

In the current paper, we addressed the relationship between phosphorylation efficiency and response dynamics focusing of multisite phosphorylation of NLS-NES modules. In contrast to degradation, phospho-regulation of localization is a more complex reversible output, opening up a much richer set of possibilities in terms of the response profiles. We used synthetic phospho-regulated nuclear localization sensors based on NLS-NES regions of CDK targets Dna2, Psy4, and Mcm2/3 of *S. cerevisiae*. Instead of a fixed CDK output, the studied phosphorylation sites and their CDK specificity affected both the net rate of CDK multisite phosphorylation of the sensor and the dynamics of the downstream process, namely, the nucleo-cytoplasmic shuttling, via differential regulation on NLS and NES. By varying the combination of phosphorylation sites, and by introducing different cyclin-specific docking motifs, we found that the dynamic output profiles of nuclear entry or exit, as a response to accumulating cyclins from G1 to mitotic exit, can exhibit very different shapes and oscillatory behaviors. The observed profiles included early ultrasensitive responses, delays followed by mitotic switches, gradual responses, biphasic responses, and different homeostatic plateaus.

Results

Switching between abrupt and gradual nuclear exit profiles of a Psy4-based CDK sensor

To create a localization sensor that exits the nucleus in response to CDK activity, we fused sfGFP to the intrinsically disordered C terminus of Psy4 (positions 315-441), a regulatory subunit of protein phosphatase PP4 containing a bipartite NLS that is inactivated by Cdk1-mediated phosphorylation (*8, 34*). We followed the nuclear shuttling of the construct using time-lapse fluorescence microscopy (**Fig 1A**). For a reference time-point during cell cycle progression, the G1/S transition was used, defined as a point where 50% of an Mcm2/3-based Cdk1 activity sensor was exported from the nucleus (**Fig 1B, C, S1B**) (*18, 35*). Psy4(full-length)-sfGFP (78 kDa) and Psy4(315-441)-sfGFP (42 kDa) were exported from the nucleus with similar dynamics following G1/S (**Fig 1C**). This confirms that the disordered C terminus could be used as a model system to study the regulation of nuclear shuttling and that the localization dynamics were not affected by a possible gain in free diffusion through the nuclear pores for the smaller protein. Also, addition of GST to Psy4(315-441)-sfGFP, increasing the molecular weight by 27 kDa, did not affect the localization dynamics, indicating that the process is dependent on regulated transport (**Fig 1C**).

Double mutation of the optimal CDK phosphorylation sites T320 and T347 to alanines leads to constant nuclear localization of Psy4 during the cell cycle (*8*) (**Fig 1A, D**). These sites are located immediately N-terminal to the two basic motifs of the bipartite NLS (**Fig 1A**), and their phosphorylation is expected to inhibit nuclear import (*8*) (**Fig 1E**). Yet, the disordered C terminus contains four additional Cdk1 consensus sites (**Fig 1A**). To study the potential complexity of the 6-site network in regulating nucleo-cytoplasmic shuttling, we performed systematic analysis using phosphorylation site mutants. First, we found that the single alanine mutation T347A did not abolish exit like the double mutant, but instead switched the rapid drop of nuclear signal to a slow gradual decline (**Fig 1D**). The T320A mutant also exhibited less steep decline, although the effect was less drastic (**Fig 1D**), but we observed no effect upon mutation of a minimal consensus site S337 (**Fig S1C**).

The gradual decline of the T347A mutant over a wide span of S and M phases (60 min) is inversely related to the gradually accumulating CDK activity (*26, 36, 37*) (**Fig S1D**). However, as this exit is not abrupt, the phosphorylation-driven switch cannot be attributed

to a specific CDK activity threshold. In contrast, the wild-type sensor exhibits abrupt switch-like exit. This raises the possibility that different dynamic shapes of CDK signaling outputs can be created via phosphorylation of multisite networks regulating the equilibrium of nucleo-cytoplasmic shuttling. As T347 is a site whose phosphorylation is predicted to hinder nuclear import, the gradual decline instead of a rapid switch is likely due to increased re-entry rate of the T347A sensor (**Fig S1E**). Thus, for the wild-type sensor, the downstream event at G1/S threshold (translocation into cytoplasm) is very efficient. The equilibrium is abruptly shifted towards exit at very low CDK activity levels via CDK-blocked re-entry. However, when re-entry is blocked less efficiently, due to the T347A mutation, the abrupt exit is switched to a gradual decline. These results exemplify how a single CDK site mutation in a 6-site phosphorylation network can switch the kinase-phosphatase module input-output function from the one with an ultrasensitive response to a graded response (*12*). Indeed, the wild-type sensor showed cell cycle-dependent phosphorylation shifts with the major change starting at 20-30 minutes after the release from G1 (**Fig 1F**), which correlates well with the microscopy profile of a fast drop in nuclear localization (**Fig 1C**). The version with T347A showed a slower accumulation of the shifts, which was also in good agreement with the slow gradual exit observed in microscopy (**Fig 1D, F**).

The abrupt trapping of the phosphorylated sensor in the cytoplasm as opposed to the leaking circulation would suggest that engineering a more efficient and specific phosphorylation of the NLS inactivating sites at the leaking sensor would restore the ultrasensitive response. To test this, we engineered sensors with increased cyclin recognition specificity. The wild-type Psy4(315-441) fragment lacks any identified cyclin docking motifs, and the addition of an optimal G1-CDK specific LP cyclin docking motif (*31*) did not significantly change its rapid exit (**Fig 1G**). In contrast, adding this LP motif to the T347A mutant transformed its gradual exit profile to an early abrupt ultrasensitive switch, and shifted the 50% exit timing by about 40 minutes (**Fig 1G**). This result suggests that the CDK thresholds and temporal order of switches based on different multisite phosphorylation patterns depend heavily on the kinetics of both phosphorylation and post-phosphorylation downstream equilibria (see also **Fig S1A**).

Cyclin specificity imposes a biphasic nuclear exit profile for the sensor in S and M phases

Surprisingly, a single alanine mutation of S364 caused a stepwise biphasic nuclear drop of the sensor (**Fig 1H, S1E**). An initial rapid export after G1/S was followed by a period of steady plateau around S phase, up to 20 minutes, after which the exit rate increased again. Apparently, as also demonstrated in more detail below, the kinase-phosphatase specificities towards the key sites in S364A sensor enables rapid phosphorylation and rapid steady state equilibrium (plateau) upon reaching the S-CDK peak, while phosphorylation of key sites in T347A sensor must be slower, allowing no equilibrium to be reached before the later mitotic cyclins start to accumulate. As S364 does not qualify as a predicted site affecting the NLS (*8*), the incomplete exit in S phase suggests that S364 could be a positive regulator of a putative NES.

To test if it is possible to shift the S phase equilibrium and the plateau height by increasing CDK activity in S phase, we used a well-defined system where the S phase cyclin *CLB5* was replaced in its locus with mitotic cyclin *CLB2* (*38*). As the intrinsic catalytic activities of CDK complexes rise gradually during the cell cycle (*2*, *3*, *33*), Clb5-Cdk1 has about an order of magnitude lower specificity towards CDK consensus phosphorylation sites compared to Clb2-Cdk1. As expected, the *clb5::CLB2* replacement (in Δ*swe1* background

(*38*, *39*)) suppressed the plateau and almost restored the dynamics of the wild-type sensor (**Fig 1H**). Similarly, when a second copy of *CLB5* was added, the plateau was shifted, although not as much as in the case of Clb2 (**Fig 1H**), which is also in agreement with *in vitro* kinetic data on the intrinsic activity differences of these two CDK complexes (*33*). Thus, the biphasic dynamics corresponded to profound differences in S- and M-CDK intrinsic activities. Intriguingly, the observed profile is an example of how CDK-regulated processes in two major phases of the cell cycle, S and M phases, could clearly manifest as two different output steady states.

A mitotic switch based on limited phospho-regulation of NLS and NES

Strikingly, the S phase plateau of the S364A mutant shifted up when the T320A mutation was added (**Fig 2A**), creating a profile with virtually no response to pre-mitotic thresholds of CDK activity. When the most C-terminal sites of the 6-site cluster, the suboptimal SP motifs, S409 and S434, were further mutated, the construct was entirely nuclear. As these sites are located at least 40 amino acids C-terminal to the NLS, their phosphorylation is not expected to affect the NLS (*8*). This suggests that, similar to S364, phosphorylation of these sites might activate a putative NES (**Fig 2B**). Psy4 is exported by Msn5, for which no NES consensus has been defined, but export of other Msn5 targets has been found to be activated by phosphorylation (*8*, *40*). Thus, the data suggested that in the T320A-S364A construct, the two mutations weaken both NLS and NES regulation, respectively. Low levels of CDK in S phase are not sufficient to shift the equilibrium towards exit while the higher mitotic levels are still sufficient for this (**Fig 2B**). To test this, we set out to increase the S-CDK activity towards the T320-S364A sensor by introducing cyclin-specific docking motifs (**Fig 2C**). Addition of an optimal G1-specific LP motif resulted in rapid export of the sensor at G1/S (**Fig 2D**). An exclusively S-Cdk1-specific NLxxxL motif (*27*) led to an abrupt partial exit, followed by a gradual decline in nuclear levels (**Fig 2D**), while addition of an RxL motif showed slightly steeper decline after the initial drop, which is in good agreement with high specificity of RxL motifs for S-Cdk1 and moderate specificity for G2-Cdk1 complex (*32*). The M-Cdk1-specific LxF motifs showed a mild effect on the slope of the exit around the time window of mitosis (**Fig 2E**). Similarly, the profile created by addition of the G2-Cdk1-specific PxF motif correlates with the expression period of G2 cyclin Clb3 between S and M phase cyclins.

Also, a sensor containing the pair T320 and T347 as the only two CDK sites left, was able to shift the equilibrium between nucleus and cytoplasm (**Fig S2A, Fig 2B**). This suggests that a basal NES activity must be present in a non-phosphorylated construct, as active export by Msn5 is necessary for nuclear exit of Psy4 and T320-T347 are predicted to affect the NLS re-entry, but not the exit rate (*8*) (**Fig 2B**). Furthermore, when either T320 or T347 was present as the single CDK consensus site, the construct was entirely nuclear (**Fig S2A**). This suggests that pT320 and pT347 work as a cooperative pair to prevent re-entry.

C-terminal truncations suggested that an NES could reside in the region around the CDK site S364 and the region from 375-441 harboring the CDK sites S409 and S434 (**Fig S2B-C**). In addition, when combined with the T347A mutation, the mutations S409A and S434A reduced the nuclear export (**Fig S2D**). However, a double mutation of S409A S434A in the wild-type template did not affect localization (**Fig S2D**). Therefore, by contrast with the S364A mutant (**Fig 2A**), we suggest that S364 is the major activator of the putative NES, while sites S409 and S434 may have a supportive role.

Next, we analyzed directly the phosphorylation of the localization modules in different cell cycle phases. For this, we arrested cells with α-factor (G1 phase), hydroxyurea (S phase), or nocodazole (mitosis) (**Fig 2F**). Separate mutations of T320A, T347A, or S364A showed a single-band downshift of the hyper-phosphorylation in nocodazole. Also, the double mutation T320A-S364A caused a dramatic loss of phosphorylation in HU, while showing a slightly prominent shift in mitosis (**Fig 2F**), which explains the absence of nuclear export of T320A-S364A sensor in the S phase. The double mutation S409A-S434A showed moderate loss of phosphorylated forms in HU and nocodazole arrest, which confirms that these sites are phosphorylated *in vivo* and may play a role in promoting nuclear exit, like observed in several forms of the sensor (**Fig 2A, S2D**).

NLS-regulating phosphorylation sites are linked to NES-activating sites via Cks1-mediated docking

Kinase assays using purified proteins and Phos-tag SDS-PAGE autoradiography revealed that phosphorylation of the wild-type sensor is dependent on Cks1, a phospho-adaptor subunit of the CDK complex that recognizes phospho-threonines but not phospho-serines as priming sites (*41, 42*) (**Fig 3A**). Cks1-dependent docking facilitates the phosphorylation of sites located on the C-terminal side of the priming sites (*42*). For example, the NLS-inactivating TP sites could prime the C-terminal NES-activating SP sites (**Fig 1A**). Such a directional chain of priming events leading to phosphorylation of SCF phospho-degrons has been found in several CDK targets (*18, 25, 27*). Phosphorylation of constructs containing T320A or T347A mutations, alone or combined, revealed that T320 and T347 are the major Cdk1 target sites, and that they are required for rapid Cks1-dependent hyper-phosphorylation (**Fig 3B**).

To further test if T320 or T347 may be the priming sites facilitating the phosphorylation of NES-activating sites, we used phospho-mimetic mutations T320E and T347E and followed their localization dynamics. The idea was to separate the two functions: while the glutamates may mimic the phospho-regulation of NLS, as reported (*35*), they cannot act as priming sites, since the phospho-mimicking EP sequences do not bind Cks1 (*41*). As expected, both T320E and T347E reduced the initial nuclear localization level of the construct confirming that these mutations inactivate the NLS (**Fig 3C**). On the other hand, after G1/S, the T320E mutant followed the same exit profile as the wild-type sensor whereas the T347E mutant showed a gradual exit path, analogous to the T347A mutant (**Fig 1D, 3C**). This result strongly suggests that phosphorylated T347 (pT347) serves as a Cks1-dependent priming site to promote the phosphorylation of the NES-activating site S364 (**Fig 3D**). Although pT320 also might act as a primer for S364, the distance between the two sites is exceeds the optimum length (*42*), which may also be reflected in slow gradual exit of the T347A sensor (**Fig 1D**). Also, the synergistic amplification from Cks1 docking is clearly evident from the finding that sensors including either the Cks1 primer site (T347) or the suboptimal sites (S364, S409 and S434) are entirely nuclear, but combining them into one sensor creates a prominent mitotic switch (**Fig S3A**).

This intriguing priming-mediated connection between NLS-inactivating and NES-activating sites further reveals that the whole 6-site CDK phosphorylation network contains a more complex signal processing scheme than initially anticipated. The priming connection may work as a system ensuring that molecules containing the NLS-inactivating pT347 site are exported decisively. In the absence of this connection, randomly distributive phosphorylation of T347 or S364 sites in a pool of molecules may either not lead to efficient export or may result in a futile export-import cycle, respectively (**Fig 3D**).

Threonine-serine swapping reveals a CDK specificity filter

As Cks1 binds phospho-threonines but not phospho-serines, we tested a Cks1-docking deficient T320S-T347S mutant sensor. This sensor was exported rapidly at G1/S, similarly to the wild-type (**Fig 3E**). There are two possible explanations for this result: either the Cks1-dependent docking is not important or the serines at sites 320 and 347 are phosphorylated more efficiently than threonines and thereby rescue the effect of disabled Cks1 docking. Interestingly, a construct with T347 as the only CDK site was almost stable over the cell cycle, but a similar construct with the T347S mutation resulted in rapid exit, dropping to 50% of G1 levels (**Fig 3E**). In constructs with T320 or S320 as the only CDK sites, the effect was similar (**Fig S3B**). These results support the possibility that phosphorylation at sites 320 and 347 occurs to a greater extent (i.e., a greater fraction of molecules) when they are serines than when they are threonines (**Fig 3F**). Also, other sensor versions with threonine-serine mutations showed a switch to a similar rapid loss of nuclear localization at G1/S (**Fig S3C-E**).

Next, we compared the dynamics of Psy4 modules with T320-T347 and S320-S347 as the only two CDK sites in a strain where *CLB5* gene is replaced with *CLB2* (*clb5::CLB2* Δ*swe1*) to obtain higher intrinsic Cdk1 activity in S phase, as described above (**Fig 1H**). While the T320S-T347S sensor oscillated with similar dynamics in wild-type and *clb5::CLB2* strains, the T320-T347 module was exported to a greater extent in the *clb5::CLB2* strain (**Fig S3F**). This suggests that S320 and S347 could be close to maximally phosphorylated already in S phase, whereas T320 and T347 do not reach full phosphorylation in the wild-type background. To assess the phosphorylation status, we analyzed the shifts in cells arrested with α-factor (G1), hydroxyurea (S phase), or nocodazole (mitosis) using Phos-tag western blotting. Indeed, as predicted, the T320S-T347S sensor and S320 sensor had reached a full shift compared to the analogous threonine variants (**Fig 3G**). While the T320-T347 sensor was phosphorylated to a greater extent in HU-arrested *clb5::CLB2* cells compared to wild-type cells, it did not reach full phosphorylation in mitotic cells of either strains (**Fig 3G**). This suggests that serines in these positions are efficiently and fully phosphorylated, but threonines are not.

We and others have previously shown using model substrate peptides that SP motifs are about 2-3 times more specific for Cdk1 complexes compared to TP motifs (*26*, *43*). Also, with Psy4 sensors, we found that the T320S-T347S mutant showed loss of hyper-phosphorylation *in vitro*, but also an increase in the phosphorylation initial velocity by 2 times (**Fig 3B**). Next, we found that *in vitro* dephosphorylation assays using a key CDK counteracting phosphatase, PP2A-Cdc55, showed higher preference for wild-type Psy4 sensor containing the two threonines compared to the T320S-T347S version (**Fig 3H, S3G**). This is in agreement with previous reports on PP2A-Cdc55 specificity (*44*, *45*). Lower CDK specificity and higher phosphatase specificity could explain why the sensors with T320 and/or T347 are less efficiently exported compared to the corresponding sensors with T-to-S mutations. In contrast, the phosphatase Cdc14, which counteracts CDK during mitotic exit showed higher specificity for the T320S-T347S sensor (**Fig 3H, S3G**), which is also in agreement with previous reported preference for phospho-serines in the case of Cdc14 (*46*, *47*). Interestingly, these data demonstrate that even highly optimal CDK sites can be only partially phosphorylated due to high phosphatase specificity.

As previously shown for several Cdk1 targets, S/TP consensus sites can be phosphorylated in G1 when the activity of cell cycle-related CDK complexes is very low

(*17*, *26*), and we found that the Psy4-based sensor was partially phosphorylated in an α-factor arrest (**Fig 1F, 2F**). However, most of these shifts were not present when an alternative approach was used for G1 arrest, suggesting that the phosphorylation was due to the MAPK Fus3 that is activated via the pheromone pathway (**Fig S4A**). Psy4 is nuclear in a pheromone-induced G1 arrest (*8*), raising the interesting possibility of a specificity filter that allows nuclear exit only in response to Cdk1, which in contrast to other proline-directed kinase possesses the Cks1 docking mechanism. The T320S-T347S sensor lacks the Cks1 docking capability, while its phosphorylated form would be more resistant to phosphatases (providing more protection from other proline-directed kinases than the threonine-based sites) (*45*). To test this, we analyzed the levels of the wild-type sensor and the T320S-T347S sensor in an α-factor arrest. Indeed, the wild-type sensor accumulated to higher levels compared to the all-Ser version in G1 (**Fig S4B, C**). Also, in an α-factor arrest, the sensor with all Cdk1 consensus sites mutated to alanine accumulated to higher nuclear concentrations compared to T320A-T347A mutant, where S364, S409 and S434 are still present (**Fig S4D, E**). This further supports that the sites S364, S409 and S434 promote nuclear export and that these sites are phosphorylated to some extent in cells arrested with α-factor.

These experiments hint that Cks1-dependent docking introduces several emergent properties. First, the priming and docking connection is specific for Cdk1 and not for other proline-directed kinases, including Fus3 (**Fig S4A-C**). Second, the low T347 phosphorylation in T320A-S364A mutant creates a lag period and the possibility to design a wide temporal resolution relative to G1/S (**Fig 2A**). Third, upon the return of the sensor into the nucleus in mitotic exit, Cdc14's inability to dephosphorylate the key site pT347 would potentially lead to later entry timing than in the all-Ser version, which has both better specificity for Cdc14 and is less efficiently multiphosphorylated due to the absence of Cks1 docking. We analyzed the timings of nuclear entry for all-Ser and wild-type sensors. As predicted, the wild-type sensor was imported later compared to the all-Ser version (**Fig S4F**). These results together suggest that Cks1-driven mechanism with phospho-priming mediated connection of NLS inactivation and NES activation is a useful property that filters off the non-specific signals of kinases other than CDK, enables to create mitotic switches, and can shift the nuclear entry timing until very low thresholds of declining M-CDK activity.

The Cdk1 inhibitor sensitivity of the G1/S triggered sensors and the concept of CDK thresholds

To test how the localization sensors would behave in the context of different Cdk1 activity dynamics we inserted them into the Cdk1-as1 strain (*48*), where Cdk1 activity is lower and can be quantitatively inhibited. The Mcm2/3-based sensor was exported with similar fast kinetics at G1/S as in a wild-type strain, and the profile was not sensitive to up to 200 nM inhibitor (**Fig 4A**). Strikingly, in the case of the Psy4-based sensor, the profile was changed from an ultrasensitive G1/S switch to a gradual export. Furthermore, even a small dose of 100 nM inhibitor, which would be insufficient to induce cell cycle arrest at a high G2/M CDK threshold (*48*), led to a dramatically flattened profile with a minor nuclear exit in the cell cycle (**Fig 4B**). A similar effect was observed with the S364A mutant sensor (**Fig 4C**). This differential inhibitor sensitivity might arise from phosphatase specificity, as the NLS-inactivating sites are serines in the Mcm2/3 sensor and threonines in the Psy4 sensor. The sensitivity to the inhibitor is highest when sites are not fully phosphorylated (see also **Fig 7D** below). Secondly, in multistep phosphorylation systems, the final inhibitor effect amplifies at each sequential step. Thus, the Psy4 sensor could be sensitive to lower doses of inhibitor because of the stepwise process involving Cks1 docking via pT347 that is crucial

for the phosphorylation of NES-inactivating site S364. The NES in Mcm2/3 seems to be not regulated by phosphorylation (*35*). Nevertheless, these results are surprising because they indicate that targets with similar phosphorylation timing (and presumably similar CDK thresholds) show very different sensitivity to Cdk1 inhibitor. These results raise alternative possibilities to interpret the use of inhibitor doses to define CDK thresholds.

A nuclear import module based on Dna2 also depends on CDK multisite phosphorylation

To study an example of CDK-activated nuclear import, we engineered a minimal model system based on the DNA replication factor Dna2. The Dna2 protein contains an intrinsically disordered N terminus with a bipartite NLS that is activated by Cdk1-mediated phosphorylation of S17 in the linker region of the NLS (**Fig 5A**) (*8*). We fused the 100 N-terminal residues of Dna2 to sfGFP and expressed it from constitutive P_{ACT1} promoter to study the regulation of Cdk1-controlled nuclear entry using time-lapse fluorescence microscopy (**Fig 5B**). Dna2(1-100)-GFP was mainly cytoplasmic in G1 phase but accumulated rapidly in the nucleus after G1/S (**Fig 5B, C**). Mutation of the Cdk1 site S17 abolished the nuclear entry of the module (**Fig 5C**), as reported previously for full-length Dna2 (*8*). Importantly, full-length Dna2 showed similar localization dynamics as the N-terminal fragment (**Fig S5A**), indicating that the key motifs regulating the localization are in the 1-100 fragment.

Next, we tested how the CDK specificity of S17 affects the dynamics of nuclear entry. We made two constructs in which the S17 motif (SPAKK) was differently mutated to a minimal consensus site (SPAQQ or SPAAK). These mutations caused about a 50% drop in the nuclear abundance during the cell cycle, but did not have a significant effect on the timing of nuclear entry (**Fig 5D**). Another full consensus CDK phosphorylation site, T4, is located 13 residues upstream of S17, at an ideal distance to act as a Cks1-dependent phospho-priming site for S17 (**Fig 5A**). To test this idea, we mutated T4 either to alanine or serine. Both mutations caused a considerable decrease in nuclear accumulation of Dna2(1-100)-GFP and also slightly delayed the timing of entry (**Fig 5E**), suggesting that T4 functions as a Cks1-dependent primer site for phosphorylation of S17. Furthermore, when the mutation of S17 to a minimal consensus site was combined with the loss of Cks1 priming by T4S mutation, no nuclear accumulation of the module was observed during the cell cycle (**Fig 5E**). This indicates that Cks1 docking is necessary to keep a substantial fraction of molecules phosphorylated at S17.

In a kinase assay followed by Phos-tag SDS-PAGE, rapid accumulation of a doubly phosphorylated form was observed, and this process was severely suppressed by Cks1 phospho-pocket mutation, confirming that Cks1 promotes multi-phosphorylation of the module (**Fig 5F**). We also performed Phos-tag western blotting of synchronized yeast cultures to directly analyze the phosphorylation of Dna2(1-100)-GFP in the cell cycle. Dna2(1-100) was unphosphorylated in a pheromone-induced G1 arrest followed by extensive phosphorylation at around 30 minutes after the release of cells from the arrest (**Fig S5B**). Analysis of the multisite phosphorylation pattern of different Dna2(1-100) mutants confirmed that both T4 and S17 are phosphorylated in a cell cycle-dependent manner (**Fig S5C**).

As with the threonine vs serine effects observed in Psy4-based constructs, a S17T mutation in Dna2 led to a profound decrease in nuclear accumulation (**Fig 5G**), and reduced phosphorylation of T17, but not S17, was also observed in Phos-tag western blotting

experiments in a T4A background (**Fig S5C**). Interestingly, the negative effect of S17T on entry was greater than that observed by mutating the S17 to a minimal consensus site (S17+3A, mutation of 17SPAK to SPAA) (**Fig 5G**). The S17T mutation caused a decrease in phosphorylation rate by about two times with both Cln2- and Clb2-Cdk1 *in vitro* (**Fig 5H**). Mutation of S17 to a minimal consensus site (S17+3A), however, led to a greater decrease in phosphorylation rate (**Fig 5H**). This suggests that factors other than CDK specificity are affected by the Ser-to-Thr mutations *in vivo*. Again, as in Psy4, we hypothesize that this could be due to higher dephosphorylation rate of TP sites compared to SP sites (*45*). *In vitro* analysis of the phosphatase specificity of Dna2(1-100) confirmed that PP2A-Cdc55 preferentially dephosphorylates the S17T mutant, while the mitotic exit phosphatase Cdc14 preferentially targets S17 (**Fig S5D**).

Next, we tested the effect of added cyclin-docking SLiMs in the Dna2-derived module. As the majority of its nuclear accumulation takes place around G1/S, we hypothesized that this could be driven mainly by the G1-specific Cln2-Cdk1 complex, which is abundant in the cytoplasm (*49, 50*). We introduced specific docking motifs for G1-, S-, and M-Cdk1 to Dna2(1-100 17SPAQQ) (**Fig S5E**). The addition of a G1-Cdk1-specific LP motif caused about 10-minute advance in the nuclear entry and an increase in the nuclear levels over the cell cycle (**Fig S5F**). Adding an S-Cdk1 specific NLxxxL motif did not affect the nuclear import dynamics of the module (**Fig S5F**), likely because the S phase cyclins are predominantly nuclear (*38*). The module containing a mitotic cyclin docking motif LxF showed similar nuclear entry at G1/S as the wild-type, but had a marked nuclear accumulation peak 40-60 minutes after G1/S (**Fig S5F**). These results indicate that the G1- and M-Cdk1 complexes play a major role in the phosphorylation of cytoplasmic targets. In contrast, the Psy4-based constructs were affected by the specificity of all four major cyclins, indicating that the nuclear export of CDK targets is affected by CDK activity in both compartments.

Programming the phosphorylation patterns to control protein oscillations in the nucleus

Our experiments have shown that the input activity of the core CDK oscillator, exemplified as a sum of gradual accumulation of different cyclins from G1 to mitosis followed by a decline at M/G1, can be processed into different output profiles of regulated dynamic processes. This can be achieved by combining the multisite phosphorylation code (*26*) and kinetics of the downstream event, which in the current case was nucleocytoplasmic shuttling. For a conclusive overview, we next demonstrate collected sets of nuclear oscillatory patterns of CDK outputs that were programmed into the studied modules using a small set of sequence elements involving a combination of phosphorylation sites and cyclin docking sites. As a primary reference profile, one can consider the gradual decline of the T347A-Psy4 sensor (**Fig 6A**) as a reverse profile of the gradual CDK input (**Fig S1D**). Our study reveals that there are many ways to transform this gradual shape into various different profiles. Interestingly, in all tested constructs, an abrupt change in the nuclear level of the Psy4 sensor occurred only around the time of G1/S (0 min) and at mitotic entry (after 20 min). Addition of the RxL motif made the switch even more abrupt than the wild-type (**Fig 6A**). A considerable delay spanning S phase (ca 20 min) could be introduced by mutating T320 and S364 and adding the M-CDK docking motif LxF. The constructs with intermediate timing between the G1/S and M phase profiles were always exported in a step-wise manner, as shown by the construct with RxL cyclin docking sites in the T320A-S364A module (**Fig 6A**).

Biphasic oscillatory profiles were also designed that have one signaling output in S phase and another in mitosis (**Fig 6B**). The level of S-phase output could be slightly modulated, for example, by introducing the T320S mutation to the S364A background (**Fig 6B**). Secondly, the gradual profile of T347A could be switched to a biphasic profile by addition of a Clb5-specific NLxxxL docking site in the middle of the construct, while smooth non-switch-like profiles were obtained when the docking site was introduced at the C terminus of the construct (**Fig 6C, S6A**). Given that the Clb5 docking motifs potentiate the phosphorylation of sites located N-terminally from the docking motif (*42*), this result suggests that the middle position helps to phosphorylate T320, imposing a stronger block to nuclear re-entry in S phase to create a bi-phasic profile. The C-terminal positioning of the docking motif would also potentiate the phosphorylation of the NES activating sites, and therefore would draw a profile with faster exit than the gradual T347A reference profile.

For the Dna2-based sensors, the entry timing after G1/S was sensitive to Cln2 specificity (addition of an optimal LP docking site) (**Fig 6D, S6B**). Secondly, the efficiency of Cks1-mediated phosphorylation is known to be dependent on the distance between primer and secondary sites with the optimal distance window being estimated to fall between 12-16 amino acids (*42*). Increasing the distance between T4 and S17 by 4 amino acids considerably delayed the entry (**Fig 6D, S6B**).

We found that different re-entry timing could also be programmed. The wild-type Psy4 module was imported roughly 5 minutes later than the Mcm2/3-based sensor (**Fig 6E**). Mutation of sites S409A and S434A and single mutation of S364A led to earlier re-entry timing and also resulted in higher nuclear levels in G1 (**Fig 6E**), presumably because the nuclear accumulation of these mutants is more dependent on dephosphorylation of the TP sites that are preferentially targeted by PP2A-Cdc55 (*45*). Interestingly, T320S and T347S mutations also advanced nuclear import (**Fig 6E**), likely because the phosphatase Cdc14 preferentially dephosphorylates SP sites (**Fig 3H**) (Bremmer *et al*., 2012; Touati *et al*., 2019).

Programming different stable nuclear plateau levels spanning from G1/S to M/G1

As observed in several cases for both Psy4- and Dna2-based sensors, manipulating the phosphorylation sites and cyclin docking motifs does not always affect the timing of shuttling, but instead leads to different steady states of nuclear levels lasting for the whole span of S and M phases. For example, a lower constant nuclear accumulation could be programmed in the Dna2 sensor by mutating S17 to a minimal consensus site (17SPAQQ or 17SPAAK) (**Fig 7A, S7A**). The nuclear levels could also be lowered by increasing the distance between T4 and S17 (T4+GGSG), resulting in less efficient Cks1-mediated phosphorylation of S17 (**Fig 6D, 7A**). Interestingly, the lowest nuclear level was observed with the S17T mutation (**Fig 7A**). Furthermore, while addition of a G1-CDK-specific docking motif shifted the timing of nuclear entry, it also increased the constant plateau level (**Fig 6D**). These results indicate that due to the different localization patterns of cyclins (*38, 49, 51*), CDK activity does not accumulate uniformly in the cytoplasm during the cell cycle. Apparently, the high cytoplasmic abundance of G1 cyclin Cln2 could result in an early peak in cytoplasmic Cdk1 activity. This may be the cause of the nearly flat overall nuclear profile of the sensor as the Dna2-based sensor is cytoplasmic in G1 and the NLS-activating phosphorylation as an entry trigger should also take place in the cytoplasm.

Similarly, in the Psy4- and Mcm2/3-based sensors, we could demonstrate a wide-range ladder of controlled steady nuclear plateaus (**Fig 7B, S7B**). The lowest constant nuclear concentration from G1/S to mitosis was achieved by addition of a G1-CDK docking motif to the wild-type Psy4 sensor, while the next step on the ladder could be achieved by further mutating the sites T320 and S364. The optimal LP motif efficiently targets G1-Cdk1 activity to phosphorylate the Psy4 module, resulting in rapid nuclear exit at G1/S, followed by a period with no further decrease in nuclear concentration, presumably due to degradation of Cln2 or because of full phosphorylation of the modules. As the T347A mutation prohibits full NLS inactivation, this mutant is expected to have higher nuclear abundance in the state where all other sites are phosphorylated. By replacing the native NES from Mcm3 with the weaker NES from Psy4, an intermediate plateau was observed. As this replacement does not affect the phosphorylation sites adjacent to the Mcm3 NLS, phospho-regulation is likely unaffected, but a different nuclear-cytoplasmic ratio is achieved due to the relative strength of NLS and NES motifs. Using just a single weak NLS-inhibiting site and S/T swapping, two higher steps can be added to the ladder (**Fig 7B**). While the module carrying S320 is partially translocated at G1/S, the module with just T347 is not affected by progression to S phase. Among other ways to fine-tune the higher levels of the nuclear plateau is to mutate the NES on the Mcm2/3-based sensor (**Fig 7B**). This leads to phosphorylation of the NLS-inactivating sites at G1/S, accompanied by rapid translocation of a small fraction and constant high nuclear levels over the cell cycle.

Discussion

Our study demonstrates that the cyclins accumulating from G1 to the mitotic peak and declining during mitotic exit can create different dynamic output shapes for CDK-regulated protein functions via phospho-regulation of NLS and NES signals. These different oscillatory patterns of CDK input-output functions depend on various parameters including the kinetics of the downstream steps (nuclear entry and exit rates), phosphatase specificity, cyclin specificity in substrate docking, and Cks1-dependent phospho-docking connections. Our data suggest that the kinetics of downstream steps may be as important as the CDK/phosphatase activity thresholds in defining the order and temporal dynamics of CDK-driven events (**Fig S1A**). We also find that linking the NLS and NES phospho-regulation via Cks1-dependent docking may play an important part in establishing the nuclear import-export equilibria of CDK targets.

We observed that CDK-dependent fast export combined with the phosphorylation-induced block of re-entry can result in a very abrupt early nuclear exit switch. On the other hand, just a single alanine mutation (T347A) in the 6-site network can turn the profile from ultrasensitive switch to a graded response. Remarkably, the gradual profile can be turned back to an abrupt switch by G1-CDK specific docking. These observations are related to one of the important challenges in kinase signaling: how to process a graded input into an

ultrasensitive all-or-none output (**Fig 7C**) (*12*). Furthermore, the T320A-S364A-Psy4 sensor was not responsive to the accumulation of CDK activity until mitosis (**Fig 2A**). However, in mitosis, an ultrasensitive nuclear exit profile was formed, which was further enhanced by addition of the M-CDK docking motif LxF (**Fig 2E**). Surprisingly, when only the suboptimal CDK site S364 site was added back, the ultrasensitive exit profile was shifted by 30 minutes, from the M phase to G1/S (**Fig 1D**). Considering the 90-minute span of the cell cycle, such reprogramming of ultrasensitive output profiles with widely separated timing would likely be difficult to design by introducing only a minor change in the number of sites from six to four using simple distributive multisite-phosphorylation-based ultrasensitivity mechanism (*12*).

To compare the mechanism of temporal resolution of CDK switches in the case of direct linear threshold-to-switch systems and the more complex equilibrium systems (NLS-NES), one has to consider the concept of the "rate-limiting step" in CDK multisite phosphorylation systems. In our previous studies we have focused on CDK multisite phosphorylation of targets with di-phospho degrons (*26*, *27*). In these cases, the rate-limiting phosphorylation step was a non-consensus CDK site, a crucial part of the degron, the end output of the Cks1-driven multisite process. Alone, without Cks1 and cyclin docking, these sites would remain unphosphorylated even at the highest mitotic thresholds of CDK (*26*). Alternatively, in the NLS-NES equilibrium type Psy4-based sensors, there are two limiting steps and two outputs. High phosphatase activity limits the phosphorylation of NLS-regulating T320-T347 (*45*), while NES regulating sites are suboptimal CDK consensus sites. Cks1-dependent docking links the NLS inactivating sites and NES activating sites. By changing the multisite phosphorylation patterns one could also tune the shape and timing of the sensor localization profile, which is a step further in complexity from the single degron. However, the common feature of the two alternative systems is the Cks1-driven CDK filter that allows only CDK but not the other proline-specific kinases to trigger the switch.

Another important outcome of the study relates to our understanding of CDK thresholds, substrate sensitivity to CDK inhibition, and the role of cyclin specificity. According to the quantitative model of CDK function (*52*, *53*), more CDK activity is required to drive mitosis than to trigger S phase, and this model is thought to be supported by the sensitivity of different transitions to Cdk1 inhibition. The Cdk1-as1 strain can be arrested at G2/M with 500 nM inhibitor and in both G1 and G2/M with a 5 μM dose, which is similar to the analogous Cdk1-as strain of *S. pombe* (*48*, *53*). Such inhibitor doses have been used to define the G1/S and G2/M CDK thresholds in both yeast model organisms (*48*, *53*). According to the threshold model, the timing of cell cycle events is a product of the direct translation of accumulating CDK activity into the sequential timing of various

switches. The faster the cyclin concentration rises the earlier the switches should take place. However, paradoxically, overexpression or deletion of major cyclins in yeast has only a minor effect on cell cycle dynamics (Oikonomou and Cross, 2011; Pirincci Ercan *et al*., 2021). Similarly, in mammalian cells, cyclin and CDK knockouts revealed that the loss of several cyclins and Cdks is tolerated (*54*).

The experiments in Figure 4B show that the execution of the phosphorylation switch of a low-threshold G1/S target, the Psy4-based sensor, is lost when Cdk1 activity is only slightly reduced with a dose of 100 nM inhibitor. Thus, we cannot exclude the possibility that the putative "high CDK threshold mitotic targets" that are responsible for low-dose (300-500 nM) inhibitor-induced G2/M arrest (*48*, *53*) may actually require low CDK activity, as seen with Psy4-like inhibitor-sensitive low-threshold early G1/S targets. In principle, the targets crucial for mitosis and the metaphase-anaphase transition could be phosphorylated at the G1/S threshold. Deletion, overexpression, or placement of *CLB2* at the *CLB5* locus does not have a major impact on the pace or sequence of cell cycle events, suggesting that the cell tolerates early accumulation of the CDK activity corresponding to late mitotic CDK thresholds.

Intriguingly, the weaker activity of Cdk1-as1 results in a longer cell cycle, as in yeast cells in poor nutrient conditions with slower cyclin accumulation (*55–57*). In rich media, as suggested by high tolerance to cyclin deletions, CDK activity accumulates excessively, perhaps to guarantee robustness. In conditions with low net CDK activity, the phosphorylation of a minimal set of targets during a narrow low threshold window (potentially including those involved in mitotic events) could be sufficient to accomplish the cycle. Inhibitor-sensitive substrates like Psy4, however, could be important for fine-tuning for better fitness in rich media with an excess of CDK activity. Indeed, this alternative view does not exclude the possibility that the targets modified at the low G1/S threshold time window have different inhibitor sensitivity. Those that need to be 100% phosphorylated to prevent relicensing and re-replication have higher phosphorylation specificity than those that can execute their downstream processes when partially phosphorylated (**Fig 7D**). Interestingly, we cannot exclude an alternative possibility that the ability of cyclin specificity to temporally resolve different switches (*26*, *32*) is not simply to time the onset of specific cell cycle processes but is instead needed to mitigate substrate competition. The cell contains hundreds of targets whose K_Ms are relatively low for particular cyclin-CDK complexes, but high for the others (*2*, *33*).

In conclusion, our results provide a broader view of the dynamics and specificity of CDK signaling, shedding light on how a single protein kinase can temporally coordinate such an intricate process as cell division. Our study also suggests that CDK-dependent phospho-regulation of NLS and NES motifs surrounded by different multisite phosphorylation patterns can potentially be a flexible way to tune and control both entry-exit timing and the nuclear levels of CDK targets. Such a toolbox of multisite phosphorylation rules, described here and in our previous studies (*26*, *27*) may prove to be useful in next-generation synthetic circuit design for synthetic biology applications that aim for better dynamic control of cellular signaling.

Materials and Methods

Yeast strains and plasmids

S. cerevisiae strains were derived from W303 and are described in **Table S1**. Gene deletions and tagging were performed using PCR and homologous recombination based approach (*58*). Mcm2/3 NLS-NES (*35*) was cloned into pRS304 with PADH1 and mCherry coding sequence. The plasmid was linearized with PacI and integrated to PADH1 locus. Psy4 and Dna2 nuclear localization modules were cloned into pRG203MX with PACT1 and superfolder GFP (*59*). pRG203MX enables guaranteed single copy integration of the vector (*60*). Prior to yeast transformation, the pRG203MX-based plasmids were linearized with SgsI.

Time-lapse fluorescence microscopy

Prior to microscopy experiments, the cells were grown at 30 °C in synthetic complete media (SC) supplemented with 2% glucose to OD600 0.2-0.6. The culture was pipetted on 0.8 mm cover glass and covered with a 1-mm thick 1.5% agarose (NuSieveTM GTGTM Agarose, Lonza) SC/glucose pad. The sample was kept under the microscope for 1 hour before starting the experiment. The experiments were carried out using Zeiss Observer Z1 microscope with a 63×/1.4NA oil immersion objective and Axiocam 506 mono camera (Zeiss). The sample was kept at 30 °C with Tempcontrol 37–2 digital (PeCon). The cells were imaged for phase-contrast, GFP and mCherry with 3x3 binning every three minutes. The experiments were up to 8 hours long and up to 12 positions were followed using ZEN software (Zeiss), an automated stage and Definite Focus. Filter set 61 HE (Zeiss) in combination with Colibri 470 and Colibri 540-580 LED modules with exposure times of 15 ms and 450 ms were used for imaging of sfGFP and mCherry, respectively. The Colibri LED modules were used at 25% power.

Image segmentation, cell tracking, and quantification of fluorescence signals was performed using MATLAB (The MathWorks, Inc.) as described in (*61*). All plots with microscopy data contain data from at least two experiments, the number of cells analyzed from each construct is presented in **Table S1**.

Western blotting

Dna2(1-100)-sfGFP and Psy4(315-441)-sfGFP were tagged with 6HA as described in (*58*). The yeast cultures were grown at 30 °C in YPD medium to OD600 0.3, followed by addition of 1 μg/ml α-factor and incubation for 2.5 hours to arrest cells in G1 phase. Then, the cells were washed thoroughly to remove α-factor and were resuspended in fresh YPD medium and grown at 30 °C. Cells from 5 ml of the culture were collected and flash frozen in liquid nitrogen every 10 minutes.

Cells were lysed by bead beating in lysis buffer containing urea. The proteins were separated using Phos-tag SDS-PAGE with 8% acrylamide, 50 μM Phos-tag and 100 μM $MnCl_2$ as described in (*62*). The electrophoresis was carried out at 15 mA for 1.5 hours. Prior to transfer, the gels were soaked in TBS-T buffer containing 10 mM EDTA for 30 minutes. The transfer to nitrocellulose membrane was performed using the standard semidry transfer with Pierce G2 Fast Blotter (Thermo Scientific). Purified anti-HA.11 epitope tag antibody (1:500) (clone 16B12, BioLegend Cat. No. 901501) and HRP-conjugated anti-mouse antibody (1:7,500) from Labas, Estonia were used to detect the 6HA-tagged proteins.

Protein purification

Dna2(1-100)-sfGFP, Psy4(315-441)-sfGFP, Sic1 and Cdc14 were cloned to pET28a and were expressed in E. coli BL21RP cells as fusion proteins with N-terminal 6xHis tag. Sic1 was expressed at 37 °C using 1 mM IPTH, while Dna2 and Psy4 constructs were expressed at 30 °C using 0.5 mM IPTG. The proteins were purified using immobilized cobalt affinity chromatography and imidazole for elution. The expression of 6xHis-Cdc14 was induced with 0.125 mM IPTG at 23 °C, followed by purification using nickel affinity chromatography.

Clb2-Cdk1 and Clb5-Cdk1 complexes were purified from yeast extract of the respective cyclin-TAP overexpression culture using tandem affinity purification method as described previously (*6, 63*). For purification of Cln2-Cdk1, Cln2 was N-terminally tagged with 3HA, overexpressed from P_{GAL1} promoter and purified using immunoaffinity chromatography as described previously (*64*). Cks1 was purified from *E. coli* BL21RP extracts as described (*65*).

PP2A-Cdc55 complex was purified from yeast cells containing 3HA-tagged Cdc55 (*66*). The yeast culture was grown in YPD to OD600=1.4, the cells were collected, snap frozen and lysed using Mixer Mill MM 400. The lysate was cleared by centrifugation and the supernatant was incubated with anti-HA agarose beads for 3 hours. The beads were washed thoroughly and PP2A-Cdc55 was eluted with buffer containing HA dipeptide.

In vitro phosphorylation assays

The general composition of the phosphorylation experiments was as follows: 50 mM Hepes-KOH, pH 7.4, 150 mM NaCl, 5 mM $MgCl_2$, 20 mM imidazole, 2% glycerol, 0.2 mg/ml BSA, 500 nM Cks1 and 500 μM ATP [(with added [γ-^{32}P]-ATP (Hartmann Analytic)]. The substrate protein concentration was 1 μM (in the linear [S] versus initial velocity range, several-fold below the estimated K_M value), cyclin-Cdk1 complex concentration was 0.2 nM. The reactions were carried out at room temperature and were stopped at the indicated time points by addition of SDS-PAGE sample buffer. For analysis of multisite phosphorylation, the proteins were separated using Phos-tag SDS-PAGE (8% acrylamide, 50 μM Phos-tag) as described in (*62*).

For the dephosphorylation assays, the Dna2- and Psy4-based purified substrate proteins were phosphorylated with Clb5-Cdk1 at room temperature for 20 (Psy4) or 60 (Dna2) minutes in the following buffer: 20 mM Tris-HCl, pH 7.4, 50 mM HEPES-KOH, pH 7.4, 210 mM NaCl, 5 mM $MgCl_2$, 80 mM imidazole, 2% glycerol, 0.2 mg/ml BSA, and 500 μM ATP [(with added [γ-^{32}P]-ATP (Hartmann Analytic)]. Then, an aliquot of the reaction was pipetted to SDS-PAGE sample buffer to measure the phosphorylated protein ^{32}P signal and a mixture containing Sic1 and either Cdc14 or PP2A-Cdc55 phosphatase was added to the rest of the phosphorylation reaction. Sic1 was added to inhibit further phosphorylation of the substrate proteins by Clb5-Cdk1. At 5, 20 and 60 minutes an aliquot of the reaction was pipetted to SDS-PAGE sample buffer to stop the dephosphorylation reaction. The samples were run on SDS-PAGE, the gels were dried and ^{32}P signals were detected using an Amersham Typhoon 5 Biomolecular Imager (GE Healthcare Life Sciences) and were quantified using ImageQuant TL (Amersham Biosciences).

References

1. J. Bloom, F. R. Cross, Multiple levels of cyclin specificity in cell-cycle control. *Nat. Rev. Mol. Cell Biol.* **8**, 149–160 (2007).

2. M. Kõivomägi, E. Valk, R. Venta, A. Iofik, M. Lepiku, D. O. Morgan, M. Loog, Dynamics of Cdk1 Substrate Specificity during the Cell Cycle. *Mol. Cell*. **42**, 610–623 (2011).

3. B. R. Topacio, E. Zatulovskiy, S. Cristea, S. Xie, C. S. Tambo, S. M. Rubin, J. Sage, M. Kõivomägi, J. M. Skotheim, Cyclin D-Cdk4,6 Drives Cell-Cycle Progression via the Retinoblastoma Protein's C-Terminal Helix. *Mol. Cell*. **0** (2019), doi:10.1016/j.molcel.2019.03.020.

4. M. Kõivomägi, M. P. Swaffer, J. J. Turner, G. Marinov, J. M. Skotheim, G1 cyclin–Cdk promotes cell cycle entry through localized phosphorylation of RNA polymerase II. *Science*. **374**, 347 (2021).

5. D. O. Morgan, *The cell cycle : principles of control* (New Science Press, 2007; https://books.google.ee/books/about/The_Cell_Cycle.html?id=ScEuiD2V6GoC&redir_esc=y).

6. J. A. Ubersax, E. L. Woodbury, P. N. Quang, M. Paraz, J. D. Blethrow, K. Shah, K. M. Shokat, D. O. Morgan, Targets of the cyclin-dependent kinase Cdk1. *Nature*. **425**, 859–864 (2003).

7. J. M. Enserink, R. D. Kolodner, An overview of Cdk1-controlled targets and processes. *Cell Div.* **5**, 11 (2010).

8. S. Kosugi, M. Hasebe, M. Tomita, H. Yanagawa, Systematic identification of cell cycle-dependent yeast nucleocytoplasmic shuttling proteins by prediction of composite motifs. *Proc. Natl. Acad. Sci. U. S. A.* **106**, 10171–10176 (2009).

9. J. D. Nardozzi, K. Lott, G. Cingolani, Phosphorylation meets nuclear import: a review. *Cell Commun. Signal. 2010 81*. **8**, 1–17 (2010).

10. D. Pirincci Ercan, F. Chrétien, P. Chakravarty, H. R. Flynn, A. P. Snijders, F. Uhlmann, Budding yeast relies on G1 cyclin specificity to couple cell cycle progression with morphogenetic development. *Sci. Adv.* **7**, eabg0007 (2021).

11. J. E. Ferrell, Tripping the switch fantastic: how a protein kinase cascade can convert graded inputs into switch-like outputs. *Trends Biochem. Sci.* **21**, 460–466 (1996).

12. J. E. Ferrell, S. H. Ha, S. H. Ha, Ultrasensitivity part II: multisite phosphorylation, stoichiometric inhibitors, and positive feedback. *Trends Biochem. Sci.* **39**, 556–569 (2014).

13. M. Thomson, J. Gunawardena, Unlimited multistability in multisite phosphorylation systems. *Nature*. **460**, 274–277 (2009).

14. J. B. Asfaha, M. Örd, C. R. Carlson, I. Faustova, M. Loog, D. O. Morgan, Multisite

phosphorylation by Cdk1 initiates delayed negative feedback to control mitotic transcription. *Curr. Biol.* **32**, 256-263.e4 (2022).

15. J. R. Pomerening, E. D. Sontag, J. E. Ferrell, Building a cell cycle oscillator: Hysteresis and bistability in the activation of Cdc2. *Nat. Cell Biol.* **5**, 346–351 (2003).

16. L. Ou, M. B. Waddell, R. W. Kriwacki, Mechanism of Cell Cycle Entry Mediated by the Intrinsically Disordered Protein, p27Kip1. *ACS Chem. Biol.* **7**, 678 (2012).

17. R. Venta, E. Valk, M. Örd, O. Košik, K. Pääbo, A. Maljavin, R. Kivi, I. Faustova, N. Shtaida, M. Lepiku, K. Möll, A. Doncic, M. Kõivomägi, M. Loog, A processive phosphorylation circuit with multiple kinase inputs and mutually diversional routes controls G1/S decision. *Nat. Commun.* **11**, 1836 (2020).

18. M. Örd, R. Venta, K. Möll, E. Valk, M. Loog, Cyclin-Specific Docking Mechanisms Reveal the Complexity of M-CDK Function in the Cell Cycle. *Mol. Cell*. **75**, 76--89.e3 (2019).

19. J. Gerardin, N. R. Reddy, W. A. Lim, The Design Principles of Biochemical Timers: Circuits that Discriminate between Transient and Sustained Stimulation. *Cell Syst.* **9**, 297-308.e2 (2019).

20. J. R. Burke, G. L. Hura, S. M. Rubin, Structures of inactive retinoblastoma protein reveal multiple mechanisms for cell cycle control. *Genes Dev.* **26**, 1156 (2012).

21. R. M. Gordley, R. E. Williams, C. J. Bashor, J. E. Toettcher, S. Yan, W. A. Lim, Engineering dynamical control of cell fate switching using synthetic phospho-regulons. *Proc. Natl. Acad. Sci.* **113**, 13528–13533 (2016).

22. S. Liokatis, A. Stützer, S. Elsässer, F. Theillet, R. Klingberg, B. van Rossum, D. Schwarzer, C. Allis, W. Fischle, P. Selenko, Phosphorylation of histone H3 Ser10 establishes a hierarchy for subsequent intramolecular modification events. *Nat. Struct. Mol. Biol.* **19**, 819–823 (2012).

23. A. Mylona, F. Theillet, C. Foster, T. Cheng, F. Miralles, P. Bates, P. Selenko, R. Treisman, Opposing effects of Elk-1 multisite phosphorylation shape its response to ERK activation. *Science*. **354**, 233–237 (2016).

24. N. A. Lyons, B. R. Fonslow, J. K. Diedrich, J. R. Yates, D. O. Morgan, D. O. Morgan, Sequential primed kinases create a damage-responsive phosphodegron on Eco1. *Nat. Struct. Mol. Biol.* **20**, 194–201 (2013).

25. M. Kõivomägi, E. Valk, R. Venta, A. Iofik, M. Lepiku, E. R. M. Balog, S. M. Rubin, D. O. Morgan, M. Loog, Cascades of multisite phosphorylation control Sic1 destruction at the onset of S phase. *Nature*. **480**, 128–131 (2011).

26. M. Örd, K. Möll, A. Agerova, R. Kivi, I. Faustova, R. Venta, E. Valk, M. Loog, Multisite phosphorylation code of CDK. *Nat. Struct. Mol. Biol.* **26**, 649–658 (2019).

27. I. Faustova, L. Bulatovic, F. Matiyevskaya, E. Valk, M. Örd, M. Loog, A new linear cyclin docking motif that mediates exclusively S-phase CDK-specific signaling. *EMBO J.* (2020), doi:10.15252/embj.2020105839.

28. B. A. Schulman, D. L. Lindstrom, E. D. Harlow, "Substrate recruitment to cyclin-dependent kinase 2 by a multipurpose docking site on cyclin A" (1998), (available at www.pnas.org.).

29. J. A. Wohlschlegel, B. T. Dwyer, D. Y. Takeda, A. Dutta, Mutational analysis of the Cy motif from p21 reveals sequence degeneracy and specificity for different cyclin-dependent kinases. *Mol. Cell. Biol.* **21**, 4868–4874 (2001).

30. S. Bhaduri, P. M. Pryciak, Cyclin-specific docking motifs promote phosphorylation of yeast signaling proteins by G1/S Cdk complexes. *Curr. Biol.* **21**, 1615–1623 (2011).

31. S. Bandyopadhyay, S. Bhaduri, M. Örd, N. E. Davey, M. Loog, P. M. Pryciak, Comprehensive Analysis of G1 Cyclin Docking Motif Sequences that Control CDK Regulatory Potency *In Vivo*. *Curr. Biol.* **30**, 4454--4466.e5 (2020).

32. M. Örd, K. K. Puss, R. Kivi, K. Möll, T. Ojala, I. Borovko, I. Faustova, R. Venta, E. Valk, M. Kõivomägi, M. Loog, Proline-Rich Motifs Control G2-CDK Target Phosphorylation and Priming an Anchoring Protein for Polo Kinase Localization. *Cell Rep.* **31** (2020), doi:10.1016/j.celrep.2020.107757.

33. M. Loog, D. O. Morgan, Cyclin specificity in the phosphorylation of cyclin-dependent kinase substrates. *Nature*. **434**, 104–108 (2005).

34. B. M. O'Neill, S. J. Szyjka, E. T. Lis, A. O. Bailey, J. R. Yates, O. M. Aparicio, F. E. Romesberg, Pph3–Psy2 is a phosphatase complex required for Rad53 dephosphorylation and replication fork restart during recovery from DNA damage. *Proc. Natl. Acad. Sci.* **104**, 9290–9295 (2007).

35. M. E. Liku, V. Q. Nguyen, A. W. Rosales, K. Irie, J. J. Li, CDK phosphorylation of a

novel NLS-NES module distributed between two subunits of the Mcm2-7 complex prevents chromosomal rereplication. *Mol. Biol. Cell*. **16**, 5026–5039 (2005).

36. B. Stern, P. Nurse, A quantitative model for the cdc2 control of S phase and mitosis in fission yeast. *Trends Genet.* **12**, 345–350 (1996).

37. M. P. Swaffer, A. W. Jones, H. R. Flynn, A. P. Snijders, P. Nurse, CDK Substrate Phosphorylation and Ordering the Cell Cycle. *Cell*. **167**, 1750--1761.e16 (2016).

38. F. R. Cross, M. Yuste-Rojas, S. Gray, M. D. Jacobson, Specialization and Targeting of B-Type Cyclins. *Mol. Cell*. **4**, 11–19 (1999).

39. F. Hu, O. M. Aparicio, Swe1 regulation and transcriptional control restrict the activity of mitotic cyclins toward replication proteins in Saccharomyces cerevisiae. *Proc. Natl. Acad. Sci. U. S. A.* **102**, 8910 (2005).

40. M. J. DeVit, M. Johnston, The nuclear exportin Msn5 is required for nuclear export of the Mig1 glucose repressor of Saccharomyces cerevisiae. *Curr. Biol.* **9**, 1231–1241 (1999).

41. D. A. McGrath, E. R. M. Balog, M. Kõivomägi, R. Lucena, M. V Mai, A. Hirschi, D. R. Kellogg, M. Loog, S. M. Rubin, Cks confers specificity to phosphorylation-dependent CDK signaling pathways. *Nat. Struct. Mol. Biol.* **20**, 1407–1414 (2013).

42. M. Kõivomägi, M. Örd, A. Iofik, E. Valk, R. Venta, I. Faustova, R. Kivi, E. R. M. Balog, S. M. Rubin, M. Loog, Multisite phosphorylation networks as signal processors for Cdk1. *Nat. Struct. Mol. Biol.* **20** (2013), doi:10.1038/nsmb.2706.

43. K. Suzuki, K. Sako, K. Akiyama, M. Isoda, C. Senoo, N. Nakajo, N. Sagata, Identification of non-Ser/Thr-Pro consensus motifs for Cdk1 and their roles in mitotic regulation of C2H2 zinc finger proteins and Ect2. *Sci. Rep.* **5**, 7929 (2015).

44. M. J. Cundell, L. H. Hutter, R. Nunes Bastos, E. Poser, J. Holder, S. Mohammed, B. Novak, F. A. Barr, A PP2A-B55 recognition signal controls substrate dephosphorylation kinetics during mitotic exit. *J. Cell Biol.* **214**, 539–554 (2016).

45. M. Godfrey, S. A. Touati, M. Kataria, A. Jones, A. P. Snijders, F. Uhlmann, PP2ACdc55 Phosphatase Imposes Ordered Cell-Cycle Phosphorylation by Opposing Threonine Phosphorylation. *Mol. Cell*. **65**, 393--402.e3 (2017).

46. S. C. Bremmer, H. Hall, J. S. Martinez, C. L. Eissler, T. H. Hinrichsen, S. Rossie, L. L. Parker, M. C. Hall, H. Charbonneau, Cdc14 phosphatases preferentially

dephosphorylate a subset of cyclin-dependent kinase (Cdk) sites containing phosphoserine. *J. Biol. Chem.* **287**, 1662–1669 (2012).

47. S. A. Touati, L. Hofbauer, A. W. Jones, A. P. Snijders, G. Kelly, F. Uhlmann, Cdc14 and PP2A Phosphatases Cooperate to Shape Phosphoproteome Dynamics during Mitotic Exit. *Cell Rep.* **29**, 2105--2119.e4 (2019).

48. A. C. Bishop, J. A. Ubersax, D. T. Pøtsch, D. P. Matheos, N. S. Gray, J. Blethrow, E. Shimizu, J. Z. Tsien, P. G. Schultz, M. D. Rose, J. L. Wood, D. O. Morgan, K. M. Shokat, A chemical switch for inhibitor-sensitive alleles of any protein kinase. *Nat. 2000 4076802*. **407**, 395–401 (2000).

49. N. P. Edgington, B. Futcher, Relationship between the function and the location of G1 cyclins in S. cerevisiae. *J. Cell Sci.* **114**, 4599–4611 (2001).

50. M. E. Miller, F. R. Cross, Distinct subcellular localization patterns contribute to functional specificity of the Cln2 and Cln3 cyclins of Saccharomyces cerevisiae. *Mol. Cell. Biol.* **20**, 542–555 (2000).

51. E. Bailly, S. Cabantous, D. Sondaz, A. Bernadac, M.-N. Simon, Differential cellular localization among mitotic cyclins from Saccharomyces cerevisiae: a new role for the axial budding protein Bud3 in targeting Clb2 to the mother-bud neck. *J. Cell Sci.* **116**, 4119–4130 (2003).

52. D. L. Fisher, P. Nurse, A single fission yeast mitotic cyclin B p34cdc2 kinase promotes both S-phase and mitosis in the absence of G1 cyclins. *EMBO J.* **15**, 850–860 (1996).

53. D. Coudreuse, P. Nurse, Driving the cell cycle with a minimal CDK control network. *Nature*. **468**, 1074–1079 (2010).

54. A. Satyanarayana, P. Kaldis, Mammalian cell-cycle regulation: several Cdks, numerous cyclins and diverse compensatory mechanisms. *Oncogene 2009 2833*. **28**, 2925–2939 (2009).

55. B. L. Schneider, J. Zhang, J. Markwardt, G. Tokiwa, T. Volpe, S. Honey, B. Futcher, Growth Rate and Cell Size Modulate the Synthesis of, and Requirement for, G 1 - Phase Cyclins at Start . *Mol. Cell. Biol.* **24**, 10802–10813 (2004).

56. A. Jasani, T. Huynh, D. R. Kellogg, Growth-Dependent Activation of Protein Kinases Suggests a Mechanism for Measuring Cell Growth. *Genetics*. **215**, 729–746 (2020).

57. R. M. Leitao, D. R. Kellogg, The duration of mitosis and daughter cell size are modulated by nutrients in budding yeast. *J. Cell Biol.* **216**, 3463–3470 (2017).

58. C. Janke, M. M. Magiera, N. Rathfelder, C. Taxis, S. Reber, H. Maekawa, A. Moreno-Borchart, G. Doenges, E. Schwob, E. Schiebel, M. Knop, A versatile toolbox for PCR-based tagging of yeast genes: new fluorescent proteins, more markers and promoter substitution cassettes. *Yeast*. **21**, 947–962 (2004).

59. J. D. Pédelacq, S. Cabantous, T. Tran, T. C. Terwilliger, G. S. Waldo, Engineering and characterization of a superfolder green fluorescent protein. *Nat. Biotechnol.* **24**, 79–88 (2006).

60. R. Gnügge, T. Liphardt, F. Rudolf, A shuttle vector series for precise genetic engineering of *Saccharomyces cerevisiae*. *Yeast*. **33**, 83–98 (2016).

61. A. Doncic, U. Eser, O. Atay, J. M. Skotheim, An algorithm to automate yeast segmentation and tracking. *PLoS One*. **8**, e57970 (2013).

62. M. Örd, M. Loog, in *Methods in Molecular Biology* (Humana Press Inc., 2020; https://pubmed.ncbi.nlm.nih.gov/32696389/), vol. 2141, pp. 779–792.

63. O. Puig, F. Caspary, G. Rigaut, B. Rutz, E. Bouveret, E. Bragado-Nilsson, M. Wilm, B. Séraphin, The Tandem Affinity Purification (TAP) Method: A General Procedure of Protein Complex Purification. *Methods*. **24**, 218–229 (2001).

64. D. McCusker, C. Denison, S. Anderson, T. A. Egelhofer, J. R. Yates, S. P. Gygi, D. R. Kellogg, Cdk1 coordinates cell-surface growth with the cell cycle. *Nat. Cell Biol.* **9**, 506–515 (2007).

65. G. J. Reynard, W. Reynolds, R. Verma, R. J. Deshaies, Cks1 is required for G(1) cyclin-cyclin-dependent kinase activity in budding yeast. *Mol. Cell. Biol.* **20**, 5858–5864 (2000).

66. S. D. Anastasia, D. L. Nguyen, V. Thai, M. Meloy, T. MacDonough, D. R. Kellogg, A link between mitotic entry and membrane growth suggests a novel model for cell size control. *J. Cell Biol.* **197**, 89–104 (2012).

Acknowledgments

The authors thank E. Valk for support and D. Morgan, J. Skotheim, P. Pryciak and D. Kellogg for valuable comments on the manuscript.

Funding:
ERC Consolidator Grant 649124 (to MLo)
Centre of Excellence for Molecular Cell Technologies TK143 (to MLo)
Estonian Research Council grant PRG550 (to MLo)

Author contributions:
Conceptualization: IF, MÖ and MLo
Methodology: IF, MÖ, MLõ and MLo
Software: MÖ
Investigation: IF, MÖ, VK, DF, IB, KP, MLõ
Resources: IF, MÖ, IB, DF, VK, MLõ, DM
Writing: IF, MÖ and MLo
Vizualization: MÖ and MLo
Supervision: IF, MÖ and MLo
Funding acquisition: MLo

Competing interests:
Authors declare that they have no competing interests

Data and materials availability:
All data are available in the main text or the supplementary materials.

Figures

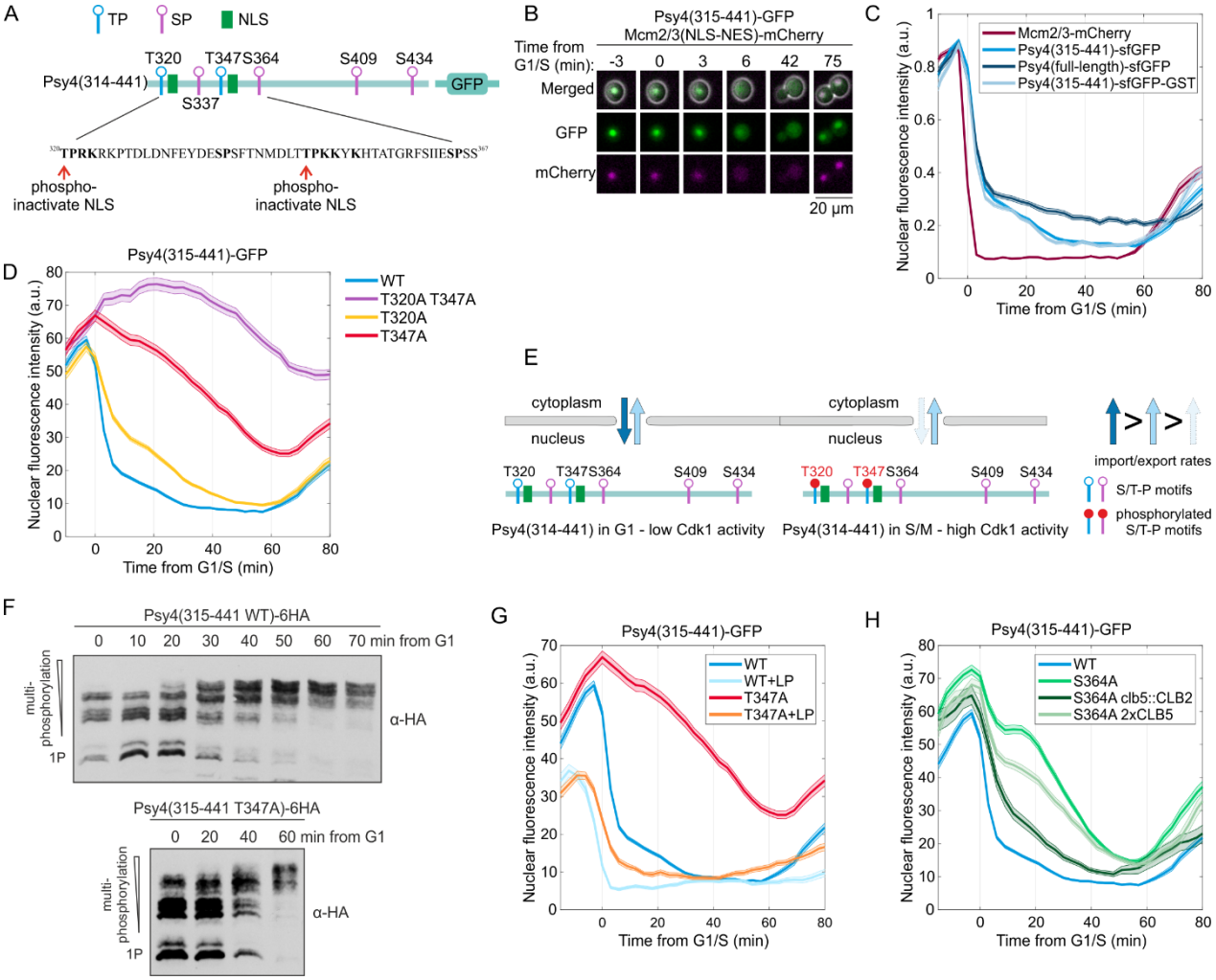

Figure 1. Multisite phosphorylation controls the nuclear export of Psy4. (A) Scheme showing the Cdk1 phosphorylation sites and NLS motifs in the disordered C terminus of Psy4 (positions 315-441). Phosphorylation of T320 and T347 inactivates the NLS (Kosugi *et al*., 2009). (B) Images showing the cell-cycle-dependent shuttling of Psy4(315-441)-GFP and Mcm2/3(NLS-NES)-mCherry sensor between the nucleus and cytoplasm. (C) Normalized nuclear fluorescence intensities of the indicated Psy4 modules during the cell cycle. Plot shows mean±SEM of cells synchronized at the time of G1/S, defined by nuclear export of 50% of the Mcm2/3 NLS-NES sensor. (D) Plot displaying mean±SEM nuclear fluorescence intensities of a population of cells expressing different Psy4-based modules synchronized at G1/S by the Mcm2/3 sensor. (E) Scheme illustrating the nuclear import/export kinetics of the Psy4 sensor without phosphorylation in G1 or upon phosphorylation in S and M phases. (F) Phosphorylation of the Psy4 modules was studied in cell cultures synchronized in G1 with α-factor and released to the cell cycle. Different phospho-forms were separated using Phos-tag SDS-PAGE. (G) Plot showing the mean±SEM nuclear fluorescence levels of the Psy4 sensors in the cell cycle. The LP motif (VLLPPFRI) was added to the C terminus of Psy4. (H) The nuclear export of Psy4-S364A module in different strains. In *clb5::CLB2* strain, an extra copy of *CLB2* is expressed from *CLB5* locus, and in *2xCLB5* strain, an extra copy of *CLB5* is expressed from an integrative plasmid. Plot shows mean±SEM nuclear Psy4-GFP fluorescence intensities.

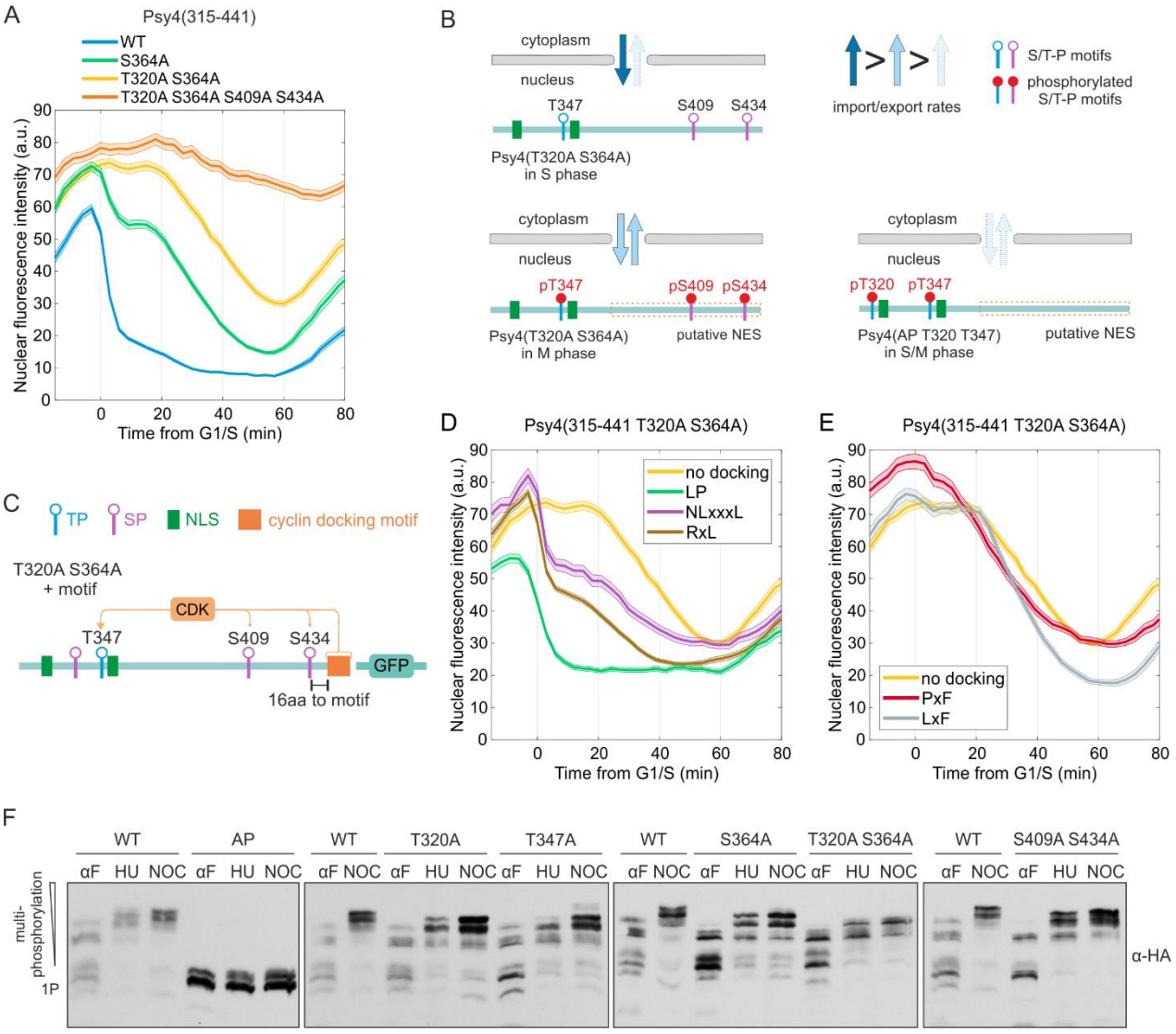

Figure 2. Combined mutations generate a mitotic localization switch. (A) The nuclear fluorescence of the indicated Psy4 modules with different phosphorylation site mutations was studied in time-lapse microscopy. Plot shows the mean±SEM Psy4-GFP nuclear fluorescence intensity. (B) Schemes illustrating the relative nuclear import/export kinetics estimated from the microscopy experiments for the indicated Psy4(315-441)-GFP sensors presented in Fig 2A and S2A. (C) Scheme showing the positioning of phosphorylation sites and added cyclin docking motifs in the Psy4 module. (D, E) The effect of cyclin docking motif addition to Psy4-T320A-S364A module. Plots show mean±SEM of the Psy4-GFP nuclear level from cells synchronized at G1/S during analysis. (F) Cells were arrested either in G1 with α-factor (αF), in S phase with hydroxyurea (HU), or in mitosis with nocodazole (NOC). The multisite phosphorylation of the indicated Psy4 module was studied using Phos-tag SDS-PAGE western blotting. AP denotes Psy4 mutant, where all CDK consensus phosphorylation sites are mutated to alanines.

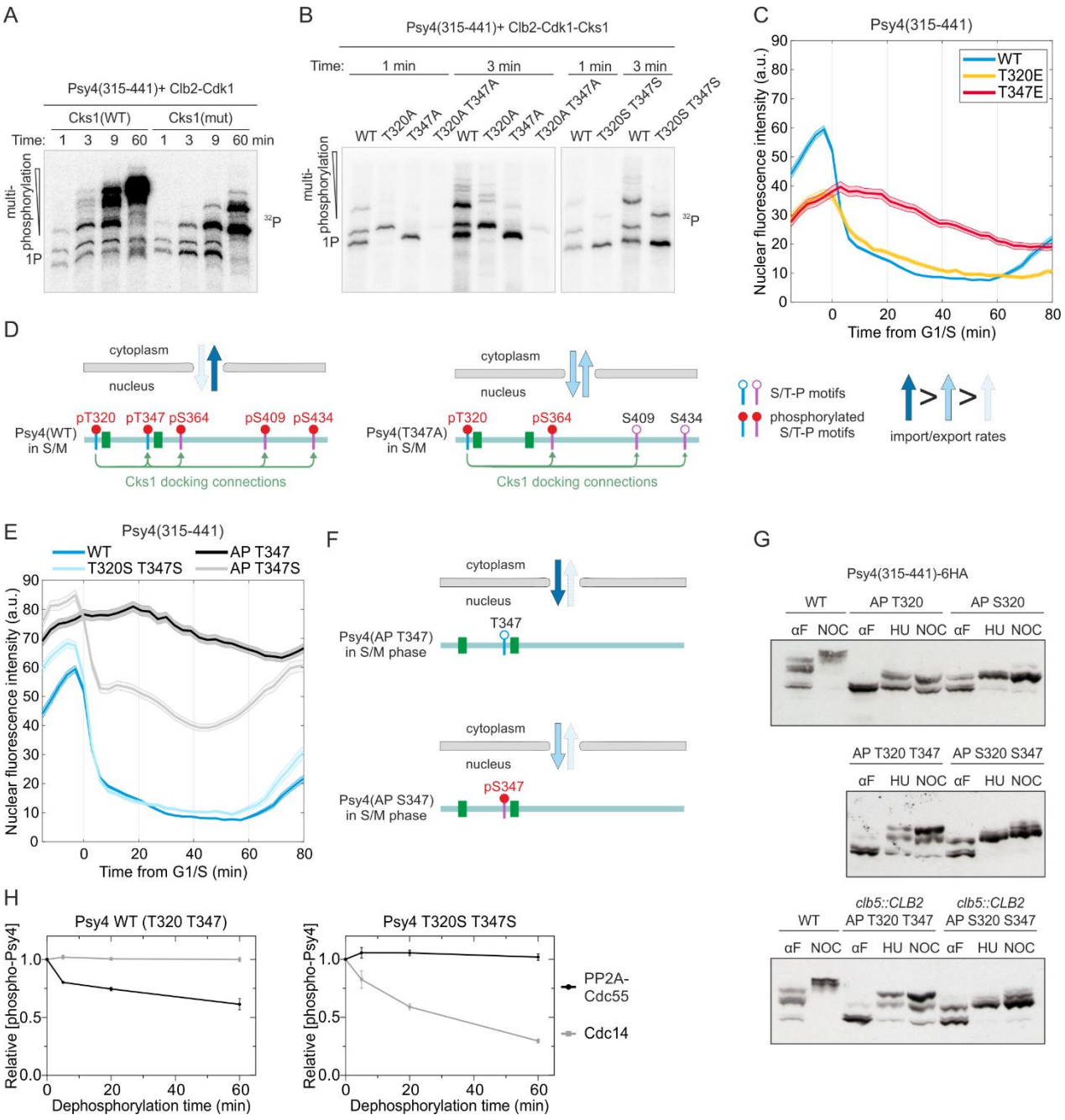

Figure 3. Multiple effects of Thr-to-Ser mutations in positions 320 and 347. (A) The multisite phosphorylation of Psy4(315-441)-GFP by Clb2-Cdk1 in complex with either wild-type or mutated Cks1 was studied *in vitro* using Phos-tag SDS-PAGE ^{32}P autoradiography. (B) *In vitro* analysis of site specificity and the contribution of Cks1 primer sites on Psy4 multisite phosphorylation by Clb2-Cdk1. The proteins were resolved on Phos-tag SDS-PAGE, ^{32}P autoradiographs are shown. (C) The effect of phospho-mimicking mutations in positions 320 and 347 was studied in microscopy; plot displays mean±SEM of nuclear fluorescence intensities of the indicated Psy4-GFP module. (D) Schemes illustrating the effect of T347A mutation on the nuclear import/export kinetics and Cks1 docking connections in Psy4(315-441)-GFP. (E) The effect of T/S mutations on the nuclear levels of

Psy4(315-441)-GFP. Plot shows mean±SEM nuclear intensities of cells aligned at the time of G1/S. (F) Depiction of estimated relative nuclear shuttling kinetics of Psy4(315-441)-GFP with T347 or S347 as the only CDK phosphorylation site. (G) Phosphorylation pattern of Psy4 modules in synchronized cell cultures was studied using Phos-tag SDS-PAGE western blotting. (H) The effect of Thr-to-Ser mutations on the dephosphorylation rate of the Psy4 module was studied *in vitro* using PP2A-Cdc55 and Cdc14 to dephosphorylate Psy4(315-441)-GFP pre-phosphorylated by Clb5-Cdk1. Plot shows mean±standard deviation of the relative remaining phospho-^{32}P Psy4 signal at indicated time points.

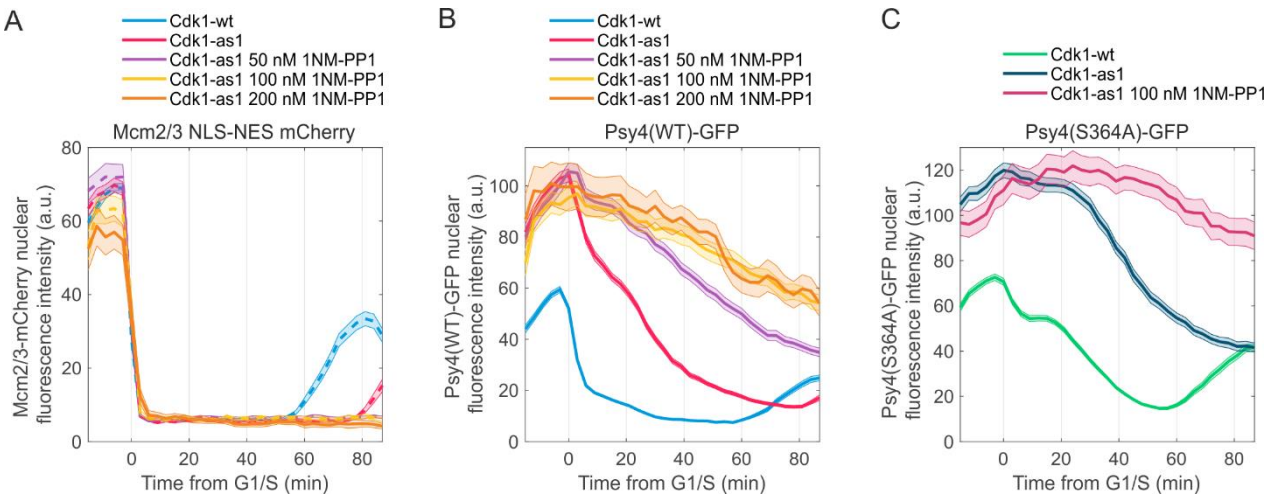

Figure 4. Differential sensitivity of G1/S targets to partial Cdk1 inhibition. (A-C) The localization dynamics of Psy4(315-441)-GFP and Mcm2/3(NLS-NES)-mCherry during the cell cycle in the presence of 1NM-PP1, the inhibitor of analog-sensitive Cdk1-as1. Plots show mean±SEM nuclear fluorescence intensities of Mcm2/3(NLS-NES)-mCherry in panel 'A', Psy4(315-441 WT)-GFP in 'B', and Psy4(315-441 S364A) in 'C'.

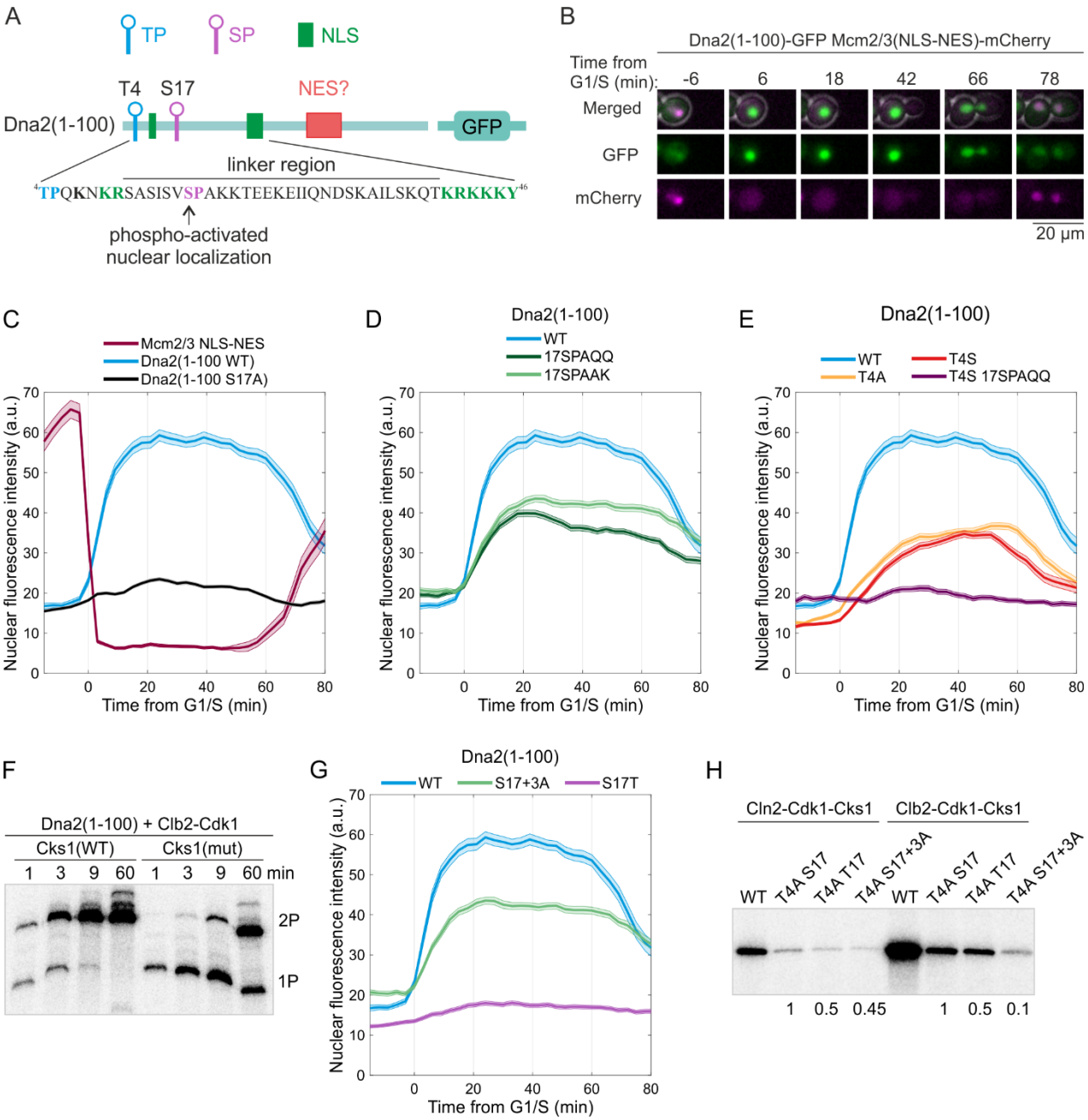

Figure 5. Cdk1-regulated nuclear import of the Dna2 module. (A) Scheme showing the Cdk1 phosphorylation sites and localization motifs in the intrinsically disordered N terminus of Dna2, positions 1-100. (B) Microscopy images showing the localization of Dna2(1-100)-GFP and Mcm2/3(NLS-NES)-mCherry during the cell cycle. Imaging was done with 3-minute interval, a selection of time points is shown. (C-E) Mean nuclear fluorescence levels of the indicated proteins during the cell cycle in a population of cells synchronized at the point of 50% nuclear export of Mcm2/3 NLS-NES sensor (denoted as time of G1/S). The plot shows mean±SEM. (F) ^{32}P autoradiographs of Phos-tag SDS-PAGE gels showing the Cks1-dependence of the multisite phosphorylation of Dna2(1-100) by Clb2-Cdk1. (G) The effect of S17T mutation on the nuclear import of Dna2(1-100)-GFP. Plots show mean±SEM.

(H) *In vitro* phosphorylation analysis of the indicated Dna2(1-100) mutants using Cln2- and Clb2-Cdk1. ^{32}P autoradiograph showing Dna2(1-100) phosphorylation under initial velocity conditions is shown.

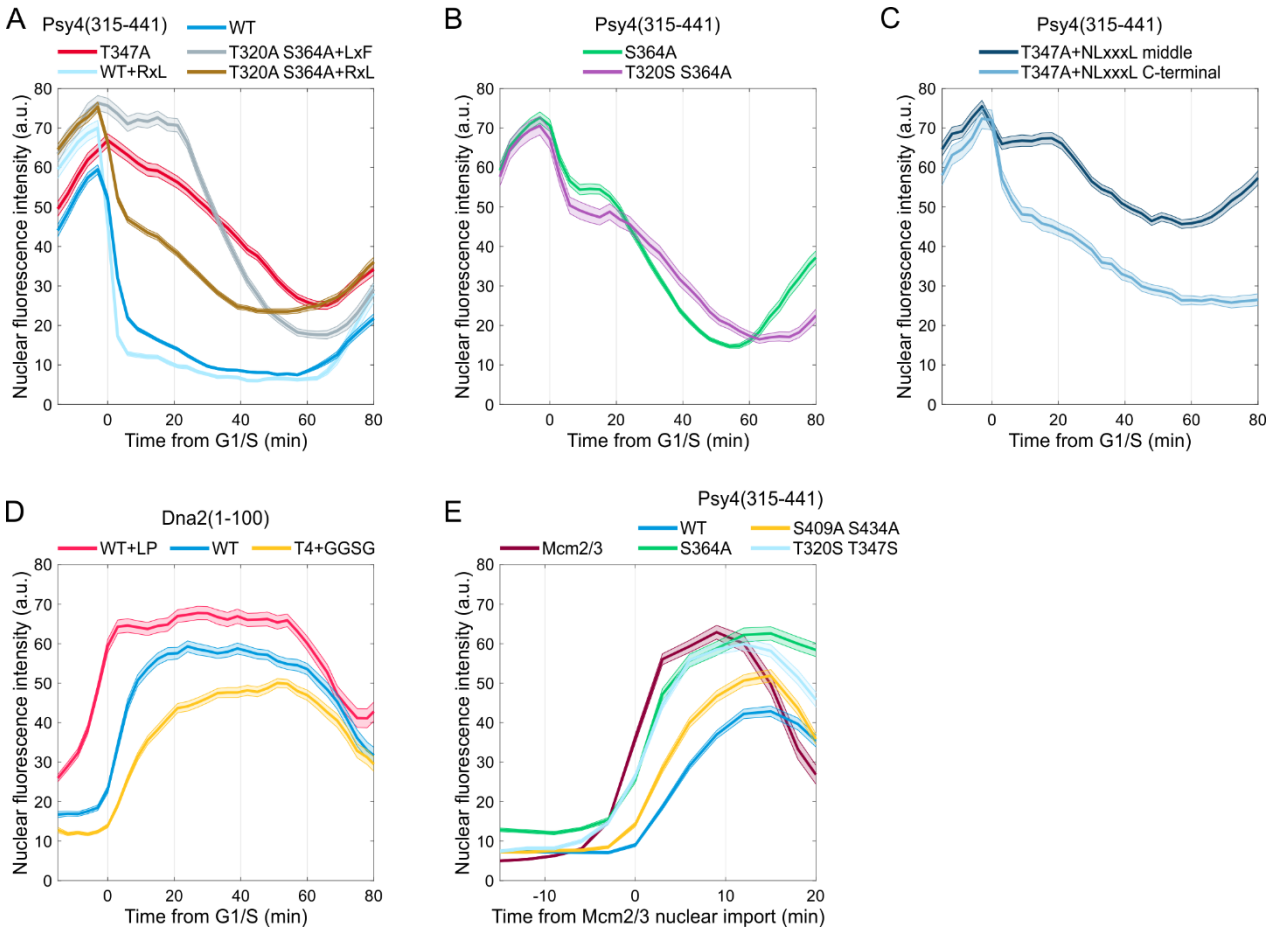

Figure 7. Encoding of CDK-regulated localization modules with different output dynamics. (A-C) Plots showing mean±SEM nuclear fluorescence intensities of the indicated Psy4(315-441)-GFP modules during the cell cycle. In panels 'A' and 'B', T347A, T320A S364A+RxL, T320A S364A+LxF and S364A have been replotted from data presented in Figure 1 and 2 to illustrate different principles. (D) Plot displaying the timing of nuclear import of different Dna2(1-100)-GFP modules. Mean±SEM of the nuclear fluorescence is shown. (E) Nuclear import of Psy4(315-441)-GFP in late mitosis was studied in time-lapse microscopy by synchronizing the cells at the nuclear import of 50% of the Mcm2/3-mCherry sensor. Plot shows mean±SEM nuclear fluorescence levels.

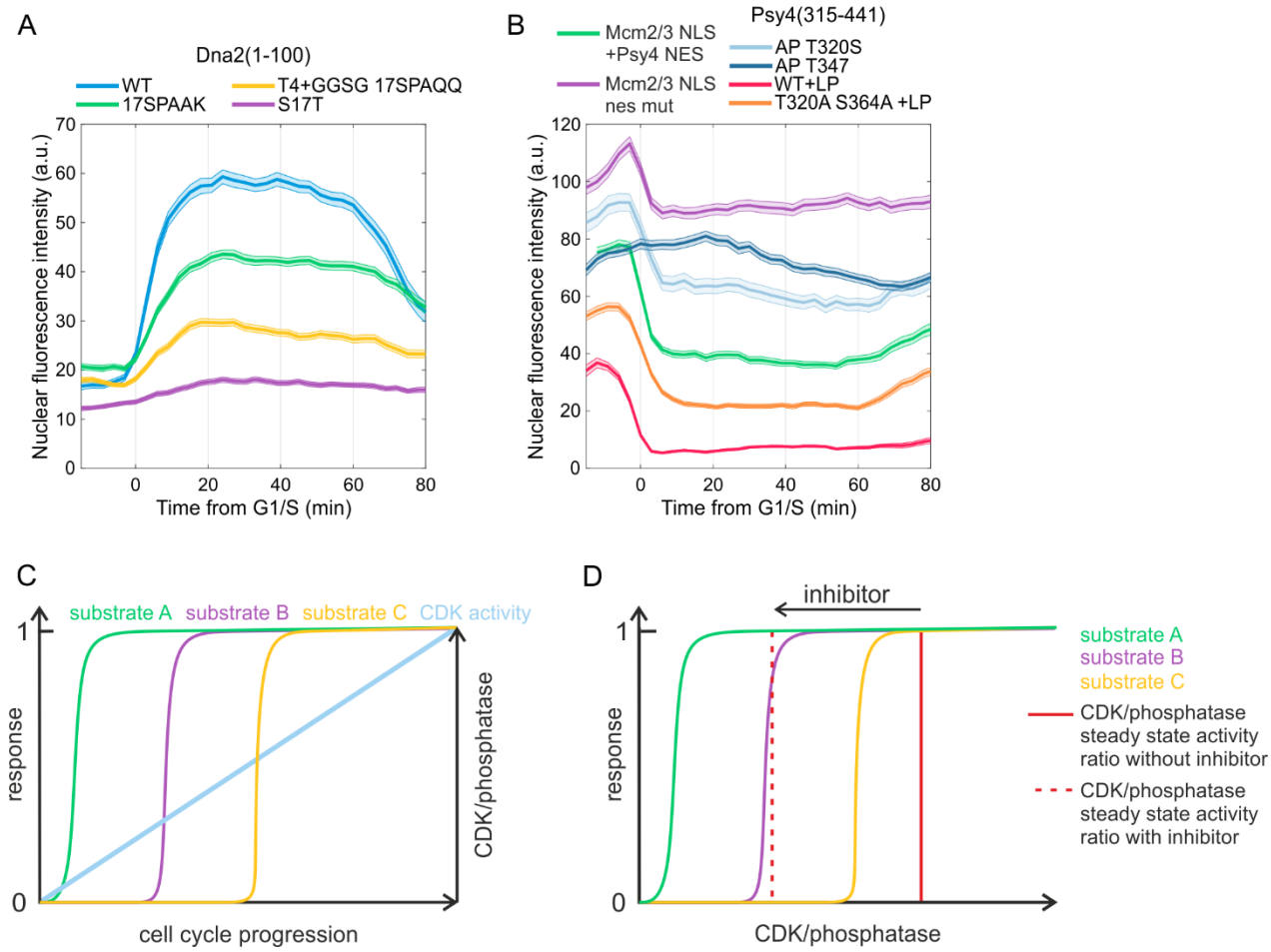

Figure 8. Programming CDK signaling modules with different stable plateau levels. (A, B) Plots displaying mean±SEM nuclear fluorescence intensities of Dna2-, Psy4-, and Mcm2/3-based localization modules measured in unperturbed cell cycles of single cells in time-lapse microscopy experiments. The schemes for the modules used in 'B' are shown in Figure S7B. In panel 'A', WT and S17T have been replotted from Fig 5G for comparison with other constructs. In panel 'B', different Psy4 constructs have been plotted together from earlier figures. (C) Scheme showing an ultrasensitive response of substrates A, B and C, triggered at different ratios of kinase/phosphatase activities as the CDK activity increases. (D) Scheme illustrating the effect of partial kinase inhibition (by addition of 1NM-PP1) on the response triggered by phosphorylation of substrates A, B and C. Addition of inhibitor decreases the ratio of kinase to phosphatase activities, leading to full inhibition of substrate C response, partial inhibition of substrate B response, and no effect to substrate A response.

Science Advances
AAAS

Supplementary Materials for

A synthetic biology approach reveals diverse and dynamic CDK response profiles via multisite phosphorylation of NLS-NES modules

Ilona Faustova, Mihkel Örd, Viacheslav Kiselev, Dmytro Fedorenko, Irina Borovko, Dags Macs, Kaur Pääbo, Marko Lõoke, and Mart Loog*

*Corresponding author. Email: mart.loog@ut.ee

This PDF file includes:

Figs. S1 to S7

Other Supplementary Materials for this manuscript include the following:

Table S1

Data S1

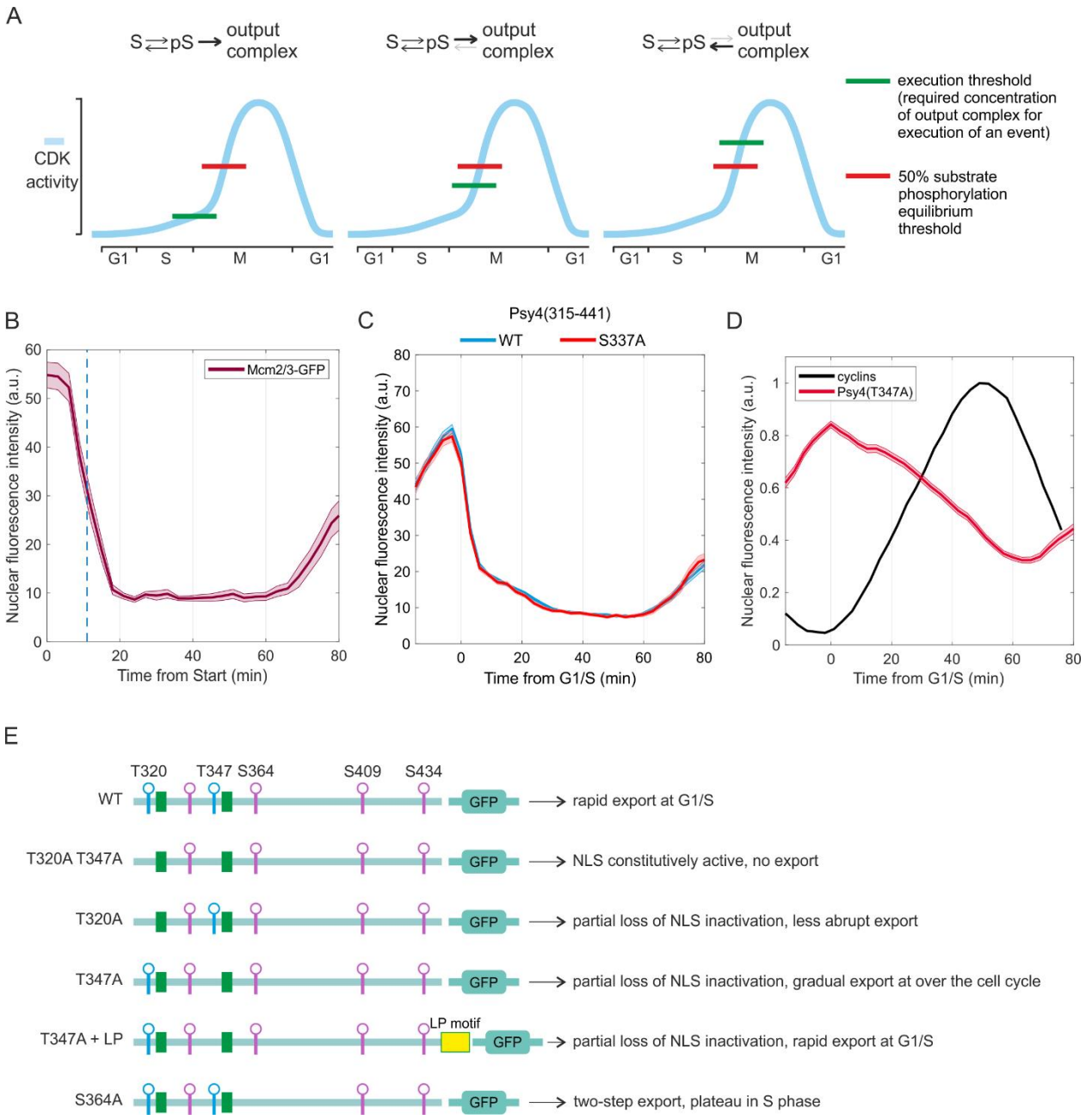

Fig. S1. Accumulation of cyclins in the cell cycle. (A) Diagrams illustrating the effect of the rate of the process downstream of phosphorylation on the threshold of CDK switch. With the same CDK specificity of the substrate (determining the equilibrium of phosphorylation), an irreversible output, such as protein degradation triggered by phosphorylation of SCF-Cdc4 di-phosphodegrons, can occur at much lower CDK activity compared to reversible outputs. (B) The timing of Mcm2/3-GFP sensor nuclear export was measured relative to Start in time-lapse microscopy using the nuclear export of Whi5-mCherry as a marker for Start point (67). Plot shows mean±SEM of Mcm2/3-GFP nuclear abundance from individual cells. 50% of Mcm2/3 sensor is exported around 11 minutes after Start. (C) Plot showing mean±SEM nuclear fluorescence intensities of wild-type and S337A Psy4(315-441) sensors in cells synchronized at G1/S. (D) Plot showing the accumulation of cyclins and nuclear export of the Psy4-T347A module during the cell cycle. The cyclin accumulation (Cln2, Clb5, Clb4, Clb3, Clb2 and Clb1) was measured relative to Start using Citrine-tagged cyclins in (26). Here, the cyclin abundance data was plotted relative to G1/S based on the 11-minute shift observed in panel 'B'. (E) Schemes showing the Psy4(315-441) constructs used in Figure 1.

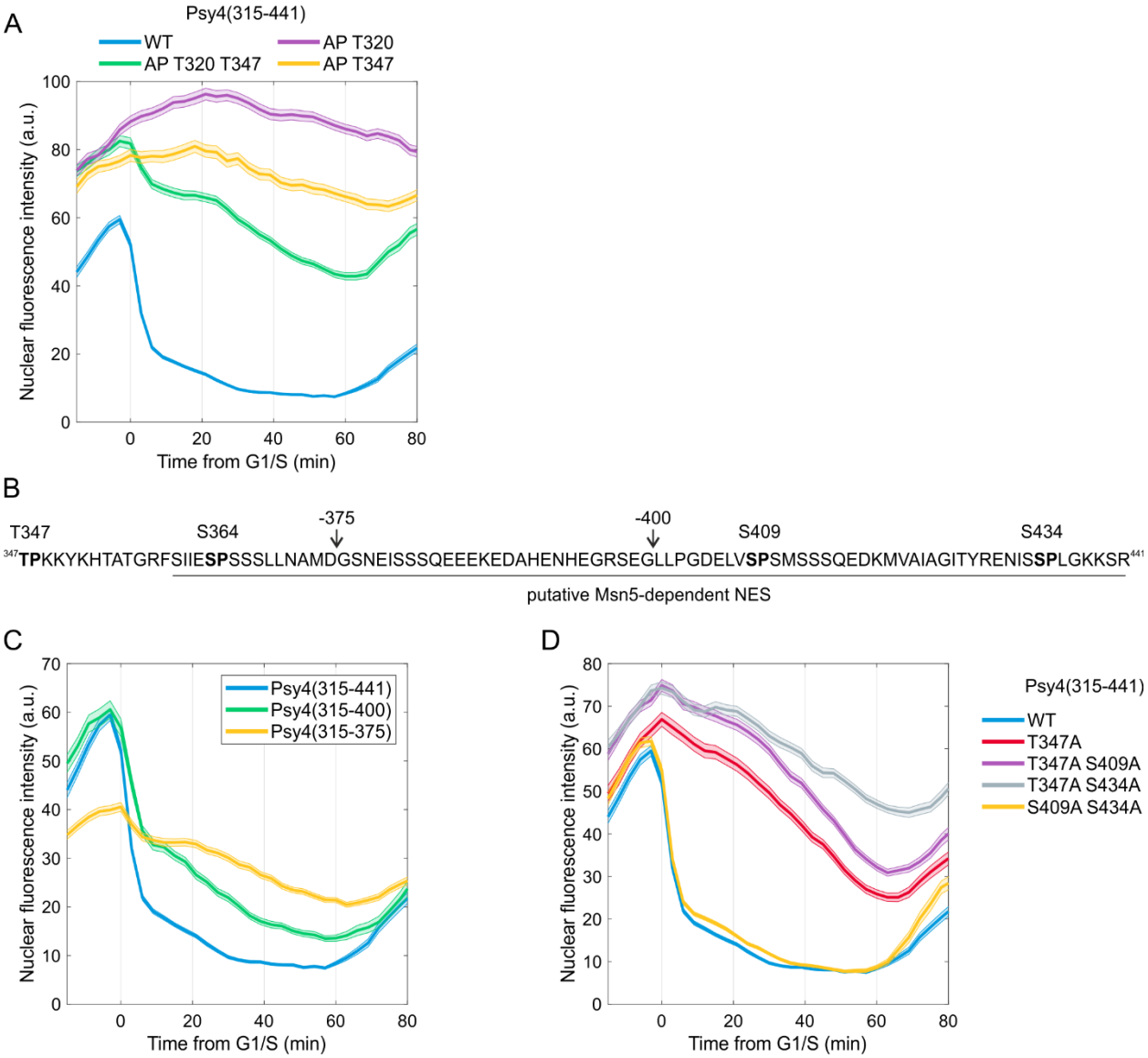

Fig. S2. The C terminus of Psy4 carries nuclear export activity that is promoted by phosphorylation of S364, S409A and S434. (A, C, D) Plots displaying the mean±SEM nuclear fluorescence intensities of the indicated Psy4(315-441)-GFP module over the cell cycle. (A) 'AP' denotes Psy4 mutant with alanine mutations at all CDK consensus sites except the ones indicated as intact (T320 and/or T347). (B) Amino acid sequence of Psy4(347-441) showing the truncations studied in panel 'C'. (C) The nuclear localization profiles of shorter Psy4 fragments were analysed to map the NES region.

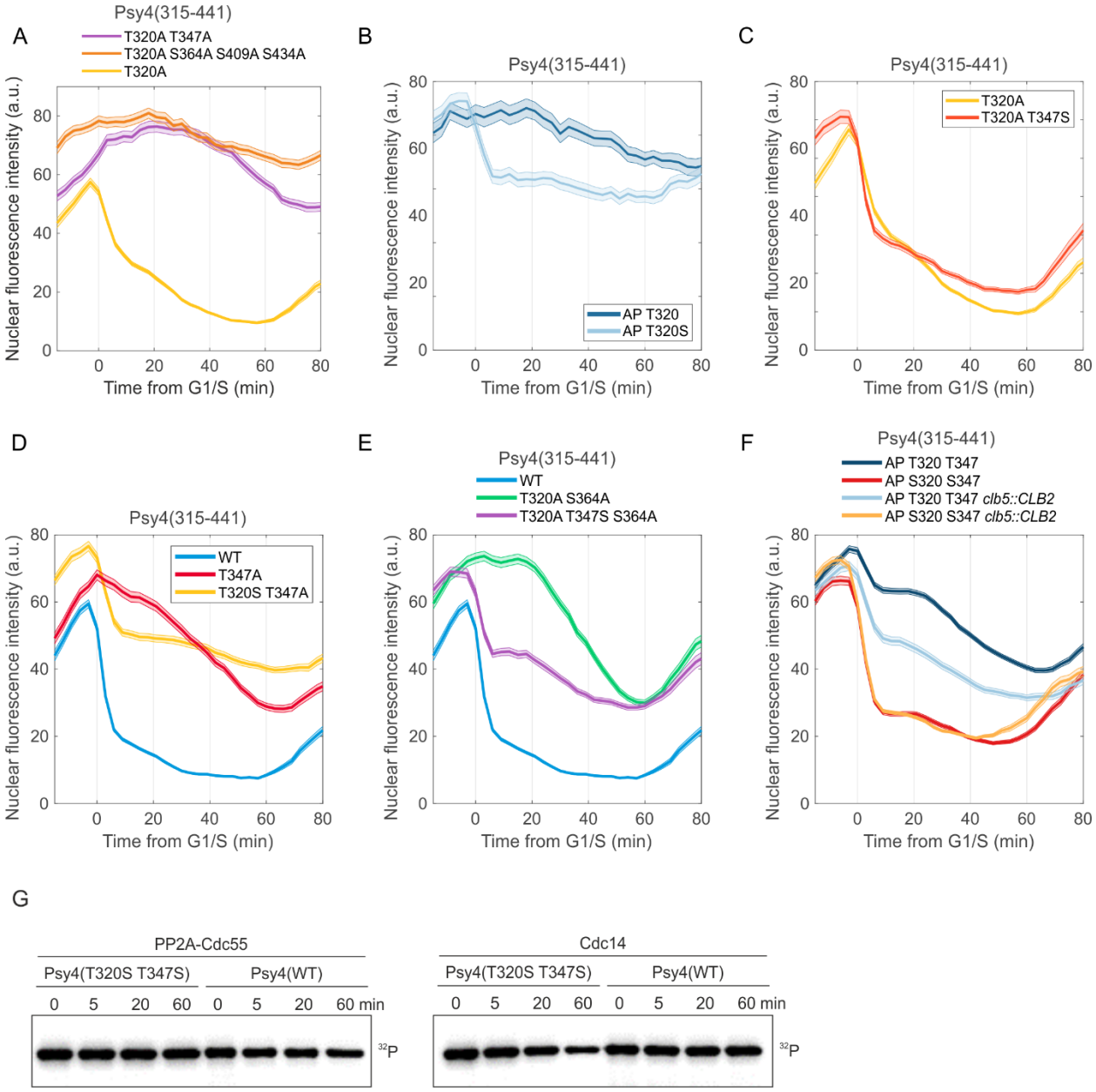

Fig. S3. Earlier phosphorylation of SP sites in the Psy4 module. (A-F) Time-lapse microscopy analysis showing mean±SEM nuclear Psy4-GFP fluorescence intensities from cells synchronized at G1/S during the analysis. (B) In Psy4-AP T320 and AP T320S, all CDK consensus sites but T320 are mutated to alanine (T347A S364A S409A S434A). (F) In clb5::CLB2 strain, SWE1 is deleted and an extra copy of CLB2 is expressed from the CLB5 locus. (G) ^{32}P autoradiographs showing the dephosphorylation of either wild-type Psy4 module or T320S-T347S module by phosphatases PP2A-Cdc55 and Cdc14. The experiment was repeated twice, a representative example is shown.

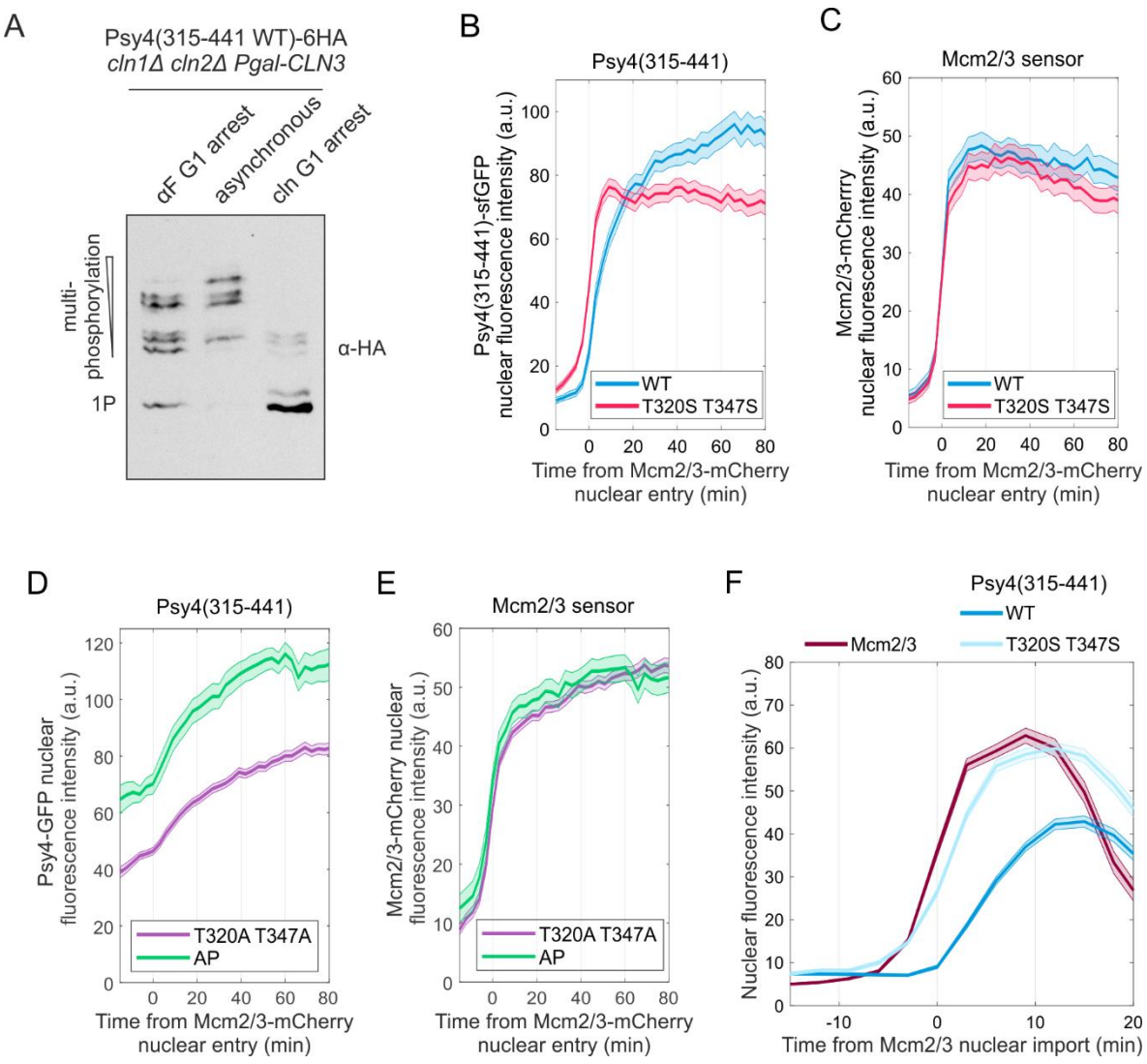

Fig. S4. Thr-to-Ser mutations affect phosphorylation in G1 and Psy4 nuclear entry in mitosis. (A) Comparison of Psy4(315-441)-GFP-6HA multisite phosphorylation in ansynchronous culture, α-factor-induced G1 arrest (MAPK active), and G1 arrest caused by G1 cyclin depletion (cln1 cln2 PGAL1-CLN3 strain grown in medium containing glucose to suppress CLN3 expression). (B-E) The nuclear level of the indicated Psy4 mutants (panels B and D) and of Mcm2/3-mCherry in the strains expressing different Psy4 modules (panels C and E) in cells arrested in G1 with α-factor was measured in time-lapse microscopy. Plots show mean±SEM nuclear fluorescence intensities from a population of cells synchronized in the analysis at the time of nuclear import of 50% of the Mcm2/3-mCherry module. AP denotes the Psy4 module, where all CDK consensus sites have been mutated. (F) Plot showing the nuclear import of the indicated Psy4 modules. The cells were synchronized during the analysis at the point of 50% nuclear import of Mcm2/3 in late mitosis. Plot shows mean±SEM Psy4-GFP nuclear fluorescence intensities.

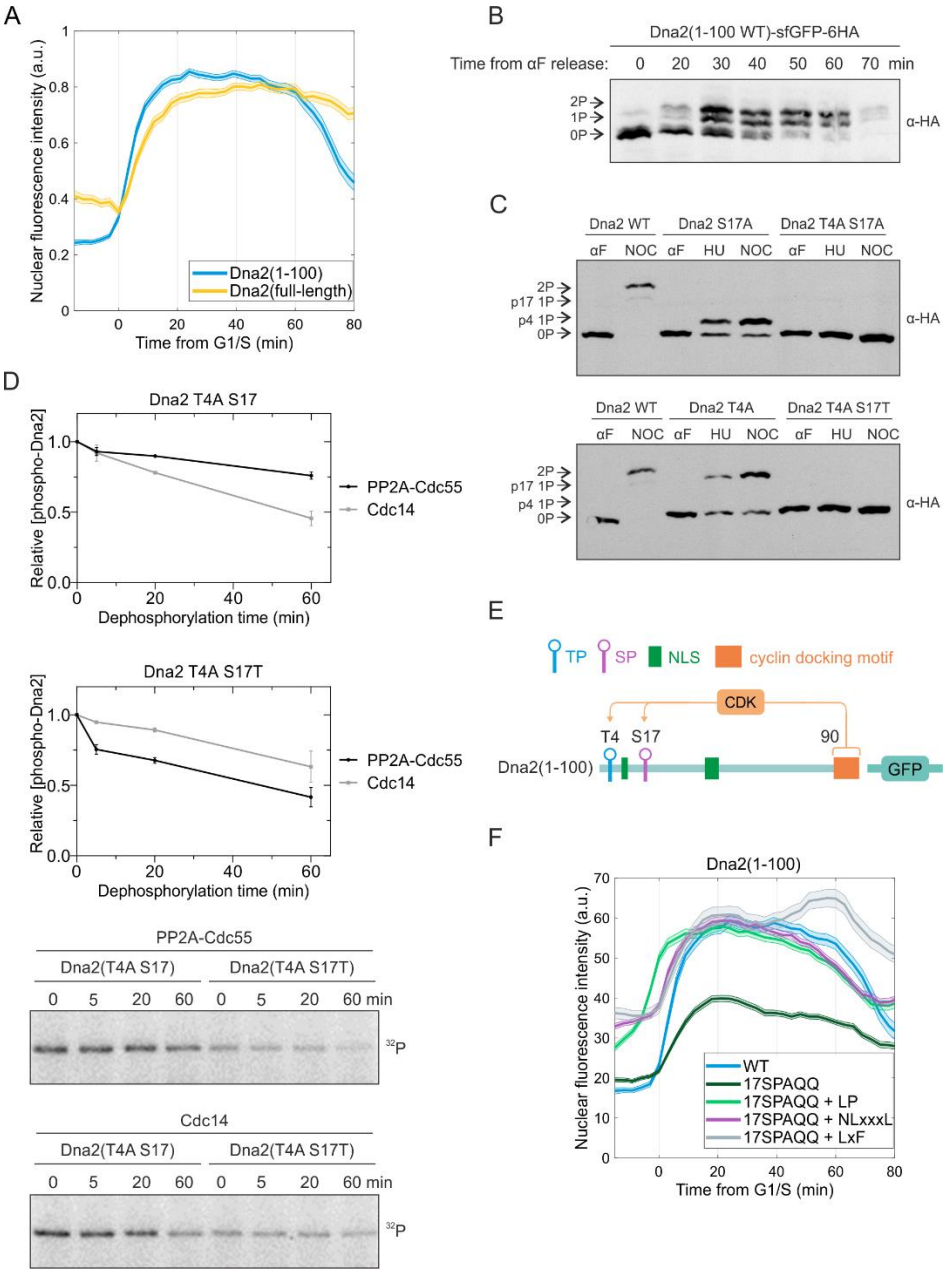

Fig. S5. Phosphorylation analysis of the Dna2 module. (A) Normalized nuclear fluorescence intensities of Dna2(1-100) and full-length Dna2 GFP fusion proteins during the cell cycle. Plot shows mean±SEM. (B) Multisite phosphorylation of Dna2(1-100)-GFP-6HA was studied using Phos-tag western blotting of synchronized cell cultures released from pheromone-induced G1 arrest. (C) Analysis of phosphorylation of different Dna2(1-100) phosphorylation site mutants in cells arrested in different cell cycle phases. α-factor (αF) causes G1 arrest, hydroxyurea (HU) S phase arrest, nocodazole (NOC) mitotic arrest. For greater resolution, the longer electrophoresis was carried out for the blots in panel 'C' compared to panel 'B'. (D) Dephosphorylation assays to study the serine/threonine specificity of phosphatases PP2A-Cdc55 and Cdc14 in dephosphorylation of Dna2(1-100). The substrate protein was first phosphorylated with Clb5-Cdk1 in the presence of ^{32}P-ATP, followed by inhibition of Cdk1 by addition of Sic1. The dephosphorylation reaction was stopped at indicated time points. The plots show mean±standard deviation of the relative remaining phospho-protein from two experiments. Representative ^{32}P autoradiographs are shown below. (E) Scheme of Dna2(1-

100) showing the addition of cyclin docking motifs to the C terminus of Dna2 module. (F) Plot showing mean±SEM nuclear fluorescence intensities of the indicated Dna2 modules.

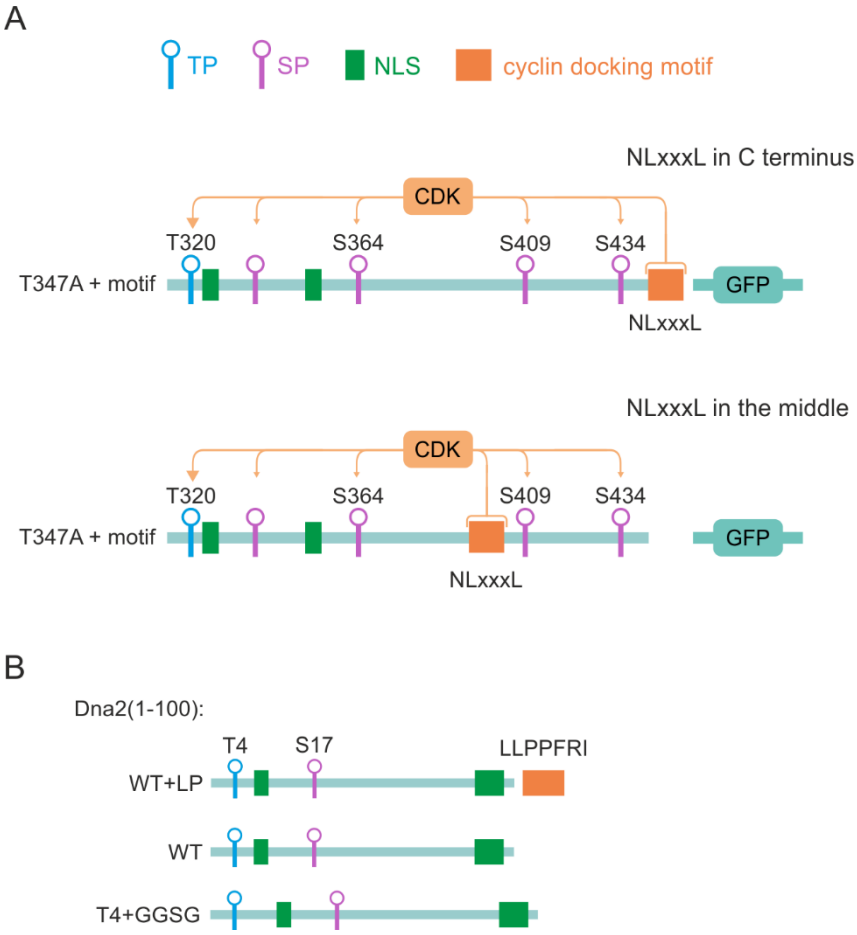

Fig. S6. Design of CDK-regulated nuclear localization modules. (A) Schemes of Psy4(315-441 T347A) modules with the cyclin docking motifs introduced in different positions. (B) Schemes showing Dna2 nuclear import modules. In "T4+GGSG", the GGSG linker was introduced after T4 to increase the distance between T4 and S17.

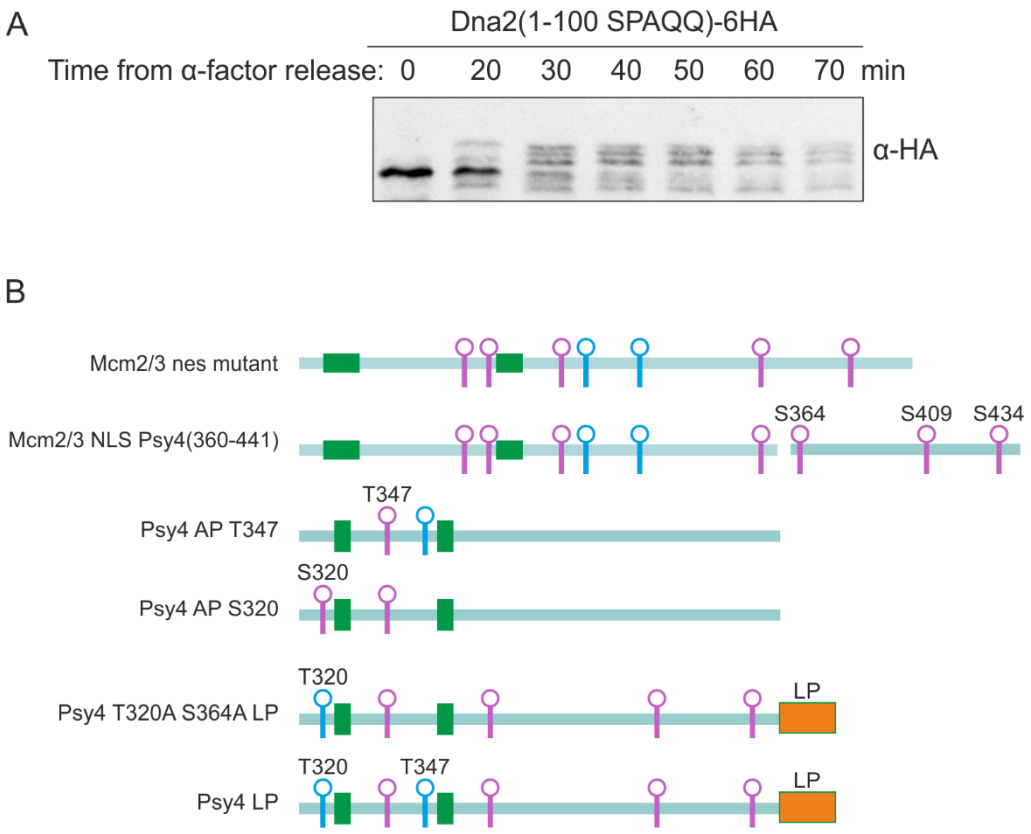

Fig. S7. Stable plateaus in CDK-regulated localization modules. (A) Multisite phosphorylation of the Dna2(1-100 17SPAQQ)-GFP-6HA was studied using Phos-tag western blotting of synchronized cell cultures released from pheromone-induced G1 arrest. (B) Schemes showing the positioning of phosphorylation sites, localization motifs and cyclin docking motifs in the Psy4- and Mcm2/3-based modules used in Figure 8B.

NON-EXCLUSIVE LICENCE TO REPRODUCE THESIS AND MAKE THESIS PUBLIC

I, Viacheslav Kiselev,

(*author's name*)

1. herewith grant the University of Tartu a free permit (non-exclusive licence) to

reproduce, for the purpose of preservation, including for adding to the DSpace digital archives until the expiry of the term of copyright,

Cdk1-mediated phosphoregulation of NLS-NES modules,

(*title of thesis*)

supervised by Associate Professor, PhD Ilona Faustova and Researcher, PhD Mihkel Örd.

(*supervisor's name*)

2. I grant the University of Tartu a permit to make the work specified in p. 1 available to the public via the web environment of the University of Tartu, including via the DSpace digital archives, under the Creative Commons licence CC BY NC ND 4.0, which allows, by giving appropriate credit to the author, to reproduce, distribute the work and communicate it to the public, and prohibits the creation of derivative works and any commercial use of the work from ***27/05/2025*** until the expiry of the term of copyright.

3. I am aware of the fact that the author retains the rights specified in points 1 and 2.

4. I confirm that granting the non-exclusive licence does not infringe other persons' intellectual property rights or rights arising from the personal data protection legislation.

Viacheslav Kiselev

27/05/2022